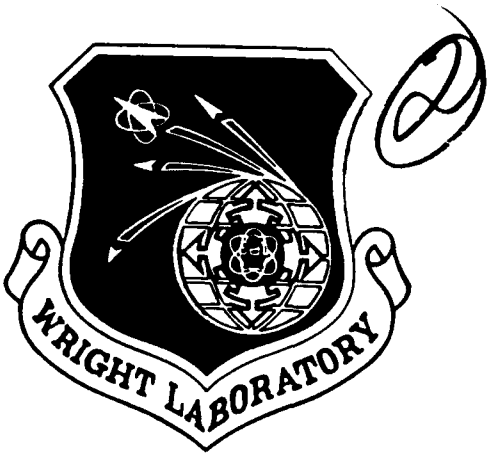

WL-TR-91-2074

ELECTRON INTERACTIONS WITH NON-LINEAR POLYATOMIC MOLECULES AND THEIR RADICALS AND IONS

Ashok Kumar Jain

Physics Department, Florida A&M University, Tallahassee, Fl 32307
&
Supercomputer Computations Research Institute (SCRI),
Florida State University, Tallahassee, Fl 32306

June 1991

INTERIM REPORT FOR PERIOD JUNE 1990 - JUNE1991
Approved for public release; distribution is unlimited

AERO PROPULSION AND POWER DIRECTORATE
WRIGHT LABORATORY
AIR FORCE SYSTEMS COMMAND
WRIGHT - PATTERSON AIR FORCE BASE, OHIO 45433-6563

NOTICE

WHEN GOVERNMENT DRAWINGS, SPECIFICATIONS, OR OTHER DATA ARE USED FOR ANY PURPOSE OTHER THAN IN CONNECTION WITH A DEFINITELY GOVERNMENT-RELATED PROCUREMENT, THE UNITED STATES GOVERNMENT INCURS NO RESPONSIBILITY OR ANY OBLIGATION WHATSOEVER. THE FACT THAT THE GOVERNMENT MAY HAVE FORMULATED OR IN ANY WAY SUPPLIED THE SAID DRAWINGS, SPECIFICATIONS, OR OTHER DATA, IS NOT TO BE REGARDED BY IMPLICATION, OR OTHERWISE IN ANY MANNER CONSTRUED, AS LICENSING THE HOLDER, OR ANY OTHER PERSON OR CORPORATION; OR AS CONVEYING ANY RIGHTS OR PERMISSION TO MANUFACTURE, USE, OR SELL ANY PATENTED INVENTION THAT MAY IN ANY WAY BE RELATED THERETO.

THIS REPORT HAS BEEN REVIEWED BY THE OFFICE OF PUBLIC AFFAIRS (ASD/PA) AND IS RELEASABLE TO THE NATIONAL TECHNICAL INFORMATION SERVICE (NTIS). AT NTIS IT WILL BE AVAILABLE TO THE GENERAL PUBLIC INCLUDING FOREIGN NATIONS.

THIS TECHNICAL REPORT HAS BEEN REVIEWED AND IS APPROVED FOR PUBLICATION.

Alan Garscadden.

ALAN GARSCADDEN
Power Components Branch
Aerospace Power Division
Aero Propulsion Laboratory

Lowell D. Massie

LOWELL D. MASSIE
Chief, Power Components Branch
Aerospace Power Division

FOR THE COMMANDER

Michael D Braydich

MICHAEL D. BRAYDICH, Lt Col, USAF
Deputy Director
Aerospace Power Division
Aero Propulsion & Power Directorate

IF YOUR ADDRESS HAS CHANGED, IF YOU WISH TO BE REMOVED FROM OUR MAILING LIST, OR IF THE ADDRESSEE IS NO LONGER EMPLOYED BY YOUR ORGANIZATION PLEASE NOTIFY WL/POOC, WRIGHT-PATTERSON AFB, OH 45433-6563 TO HELP MAINTAIN A CURRENT MAILING LIST.

COPIES OF THIS REPORT SHOULD NOT BE RETURNED UNLESS RETURN IS REQUIRED BY SECURITY CONSIDERATIONS, CONTRACTUAL OBLIGATIONS, OR NOTICE ON A SPECIFIC DOCUMENT.

UNCLASSIFIED

SECURITY CLASSIFICATION OF THIS PAGE

REPORT DOCUMENTATION PAGE

Form Approved OMB No. 0704-0188

1a. REPORT SECURITY CLASSIFICATION UNCLASSIFIED	1b. RESTRICTIVE MARKINGS N/A
2a. SECURITY CLASSIFICATION AUTHORITY N/A	3. DISTRIBUTION/AVAILABILITY OF REPORT Approved for Public Release; Distribution Unlimited
2b. DECLASSIFICATION/DOWNGRADING SCHEDULE N/A	
4. PERFORMING ORGANIZATION REPORT NUMBER(S) N/A	5. MONITORING ORGANIZATION REPORT NUMBER(S) WL-TR-91-2074
6a. NAME OF PERFORMING ORGANIZATION Florida A&M University 6b. OFFICE SYMBOL (*If applicable*)	7a. NAME OF MONITORING ORGANIZATION Aero Propulsion & Power Dir. (WL/POOC) Wright Laboratory
6c. ADDRESS (*City, State, and ZIP Code*) Physics Department, Florida A&M University Tallahassee, FL 32307	7b. ADDRESS (*City, State, and ZIP Code*) Wright-Patterson AFB, OH 45433-6563
8a. NAME OF FUNDING/SPONSORING ORGANIZATION Wright Laboratory 8b. OFFICE SYMBOL (*If applicable*) WL/POOC	9. PROCUREMENT INSTRUMENT IDENTIFICATION NUMBER F33615-90-C-2032
8c. ADDRESS (*City, State, and ZIP Code*) WL/POOC-3 Wright-Patterson AFB, OH 45433-6563	10. SOURCE OF FUNDING NUMBERS PROGRAM ELEMENT NO. 62203F; PROJECT NO. 2003; TASK NO 12; WORK UNIT ACCESSION NO. 03

11. TITLE (*Include Security Classification*)
Electron Interactions With Non-linear Polyatomic Molecules And Their Radicals And Ions

12. PERSONAL AUTHOR(S)
Jain, Ashok Kumar

13a. TYPE OF REPORT	13b. TIME COVERED	14. DATE OF REPORT (*Year, Month, Day*)	15. PAGE COUNT
Interim	FROM 90/06/07 TO 91/06/06	91 June	119

16. SUPPLEMENTARY NOTATION

17. COSATI CODES			18. SUBJECT TERMS (*Continue on reverse if necessary and identify by block number*)
FIELD	GROUP	SUB-GROUP	Electrons, Molecules, Cross Sections, Rotational Excitation, Scattering, Atomic and Molecular Physics
2009			

19. ABSTRACT (*Continue on reverse if necessary and identify by block number*)

The low energy electron collisions with CH_4, SiH_4, H_2O, NH_3, and GeH_4 has been studied for elastic and rotational excitation channels. A parameter-free ab initio approach is employed in which electron-exchange interaction is treated exactly and the polarization effects via perturbation theory. The integro-differential coupled equations are solved iteratively to yield scattering parameters. Detailed results are obtained for differential, integral, and momentum transfer cross sections. The agreement with experimental data for all the parameters is very good.

20. DISTRIBUTION/AVAILABILITY OF ABSTRACT	21. ABSTRACT SECURITY CLASSIFICATION	
☒ UNCLASSIFIED/UNLIMITED ☐ SAME AS RPT. ☐ DTIC USERS	UNCLASSIFIED	
22a NAME OF RESPONSIBLE INDIVIDUAL Patrick D. Kee, 2/Lt, USAF	22b. TELEPHONE (*Include Area Code*) 513 255-2923	22c. OFFICE SYMBOL WL/POOC

DD Form 1473, JUN 86 *Previous editions are obsolete.*

SECURITY CLASSIFICATION OF THIS PAGE

UNCLASSIFIED

PREFACE AND ACKNOWLEDGEMENTS

This work was accomplished during the period June 1990 through June 1991 under the Air Force Contract F33615-90-C-2032. The Air Force contract manager was Lt. Patrick D Kee and the contract officer was Rebecca B O'Kelley. This technical report entitled *Electron Interaction with Non-Linear Polyatomic Molecules and their Radicals and Ions*, was prepared at the Physics Department, Florida A& M University, Tallahassee, Florida.

We would like to thank the Florida State University's Supercomputer Research Institute (SCRI) for providing supercomputer time on the CRAY-YMP machine. In addition supercomputer time on the NMFECC CRAY-2 machine at Livermore was also made available to us through SCRI, which is partially funded by the US Department of Energy through contract no. DE-FC05-85ER250000. We extend our thanks to SCRI staff for their help throughout the execution of this work. We would like to take this opportunity to thank specially to Joe Lannutti (Director, SCRI), Chris Lacher (Chairman, Resource Allocation Committee), Robert Holden (Manager, Supercomputing group), Jay Sollohub, Doug Lee, Tom Combs, Dianne Brantly, Susan Fell, and many others at the SCRI and innovation park facilities.

A part of the present research work was performed in collaboration with Professor F A Gianturco (Department of Chemistry, University of Rome, Italy) and Dr. D G Thompson (Department of Applied Mathematics and Theoretical Physics, The Queen's University of Belfast, N Ireland). A travel grant from NATO (CRG 890470) is thankfully acknowledged. We wish to thank Drs. K L Baluja and Shanthi Rao for carrying out some calculations for this project. It is also a pleasure to thank our colleagues at the Physics Department, FAMU. We are grateful to Drs. L Boesten, T W Shyn, O Sueoka, H Tanaka, M Hayashi, and C Szmytkowski for sending their experimental data prior to publication.

We owe a considerable debt of gratitude to our President Frederick S Humphries for his continuous support, inspiration, and encouragement for the success of this progress report. Appreciation is expressed to Dr. Franklin Hamilton and his staff at the Sponsored Research Office (FAMU) for their administrative support. Our special thanks are to the Purchasing and Comptroller's offices for dealing with the budget part of the project. Finally, we express our gratitude to our Dean, Dr. Aubrey M Perry and his staff of the College of Arts and Science for their extremely helpful cooperation.

TABLE OF CONTENTS

1. INTRODUCTION

This report describes the progress of the project entitled " **Electron Interactions with Non–Linear Polyatomic Molecules and their Radicals and Ions** " for the period June 1990 to June 1991. The present theoretical research was carried out under the auspices of AirForce contract No. F33615-90-C-2032. The work was performed at the Physics Department, Florida A&M University, Tallahassee, Florida with the direct supervision and participation of Dr. Ashok K. Jain, Principal Investigator (PI). A part of this project was performed in collaboration with Professor F A Gianturco (Department of Chemistry, University of Rome, Italy) and Dr. D G Thompson (Department of Applied Mathematics, The Queen's University of Belfast, N. Ireland). The collaboration with the University of Rome was partially funded by the NATO (under contract No CRG 890470) in terms of a 2–year travel grant. The computational work was fully supported by the FSU's Supercomputer Research Institute (SCRI) in terms of supercomputer time on the CRAY-YMP (at Tallahassee) and on the NMFECC CRAY-2 machine (at Livermore).

The overall goal of this project is to develop state–of–the–art computer programs and to perform calculations on various elastic and inelastic cross sections for low energy electron collisions with non–linear polyatomic molecules and their ions and radicals. It is a well known fact that such a project involves a large amount of computing because of complexities involved in the dynamics of the collision system. Our main purpose is to produce a reliable set of useful cross section data for elastic as well as inelastic processes without involving any fitting procedure. When electrons interact with neutral molecular targets, time considerations of the electronic and nuclear motions allow us to treat rotational, vibrational, and electronic processes rather independently. This is the so–called adiabatic–nuclei–approximation (ANA) which has made *ab initio* electron–molecule calculations a dream come true. Even under the great simplifications introduced by the ANA formulation, the treatment of electron–polyatomics is still a very difficult problem owing to, for example, the multicenter nature of the interaction, the presence of non–local electron exchange, charge correlation and polarization effects and the opening of several other rearrangement channels .

For the simple case of elastic (including rotational excitation processes) scattering at the static–exchange level (neglecting short range correlation and long range polarization effects), the solution of inhomogenous integro-differential coupled equations *iteratively* is

an arduous task for the case of non–linear targets. Consequently, it is not surprising that just a few years ago, most of the electron–polyatomic calculations were carried out by employing model potentials for exchange and polarization effects [1]. For the first time, our group developed scattering codes [2–7] which solve electron–polyatomic scattering equation iteratively to treat electron exchange effects exactly. To implement short range correlation and long range polarization effects correctly is still an open problem. We, however, include these charge distortion effects non–empirically using the perturbative techniques.

In brief, the electron–molecule problem is set up in the single–center–expansion (SCE) scheme under the body–fixed (BF) coordinate system in the ANA close–coupling formulation. The continuum electron function is obtained numerically for each irreducible representation of the molecule point group. The convergence of bound and continuum functions with respect to SCE size is tested properly to make this approach meaningful. No fitting procedure is involved in all the cross sections discussed here. In addition, unlike the basis–set dependent L^2 type approaches [8], this method is free from producing any spurious effects in the cross sections; thus given no previous information, theoretical or experimental, the present method is capable of predicting differential as well as integral cross sections for various elastic and inelastic dynamical processes.

In Section 2, we provide a summary of work completed so far, and Section 3 gives a list of published (or accepted) and submitted papers during the period June 1990 to June 1991. The theory of the present calculations is presented in Section 4 and Section 5 provides the corresponding numerical details and a list of computer programs employed for this work. In Section 4, we also discuss our recent method [6] on a most efficient use of an iterative scheme in terms of computer time without sacrificing any numerical accuracy.

In Section 6, we discuss our main calculations on the rotationally elastic, inelastic and summed cross sections for electron collisions from CH_4, SiH_4, H_2O, NH_3, and GeH_4 molecules in the energy range of 0–20 eV. For all these species, experimental data on the differential (DCS), integral and momentum transfer cross sections are available for comparison. For the e–CH_4 case, there are experimental data on the rotational excitation process as well. In Section 7 we analyse the effect of gas temperature on the cross sections and confirm several theorems of Shimamura [9–15]. Finally, concluding remarks on the finished work and comments on the continuation of this project for the second year are made in Section 8.

2. SUMMARY OF WORK PERFORMED (June 1990 – May 1991)

1. The electron scattering from SiH_4 molecules at 0.01–20 eV now has been published [Ashok Jain and D G Thompson, J. Phys. **B24**, 1087 (1991), Ref. 5]. The exchange (exactly) and polarization (approximately but parameter–free) are included to make a direct comparison with experimental data. This is a detailed study on the low–energy behaviour of electrons in silane gas. Our *ab initio*, parameter–free calculations clearly exihibit the cross section minimum below 1 eV and a shape–resonance feature around 2–4 eV; this is in agreement with measured data. No any other *ab initio* calculation (with polarization effects) on the e–SiH_4 low–energy cross sections with such details and amount of cross section data is available in the literature.

2. In order to treat exchange effects exactly in an efficient way, we have suggested and tested a new optimized *iterative* scheme to solve the integro–differential equations more economically. The new scheme is more suitable for the case of polar molecules where convergence problems are severe. In the optimized scheme, the continuum wavefunction of the electron with full iterative procedure is calculated only once at a selected energy, say E, i.e., $f_{\ell\ell'}(r;E)$. The $f_{\ell\ell'}(r;E)$ is employed as a starting point for iterative scheme at other energies. We found for the H_2O case (and very rcently for the NH_3 case also) that the number of iterations required in the optimised scheme is smaller, by a factor of two to three, than the usual one [6]. Further, we noticed that the exact–exchange treatment is necessary for low partial waves only. The non–penetrating higher partial waves can be described by a simple model exchange potential under the density functional theory. Thus, the new scheme, which is very economical and essential to treat polar molecules, can be described as follows. For low partial waves (say $\ell = \ell_E$), we consider full exact–exchange calculation; for $\ell \geq \ell_E$, say up to $\ell = \ell_M$, we employ a model exchange (for example the free–electron–gas exchange) approximation; and finally for very high partial waves $\ell \geq \ell_M$, say $\ell = \ell_{UB}$, we use unitarised Born approximation. A paper on the optimized iterative scheme with test calculations on the e–H_2O system has been published recently [Ashok Jain, F A Gianturco and D G Thompson, J. Phys. **B24**, L225 (1991), Ref. 6].

3. We have investigated in great detail the effects of gas temperature on the rotational excitations in a molecule (CH_4 and SiH_4) by slow electron impact. We have found that the rotational excitation process is sensitive to gas temperature in an experimental

situation and one should be careful in comparing theoretical rotational excitation cross sections with measurements. In particular, for example, the theory predicts zero cross sections at zero angle for the $0 \rightarrow 3$ rotational transition in a spherical top molecule, while measurements (on the CH_4 molecule) give non-zero DCS in the forward direction [16].

4. We have studied various approximations to include polarization effects in the e–SiH_4 collisions at low energies. In this calculation, we have employed two types of parameter-free model polarization potentials alongwith exact-exchange effects. Our conclusion is that a polarization potential determined from polarised-orbital type approach is a better model than the one from the target density functional theory.

5. The calculations on low-energy electron scattering with H_2O and NH_3 gases are now almost complete. We are currently testing convergence of the differential and total cross sections for these polar gases, for which the ANA theory fails in the forward direction. Our preliminary results on the differential as well as integral quantities compare reasonably well with the experiment [A Jain and D G Thompson, 1991, under preparation].

6. In addition, we have developed a single-center computer program [17] to expand molecular quantities (orbitals, density, static potential etc.) around the center-of-mass (COM) of the target from the calculations of Quantum Chemistry codes such as the HONDO or GAUSSIAN. This work is being done in collaboration with the group at Chemistry Department, University of Rome, Italy. We are in the process of studying some big molecules such as the GeH_4, CF_4, SF_6, etc.. The first calculations on the e–GeH_4 collisions have been carried out and results submitted for publication [18].

The computing facilities, provided by the FSU's SuperComputer Research Institute (SCRI), have been excellent in order to carry out the above programs effectively. We have made use of supercomputers (CRAY-2 at the NMFECC, Livermore and CRAY-YMP at the SCRI, Tallahassee) through the FSUCC allocation committee. Most of the graphical work and small calculations were carried out at the FSU's and SCRI's VAX machines which serve as front-end system for the supercomputers.

3. LIST OF PUBLICATIONS (June 1990 – May 1991)

Papers Published/Accepted:

1. " Theoretical Study of Low-energy Electron-SiH_4 Collisions using Exact Exchange plus Parameter-Free Polarization Potential, " by **Ashok Jain** and **D G Thompson**. J. Phys. **B24**, 1087 (1991).

2. " Effect of the Gas Temperature on the Rotational Excitation of Spherical Top Molecules by Low Energy Electrons: CH_4 and SiH_4.," by **Ashok Jain**. (to appear in Z. Phys. D, Atoms, Molecules and Clusters, 1991)

3. " Exact-Exchange Treatment in Electron-Polyatomic Molecules in a Computationally Optimised Iterative Scheme, " by **Ashok Jain, F A Gianturco** and **D G Thompson**, J. Phys. **B24**, 255 (1991).

4. " Polarization Effects in Low-Energy Electron Scattering from Silane Molecules Treating Electron Exchange Correlation Exactly, " by **Ashok Jain**, Phys. Rev. **A44**, 772 (1991)

Papers Submitted for Publication

5. " Differential, Integral and Momentum Transfer Cross Sections for Electron Scattering with Germane (GeH_4) Molecules at 1-100 eV, " by **Ashok Jain, K L Baluja, V Di Martino** and **F A Gianturco**. (Accepted in Chem. Phys. Lett., 1991)

Papers under preparation

6. " Slow Electron Collisions with H_2O Molecules in an Exact-Exchange plus Parameter-free Polarization Potential Model, " by **Ashok Jain** and **D G Thompson**. (to be submitted to J. Phys. B).

7. " A Theoretical Study of Slow Electron Impact from Ammonia (NH_3) Gas: Rotationally Elastic, Inelastic and Summed Cross Sections, " **Ashok Jain** and **D G Thompson** (to be submitted in Phys. Rev. A, 1991).

4. REVIEW OF THEORETICAL APPROACH

When low–energy electrons interact with molecular targets, several processes, elastic and inelastic, can take place in the present energy region (E $\leq$ 20 eV),

$$e^- + A_nB_m \rightarrow e^- + A_nB_m \qquad (elastic)$$
$$\rightarrow e^- + (A_nB_m)^* \quad (inelastic; \quad vibrational\ and/or\ rotational)$$

(There are also other inelastic processes such as the electronic excitation, dissociative, associative, or ionization channels.) The basic Schrödinger equation involves an interaction Hamiltonian and the corresponding wave function of the total system,

$$(H_{int} - E)\Psi_T(\mathbf{r}, \mathbf{r}_i, \mathbf{R}) = 0, \tag{4.1}$$

where the electron–molecule Hamiltonian is given by,

$$H_{int} = H_{elec}(\mathbf{r}_i; \mathbf{R}) + V_{int}(\mathbf{r}, \mathbf{r}_i, \mathbf{R}) + H_{nuc}(\mathbf{R}). \tag{4.2}$$

Here $\mathbf{r}$ represents the projectile electron's coordinate and $\mathbf{r}_i$ and $\mathbf{R}$ collectively represent the target electronic and nuclear coordinates respectively. It is not possible to solve equation (1) exactly for any of the channels or collision systems. We first describe the iterative techniques to solve integro–differential (see below) equation under the SCE formalism.

4.1. Single-Center-Expansion (SCE) Iterative Method

In order to obtain various elastic and inelastic cross sections (differential as well as integral), we make use of the adiabatic–nuclei–approximation (ANA) [19] and set up our scattering equations in the SCE scheme under the close–coupling formalism. The FNA is generally a very good approximation except in certain cases: for example, near threshold and sharp shape–resonance energy regions, for polar molecules, etc.

In the body-fixed (BF) frame of reference, the time-independent Schrödinger equation of the electron-molecule system reads as (omitting the parametric dependence on internuclear coordinates $\mathbf{R}$),

$$[-\frac{1}{2}\vec{\nabla}_r^2 + H_{\rm elec}(\mathbf{r}) + V_{\rm int} - E]\Psi_{\rm T}(\mathbf{r}, \mathbf{r}_i) = 0, \tag{4.1.1}$$

where the operators in the bracket are respectively the kinetic energy operator of the scattered electron, the unperturbed molecular target Hamiltonian, the interaction potential of the electron-molecule complex and the total energy of the system. The total wave function $\Psi_{\rm T}$ can be expanded such that,

$$\Psi_{\rm T} = A\sum_{i=1}^{n} \Phi_i(\mathbf{r_1}, \mathbf{r_2}, \ldots \mathbf{r_Z}) F_i(\mathbf{r}), \tag{4.1.2}$$

where Φ_i are the target electronic states and any other suitable pseudostates that can represent the target response function to the polarization of the molecule because of the incoming electron. The continuum function $F_i(\mathbf{r})$ describes the projectile motion in molecular state i and A is the usual antisymmetrization operator to ensure Pauli principle. In the expansion (4.1.2), we have neglected the correlation functions of the $(N+1)$-electron-molecule complex.

We can assume that the center of the electron-molecule system is at the center-of-mass (COM) of the target. The spin of the scattered electron is coupled with the total spin of the molecule to form an eigenstate of $\mathbf{S}^2$ and its projection along the symmetry axis (say $\mathbf{S}_z$) corresponding to the total spin quantum number S and its substate M_S which are *constants of motion* during the collision. Each of these eigenstates can be expanded over the set of angular functions according to the prescriptions of a BF frame of reference which provides the basis of an irreducible representation (IR) $p\mu$ of the molecular symmetry point group. Thus we can write the total wave function as,

$$\Psi_T^{p\mu SM_S} = \sum_{i=1}^{n}\sum_{\ell h} \Phi_{i\ell h}^{p\mu SM_S}(\mathbf{r}_1, \mathbf{r}_2 \ldots \mathbf{r}_Z, \hat{\mathbf{r}}, \sigma)(r)^{-1} F_{i\ell h}^{p\mu SM_S}(\mathbf{r}), \tag{4.1.3}$$

where σ is the spin variable of the scattered electron. The functions Φ in equation (4.1.3) are defined as,

$$\Phi_{i\ell h}^{p\mu SM_S} = \sum_{M_{S_i} m_{s_i}} \phi_i^{p_i \mu_i S_i M_{S_i}}(\mathbf{r}_1, \mathbf{r}_2, \ldots \mathbf{r}_Z) X_{\ell h}^{p\mu}(\hat{\mathbf{r}}') \eta(\frac{1}{2}, m_{s_i}) C_{M_{S_i} m_{s_i} M_S}^{S_i \ \frac{1}{2} \ S}, \qquad (4.1.4)$$

where η's are electron spin functions for the scattered electron and C's are the Clebsch–Gordon coefficients. The bound orbitals ϕ_i describe Z–electron target wave function used in expansion (4.1.4), each transforming like a particular IR of the molecular point group and with a specific total spin eigenstate. The main molecular symmetry axis defines the M_S direction.

As a standard technique, we now project the scattering equation onto the channel functions and obtain the well known coupled integro–differential equations for each scattered electron channel function ($p\mu S$):

$$[\frac{d^2}{dr^2} - \frac{\ell_i(\ell_i+1)}{r^2} + k_i^2] F_{i\ell h}^{p\mu S}(r) = 2 \sum_{i'=1}^{n} \sum_{\ell' h'} [V_{i\ell h, i'\ell' h'}^{p\mu S}(r) + W_{i\ell h, i'\ell' h'}^{p\mu S}(r)], \qquad (4.1.5)$$

4.2 Static and Exchange Interactions

The direct potential matrix $V^{p\mu S}$ defines the coupling between two channel functions through the Coulomb operator (for details see Ref. 1). The exchange interaction is represented by the non–local term, $W^{p\mu S}$, which gives rise to the integro–differential nature of the coupled scattering equations. We do not give all the details here for obvious reasons (see Ref. 1 for full details). For a closed–shell molecule, belonging to the totally symmetric $^1A_1$ IR of the molecular point group, equation (4.1.5) does not depend on the spin quantum numbers. The equation (4.1.5) is known as the static–exchange interaction of the electron–molecule system if we retain only the ground state ($i = 1$) of the target. From a numerical point of view, it is convenient to include the target distortion (polarization) effects via a model potential added to the direct potential matrix in equation (4.1.5). At short distances, the correlation effects can be treated in a similar fashion. The exchange term in equation (4.1.5) is basically of the following type,

$$W^{p\mu} = \sum_{\alpha} \int \phi_{\alpha}^{*}(\mathbf{x}) |\mathbf{r} - \mathbf{x}|^{-1} F^{p\mu}(\mathbf{x})\, d\mathbf{x} \phi_{\alpha}(\mathbf{r}), \tag{4.2.1}$$

Recently a program has been developed to treat $W^{p\mu}$ exactly under the iterative procedure[2]. Under the static–exchange plus (model) polarization (SEP) model, the integro–differential coupled equation to be solved for a closed–shell system for each symmetry $p\mu$ is rewritten from Eq. (4.1.5) as (suppressing the $p\mu$ symbol for simplicity)

$$[\frac{d^2}{dr^2} - \frac{\ell(\ell+1)}{r^2} + k^2] F_{\ell h}(r) = 2 \sum_{\ell' h'} [V^{\rm st}_{\ell h, \ell' h'}(r) + V^{\rm pol}_{\ell h, \ell' h'} + W_{\ell h, \ell' h'}(r)], \tag{4.2.2}$$

The potential matrix $V^{\rm st}_{\ell h, \ell' h'}$ in Eq. (4.2.2) is determined from the following expression for the static potential

$$V_{\rm st}(\mathbf{r}) = \int |\Phi_0|^2 \{ \sum_{j=1}^{Z} |\mathbf{r} - \mathbf{r_j}|^{-1} d\mathbf{r_1} d\mathbf{r_2} \cdots d\mathbf{r_Z} \} - \sum_{i=1}^{M} Z_i |\mathbf{r} - \mathbf{R_i}|^{-1}. \tag{4.2.3}$$

where Φ_0 is the target ground state wavefunction given as a single Slater determinant of one–electron Z spin orbitals $\phi_i(\mathbf{r})$ and M the number of nuclei in the molecule.

In a model exchange problem, the non–local exchange term in the right hand side of Eq. (4.2.2) can be replaced by a local potential, say $V^{\rm ex}_{\ell h, \ell' h'}(r)$. A very popular form of $V^{\rm ex}(r)$ has been the free–electron–gas–exchange(FEGE) approximation which was modified by Hara [20] (to be denoted by HFEGE) for electron-molecule collisions. In the HFEGE, the $V^{\rm ex}$ reads as

$$V^{\rm ex}(\mathbf{r}) = \frac{2}{\pi} k_F(\mathbf{r}) \{ \frac{1}{2} + \frac{1-\eta^2}{4\eta} \ln |\frac{1+\eta}{1-\eta}| \}, \tag{4.2.4}$$

where, $k_F(\mathbf{r}) = (3\pi^2 \rho_0(\mathbf{r}))^{\frac{1}{3}}$ and $\eta = (k^2 + 2I + k_F^2)^{\frac{1}{2}} / k_F$. Here I is the ionization potential of the target and $\rho_0(\mathbf{r})$ is the unperturbed charge density of the molecule. Several versions of HFEGE are available by varying the value of I [21]. Thus, writing the integro–differential equation (4.2.2) in a convenient matrix form, $\mathbf{LF} = \mathbf{WF}$ where $\mathbf{WF}$ is the exchange term,

the iterative scheme is $\mathbf{LF}^i = \mathbf{WF}^{i-1}$, where $i = 0, 1, \ldots$. In order to start the solution, we chose $\mathbf{F}^0$ to be the solution obtained from the HFEGE potential (4.2.4). Our earlier scattering code (POLY, see Section 5.3) has been modified for the solution of Eq. (4.2.2). The new code (POLYEX) is now working successfully on the CRAY-2 and FSU's VAX and CRAY-YMP systems.

4.3 Polarization Interaction

It is very hard to include polarization effects accurately; however, the asymptotic form is known exactly, i.e.,

$$V_{\rm pol}(r,\theta,\phi) = \frac{-1}{2r^4}[\alpha_0(4\pi)^{\frac{1}{2}} S_0^{01} + \alpha_2(\frac{4}{5}\pi)^{\frac{1}{2}} S_2^{01} + \alpha_2^1(\frac{4}{15}\pi)^{\frac{1}{2}} S_2^{21}], \qquad (4.3.1)$$

where the S_ℓ^{mq} is a real spherical harmonic (see Ref. 1 for its definition and various properties), (r,θ,ϕ) are the coordinates of the projectile referring to the center of the target and the spherical (α_0) and nonspherical (α_2 and α_2^1) polarizabilities are expressed in terms of the polarizability tensor α_{ii} of the target, namely,

$$\alpha_0 = \frac{1}{3}(\alpha_{11} + \alpha_{22} + \alpha_{33});\ \alpha_2 = \frac{2}{3}(\alpha_{33} - \frac{1}{2}\alpha_{11} - \frac{1}{2}\alpha_{22});\ \alpha_2^1 = \alpha_{11} - \alpha_{22}.$$

In order to represent the $V^{\rm pol}$ at short distances, one has to introduce some kind of adjustable parameter(s) in the cut–off function which is multiplied to the right hand side of equation (4.3.1). The value of the unknown parameter is determined by the fitting procedure. An important development was made by our group in evaluating an approximate parameter–free polarization potential [22] based on the second–order perturbation theory [23] and the criterion of Temkin [24]. In this method, the molecule is supposed to be in an electric field $\mathbf{E} = E\hat{\mathbf{r}}$ (produced by the incoming electron) at $\mathbf{r}(r\theta\phi)$, which results in an extra potential energy V, the leading term of which is given by,

$$\begin{aligned} V(\mathbf{r}_1, \mathbf{r}_2, \ldots \mathbf{r}_Z; \mathbf{E}) &= \mathbf{E} \cdot \sum_{i=1}^{Z} \mathbf{r}_i \\ &= E \sum_{i=1}^{Z} r_i\, \hat{\mathbf{r}} \cdot \hat{\mathbf{r}}_i \end{aligned} \qquad (4.3.2)$$

The energy of the molecule in the electric field can be expanded as a Taylor series in $E_i(i = 1, 2, 3)$, the components of $\mathbf{E}$ along the axes of our coordinate system. The second order energy reads as

$$W_2 = \frac{1}{2} \sum_{ij} E_i \alpha_{ij} E_j, \tag{4.3.3}$$

In the method of Pople and Schofield [23], the first order wave function Φ_1 is expanded in terms of ground-state Φ_0 functions as

$$\Phi_1 = \Phi_0 \sum_{i=1}^{Z} f(\mathbf{r}_i) \cdot \mathbf{E}, \tag{4.3.4}$$

where unknown coefficients f's are determined variationally from the following expression of W_2, i.e.,

$$W_2 = \langle \Phi_1 | H_{mol} - W_0 | \Phi_1 \rangle + 2 \langle \Phi_0 | V | \Phi_1 \rangle. \tag{4.3.5}$$

The success of this parameter-free model for the polarization potential (to be denoted as the JT polarization approximation) along with an exact treatment of exchange has been exceptional in our recent investigation of the low-energy electron-CH_4 interactions [3]. This is demonstrated in the following Fig. 4.1, where we have shown our elastic (rotationally summed) DCS for the e-CH_4 system at 0.6 eV. There is no other ***ab initio*** result at this rather low energy and therefore, we have compared our calculations in three models: one, SEP(JT) (exact exchange plus JT potential), solid line; two, SEP(CP), (exact exchange plus the correlation-polarization (CP) [25] potential) and; third, MEP(JT) (model-exchange (HFEGE) plus JT potentials [22]). The experimental data in figure 4.1 are taken from Sohn *et al* [26]. We are dealing here with the DCS which are very sensitive to the theoretical model and this is clearly seen in Fig. 4.1. The shape of the DCS is greatly affected by the approximations for exchange and polarization interactions. Our SEP(JT) model, which is employed in the present project, is a most successful approximation. Our earlier results [22,27] using JT potential along with HFEGE approximation (plus the orthogonalization technique [21]) for exchange are not recommended now in the low-energy region. We emphasize here that it is essential to include exchange effects exactly in

any low–energy electron–molecule scattering problem. The use of another parameter–free model for the polarization potential based on the correlation energy of the target [25] is good enough only at higher energies (above 1 eV) [3]; however, at very low energies, polarization effects are best represented in a much sophisticated *ab initio* polarized–orbital type approach [22].

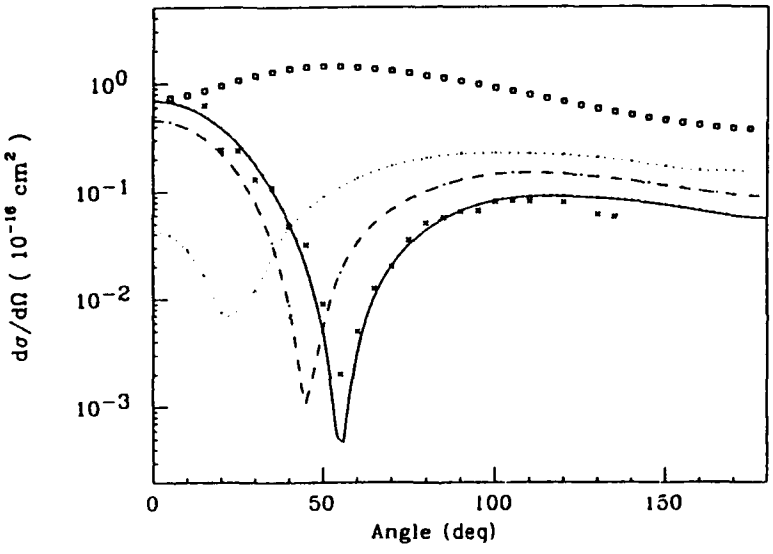

Fig. **4.1** *Elastic differential cross sections for the* **e–CH_4** *scattering at 0.6 eV: Theory: solid line, exact–exchange plus* **JT** *polarization model; dashed line, exact– exchange plus* **CP** *polarization model* **[25]**; *dotted line, model exchange* **(HFEGE)** *plus orthogonalization including* **JT** *polarization potential. The open squares represent the static–exchange (no polarization) results. Expt.:* ×, **Sohn** *et al.* **[26]**

4.4 Cross Section Formulae

We now summarise our cross section formulae. As a special case, we will provide explicit expressions in the simple case of spherical molecules such as the CH_4, SiH_4 etc.. For full details we refer to our review article [1]. In this project, we have investigated mainly the rotationally elastic, inelastic and summed channels for differential, integral, momentum transfer and energy-loss cross sections. As mentioned above, we solve our scattering problem in the fixed-nuclei approximation under the BF frame of reference. In order to obtain physical parameters, we transform the BF scattering amplitude, $f(\hat{\mathbf{k}}\cdot\hat{\mathbf{r}})$ ($\hat{\mathbf{k}}$ and $\hat{\mathbf{r}}$ are respectively the initial and final directions of the projectile) into the space-fixed amplitude $f(\hat{\mathbf{k}}\cdot\hat{\mathbf{r}}';\alpha\beta\gamma)$ (where $\hat{\mathbf{r}}'$ now refers the direction of scattered electron with respect to SF coordinate system and $(\alpha\beta\gamma)$ are the three Euler angles) by making use of rotation matrices. The SF scattering amplitude is given by,

$$f(\hat{\mathbf{k}}.\hat{\mathbf{r}}';\alpha\beta\gamma) = \sum_{\ell h m \ell' h' m' \lambda p \mu} \frac{1}{ik}\pi(2\ell+1)^{\frac{1}{2}} i^{\ell-\ell'} b^{p\mu}_{\ell h m} b^{p\mu}_{\ell' h' m'} Y^{\lambda}_{\ell'}(\hat{\mathbf{r}}') \times \mathbf{D}^{\ell'}_{\lambda m}(\alpha\beta\gamma)\mathbf{D}^{\ell}_{0m}(\alpha\beta\gamma)(\mathbf{S}^{p\mu}_{\ell h,\ell' h'} - \delta_{\ell\ell'}\delta_{hh'}), \tag{4.4.1}$$

where b's are defined earlier[1], $\mathbf{D}$'s are the rotation D-matrices and $\mathbf{S}$ is the scattering S-matrix. In the impulse approximation [28], the scattering amplitude for a particular rotational transition $JKM \rightarrow J'K'M'$ is written as,

$$f(JKM \rightarrow J'K'M') = \langle \psi_{JKM} | f(\hat{\mathbf{k}}.\hat{\mathbf{r}}';\alpha\beta\gamma) | \psi_{J'K'M'} \rangle, \tag{4.4.2}$$

where $|\psi_{JKM}\rangle$ is the rotational eigenfunctions of a molecule (asymmetric, symmetric or spherical tops) which are given in standard texts. Expressions for a general asymmetric top are discussed in Ref. 1. Here we discuss formulae for spherical tops only. The differential cross section for the $J \rightarrow J'$ transition is obtained by summing over all final magnetic substates $K'M'$ and averaging over all initial substates KM, i.e.,

$$\frac{d\sigma}{d\Omega}(J \rightarrow J') = \frac{k'}{k}\frac{1}{(2J+1)^2}\sum_{KMK'M'} |f(JKM \rightarrow J'K'M')|^2, \tag{4.4.3}$$

where k' is the wavenumber of the scattered electron given by the relation

$$2k'^2 = 2k^2 + E_J - E_{J'} \quad . \tag{4.4.4}$$

For a spherical top molecule, the energy of the Jth level is given by $E_J = BJ(J+1)$, where B is the rotational constant of the molecule in question. It is convenient to express the DCS in terms of Legendre polynomials,

$$\frac{d\sigma}{d\Omega}(J \to J') = \frac{k'}{k} \sum_{L}^{2\ell_{max}+1} A_L(J \to J') P_L(\cos\theta). \tag{4.4.5}$$

Here θ is the scattering angle between the vectors $\hat{\mathbf{k}}$ and $\hat{\mathbf{r}}'$. The expansion A_L coefficients are found to be [27],

$$A_L(J \to J') = \frac{(2J'+1)(2L+1)(-1)^L}{4k^2(2J+1)} \sum_{l l' \bar{l} \bar{l}'} [(2l+1)(2l'+1)(2\bar{l}+1)(2\bar{l}'+1)]^{\frac{1}{2}} i^{l-l'}(-i)^{\bar{l}-\bar{l}'}$$
$$\begin{pmatrix} \bar{l} & l & L \\ 0 & 0 & 0 \end{pmatrix} \begin{pmatrix} l' & \bar{l}' & L \\ 0 & 0 & 0 \end{pmatrix} \sum_{j=|J-J'|}^{J+J'} (-1)^j W(l l' \bar{l} \bar{l}'; jL) M_{l l'}^{j m_j} M_{\bar{l} \bar{l}'}^{j m_j *} \tag{4.4.6}$$

where the M–matrix is defined as

$$M_{l l'}^{j m_j} = \sum_{m m' h h' p \mu} (-1)^m \, \bar{b}_{lhm}^{p\mu} \begin{pmatrix} l & l' & j \\ m & m' & -m_j \end{pmatrix} \bar{b}_{l' h' m'}^{p\mu} \, \mathbf{T}_{lh,l'h'}^{p\mu} \quad . \tag{4.4.7}$$

Here, as usual, the $\mathbf{T}$–matrix is defined in terms of the $\mathbf{S}$–matrix as $\mathbf{T} = (\mathbf{S} - \mathbf{1})$ where $\mathbf{S} = (\mathbf{1} + \mathbf{iK})(\mathbf{1} - \mathbf{iK})^{-1}$. The scattering $\mathbf{K}$ matrix for each symmetry $(p\mu)$. In equation (4.4.7) $\begin{pmatrix} a & b & c \\ d & e & f \end{pmatrix}$ is a $3-j$ symbol, $W(abcd;ef)$ is the well known Racah coefficient and the $b_{lhm}^{p\mu}$ coefficients are the expansion terms in the definition of symmetry–adapted basis functions in terms of real spherical harmonics [1]. From equation (4.4.5), it is easy to find simple forms of the total (σ_t) and momentum transfer (σ_m) cross sections in terms of A_L coefficients, namely

$$\sigma_t^{JJ'} = 4\pi A_0(J \to J') \quad ; \quad \sigma_m^{JJ'} = 4\pi[A_0(J \to J') - \frac{1}{3} A_1(J \to J')]. \tag{4.4.8}$$

It is easy to determine A_0 and A_1 coefficients for σ_t and σ_m rather than the full expansion (4.4.6) for the DCS. For example, the A_0 and A_1 are given by the following simpler expressions,

$$A_0 = \frac{1}{4k^2} g(JJ') \sum_{\ell\ell' j m_j} (-1)^{\ell+\ell'} |M_{\ell\ell'}^{j m_j}|^2, \tag{4.4.9}$$

and

$$\begin{aligned} A_1 = \frac{3}{4k^2} g(JJ') \sum_{\ell\ell' j m_j} (-1)^{\ell+\ell'+j} [& \{(\ell+1)(\ell'+1)\}^{\frac{1}{2}} W(\ell\ell'\ell+1\ell'+1; j1) M_{\ell\ell'}^{j m_j} M_{\ell+1\ell'+1}^{j m_j^*} \\ & + \{\ell(\ell'+1)\}^{\frac{1}{2}} W(\ell\ell'\ell-1\ell'+1; j1) M_{\ell\ell'}^{j m_j} M_{\ell-1\ell'+1}^{j m_j^*} \\ & + \{(\ell+1)\ell'\}^{\frac{1}{2}} W(\ell\ell'\ell+1\ell'-1; j1) M_{\ell\ell'}^{j m_j} M_{\ell+1\ell'-1}^{j m_j^*} \\ & + (\ell\ell')^{\frac{1}{2}} W(\ell\ell'\ell-1\ell'-1; j1) M_{\ell\ell'}^{j m_j} M_{\ell-1\ell'-1}^{j m_j^*}] \end{aligned} \tag{4.4.10}$$

where $g(JJ')$ represents the statistical $(2J'+1)/(2J+1)$ factor. The vibrationally elastic (rotationally summed) cross sections are obtained by summing over J' for $J = 0$. The selection rule for the transition $J \rightarrow J'$ can easily be worked out from the asymptotic form of the static potential (4.2.3) which transforms as ${}^1A_1$ symmetry of the molecular point group. For any specified values of J and J', the angular momentum transfer j (Eq. 4.4.6) takes the following values,

$$|J - J'| \leq j \leq J + J' \quad ; \quad |l - l'| \leq j \leq l + l', \tag{4.4.11}$$

In addition, calculations on the polar polyatomic molecules (H_2O and NH_3) need further attention in order to remove the defficiencies of the ANA formalism towards convergence of the differential and total integral cross sections [see Refs. 29–30]. We employ the multipole–extracted–adiabatic–nuclei (MEAN) approximation [30]. In the MEAN methodology, a maximum use has been made of the first–Born–approximation (FBA) for the higher symmetries and partial waves. So far, such a program exists only for the linear molecules and we have modified our previous code [see Section 5.3]. Finally, in the MEAN approximation, the differential cross sections (DCS) for a rotational transition $J \rightarrow J'$ are written as [30],

$$\frac{d\sigma}{d\Omega}^{JJ'} = \frac{d\sigma^{\mathrm{FBA}}}{d\Omega}(J \rightarrow J') + \frac{k_{J'}}{4k_J} \sum_{l_t} [C(Jl_tJ';00)]^2 \frac{1}{k^2} \sum_{\lambda=0}^{\lambda_{\max}} (B_{\lambda,l_t} - B_{\lambda,l_t}^{\mathrm{FBA}}) P_\lambda(\cos\theta), \tag{4.4.12}$$

where the first term is the usual closed form for the rotational excitation ($J \rightarrow J'$) DCS in the space–fixed FBA; k_J and $k_{J'}$ are respectively the wave vectors in the initial and final channels; C(.....) is a Clebsch–Gordan coefficient; l_t is the angular momentum transfer during the collision; B_{λ,l_t} are the DCS expansion coefficients , expressed in terms of scattering matrix, and $B^{\rm FBA}_{\lambda,l_t}$ are the corresponding quantities in the FBA evaluated in the BF coordinate system.

The expression for the space–fixed FBA quantities are given in Ref. 1. The important quantity is the FBA differential and integral cross sections to be employed in equation (4.4.12). Here we give these expressions explicitly,

$$\frac{d\sigma}{d\Omega}(J \rightarrow J' = \frac{k'}{\pi k}\frac{(2J'+1)}{(2J+1)}\sum_{\ell m}(2\ell+1)^{-1}\left|\int_0^\infty dr\, r^2 v_{\ell m}(r) j_\ell(qr)\right|^2. \qquad (4.4.13)$$

and the integrated quantity is expressed as

$$\sigma_{0\rightarrow J'} = \frac{2(2J'+1)}{k^2}\sum_{\ell m}(2\ell+1)^{-1}\int_{|k-k'|}^{k+k'} dq\, q\left|\int_0^\infty dr\, r^2 v_{\ell m}(r) j_\ell(qr)\right|^2. \qquad (4.4.14)$$

where dipole and quadrupole terms correspond respectively from $J = 0$ to $J' = 1$ and 2. It is to be noted here that except at very low energy (below 0.1 eV) the short–range form of $v_{\ell m}(r)$ coefficients is very important. We have included these coefficients exactly at all radial distances, rather than employing the asymptotic form in terms of dipole, quadrupole, etc. moments.

5. REVIEW OF NUMERICAL DETAILS

In this Section, we provide a brief review of numerical and computational aspects of the present report. The basic ingredients are the molecular wavefunction and the Coulomb interaction to describe bound and bound-free quantities. A near-Hartree-Fock description of the target is sufficient for the present purpose. Next, we summarise the target bound functions, iterative procedure, and finally a list of computer programs employed.

5.1 Target Wavefunctions

For a polyatomic molecule, the multi-center target wavefunctions are easy to determine using standard Quantum Chemistry codes. In a single-center-expansion approach, however, determining actual electronic densities around the bound nuclei still rquires a large computational effort in order to represent correctly or with high precision the total charge distribution. Relativistic effects are neglected in our present work and the separation of electronic and nuclear motions is assumed under the usual Born-Oppenheimer approximation (BOA). To understand the nature of polyatomic electrons, it is necessary to consider the symmetry properties in terms of symmetry-adapted wave functions (SAWF).

For our purpose to study molecules like CH_4, SiH_4, GeH_4, H_2O, NH_3, etc., the SCE approach is very successful. We employed a computer code MOLMON (see Section 5.3) to generate bound orbitals at the fixed equilibrium geometry of the target. In general, the molecular orbitals are written in terms of LCAO (linear combination of atomic orbitals) centered at the COM of the molecule. In order to represent molecular states, we follow the nomenclature of Herzberg [31]. In brief, the capital letter A is used to represent one-dimensional IR with character $+1$, while for character -1, the letter B is used. For a two-dimensional IR, the letter E is used, while a three-dimensional IR is denoted by letter T. Suffixes $1, 2, 3..$ are used to distinguish different IR's with the same dimensions. The subcripts g or u differentiate between even (gerade) or odd (ungerade) representations of the same class if *inversion* symmetry also exists (for example in the case of SF_6 molecule). Lower case letters (a, b, e, t etc.) are used to denote individual orbitals. For example the ground state of the H_2O molecule is written as follows: $1a_1^2\, 2a_1^2\, 3a_1^2\, 1b_1^2\, 1b_2^2\ (^1A_1)$.

For the present set of molecules, we have included up to $\ell_{\max} = 7$ in the SCE expansion of bound and continuum orbitals. The molecular quantities (such as the total energy,

various multipole moments, etc.) obtained with the present SCE basis compare reasonably well with the experimental and other sophisticated calculations (see Ref. 27).

5.2 An Optimized Iterative Scheme

The non-local and short-range exchange-correlation effects in low-energy electron collisions with non-linear polyatomic molecules can be treated exactly by solving integro-differential coupled equations iteratively [2] (for a comprehensive review see Burke and Seaton, Ref. 32). Recently, this iterative exact-exchange program has been employed, under the adiabatic-nuclei approximation, to investigate in detail the elastic and rotational excitation processes in low energy e-CH_4 and SiH_4 collisions with and without polarization interaction [2-7]. In all these calculations on the non-polar polyatomic gases, we were able to include partial waves up to $\ell_{max} = 7$ ($n_c = 5$ for T_d symmetry, $n_c = 20$ for C_{2v} symmetry and so on; here n_c is the number of channels in the coupling scheme) and the corresponding number of iterations for any symmetry and impact energy was 20-25 or less. If the convergence is very slow, the iterative procedure may be undesirable to solve the *e-molecule problem*.

The convergence with respect to number of iterations depends on several factors such as the number of channels, impact energy, scattering symmetry, choice of starting solutions etc.. Finally, we are interested in converged cross sections. However, for a polar gas, the overall convergence problem is serious mainly because of long-range forces such as the dipole and quadrupole moments. In addition, the size of the close-coupling **K**-matrix increases rapidly with ℓ in the cases of C_{2v} (e.g., H_2O) and C_{3v} (e.g., NH_3) point groups. For example, for $\ell_{max} = 7$, we need to solve a 20×20 integro-differential coupled equation for the case of C_{2v} point group in its A_1 irreducible representation. Finally, for converged cross sections (differential and total) in the ANA, we need even a much larger value of ℓ_{max}. The calculation, therefore, becomes very (computer) time consuming if one has to solve that many channels for each iteration, scattering state, and impact energy. We suggest an economic and practical way to use the iterative scheme efficiently without sacrificing any numerical accuracy and present some actual calculations on the e-H_2O systen at the static-exchange level. In brief, we show that (1) it is sufficient to solve integro-differential coupled equations (to be called as static-exact-exchange, SEE) only for few lower partial waves (for example, $\ell_{max} = 4$ are adequate for the e-H_2O case), and for higher ℓ values, a model

exchange (for example, free-electron-gas-exchange (FEGE) Hara [20] type) calculation (to be called as static-model-exchange, SME) is quite close (within 1%) to the SEE **K**-matrix elements ; and (2), the SEE continuum wave function calculated at any energy is a very good guess to start solutions of the coupled equations at the next or other energies; this reduces the number of iterations (n) appreciably (see later) to make the calculations possible on a supercomputer.

At the static-exchange level [1], the Schrödinger equation for the continuum electron function $F^{p\mu}(\mathbf{r})$ for any irreducible representation $(p\mu)$ in the BF coordinate system can be written as (see also Section 4.1),

$$[-\frac{1}{2}\vec{\nabla}_r^2 + V_s(\mathbf{r}) - \frac{1}{2}k^2]F^{(p\mu)}(\mathbf{r}) = \sum_\alpha \int \phi_\alpha^*(\mathbf{r}')|\mathbf{r}-\mathbf{r}'|^{-1}F^{(p\mu)}(\mathbf{r}')d\mathbf{r}'\phi_\alpha(\mathbf{r}), \qquad (5.1)$$

where k is the incident electron wavevector and the static potential V_s is given by Eq. (4.2.3). Here Φ_0 is the target ground state wavefunction given as a single Slater determinant of one-electron N spin orbitals $\phi_i(\mathbf{r})$ and M is the number of nuclei in the molecule. The right hand side of Eq. (5.1) is the non-local exchange-correlation term arising from antisymmetrization of the e-molecule wave function. In the SME approach, this term is replaced by a local exchange potential and the corresponding scattering calculation becomes quite easy computationally (see Ref. 1). The function $f_{ij}(r)$ in the following will represent the radial part of the continuum function with channel indices i and j.

Finally, after projecting the integro-differential equation (5.1) onto the symmetry-adapted angular basis functions of $F^{(p\mu)}(\mathbf{r})$, we obtain a set of coupled integro-differential equations (4.2.2) which can be written in a convenient matrix form, $\mathbf{LF}^{(p\mu)} = \mathbf{WF}^{(p\mu)}$, where $\mathbf{WF}^{(p\mu)}$ is the exchange term. The iterative scheme is $\mathbf{LF}_i^{(p\mu)} = \mathbf{WF}_{i-1}^{(p\mu)}$, with $i = 1, 2, \ldots$.

To start the solution, we can choose $\mathbf{F}_0^{(p\mu)}$ to be the solutions obtained from the asymptotically adjusted FEGE potential [21]. For the case of non polar molecules [2-6] we employed the FEGE model to get $\mathbf{F}_0^{(p\mu)}$. However, such a scheme is computationally very expensive and unnecessary for the case of polar molecules. We suggest a different optimized iterative scheme which is very economic and convenient. In the following, we omit the superscript $(p\mu)$.

First, we show that one needs to solve the full integro-differentinal Eq. (4.2.2) only for a few low partial waves; for higher partial waves, a model exchange (SME) calculation

is adequate. In Table 5.1, we have shown the $\mathbf{K}^{A_1}$-matrix elements for e-H_2O collisions at 1 eV up to $\ell = 3, 4, 5$, and 6 in both the SEE and SME models. From this table it is clear that for $\ell \geq 4$, the SEE and SME elements are almost identical. In Table 5.1, we have shown only diagonal, dipole and quadrupole components; for other non-diagonal elements the situation is similar, i.e., the SEE and SME models give identical values for $\ell \geq 4$. The first-Born-approximation (FBA) dipole $K_{\ell,\ell\pm1}$ elements are almost equal to the close-coupling (SEE or SME) values for $\ell \geq 3$. The FBA quadrupole $K_{\ell,\ell\pm2}$ elements are within 10% of the exact results. This means that for higher values of angular momentum, the FBA is a very good approximation [29]. We have illustrated this scheme of low-, intermediate- and high-ℓ values in Fig. 5.1. From Fig. 5.1, it implies that for low partial waves (say $\ell_{\max} = L_e$), we need the full SEE scheme, for $\ell \geq L_e$ (say $\ell_{\max} = L_m$), we can employ the SME model and finally for $\ell \geq L_m$ (say $\ell_{\max} = L_B$), the Unitarised-Born-Approximation (UBA) [33] will be a good approximation. This partition is similar to the angular-frame-transformation (AFT) scheme of Collins and Norcross [29], but differs in implementation in an actual calculation. The UBA matrix is calculated up to a final $\ell_{\max} = L_B$ value and finally the MEAN (multipole-extracted-adiabatic-nuclei) approximation can be used to get the converged results on the differential and total cross sections [30].

We now demonstrate the second aspect of the present work. Suppose we want to determine the SEE $\mathbf{K}$-matrix at energy E_1. When $\mathbf{F}_0^{\rm SME}(E_1)$ is used to start the iterative scheme, it leads to the final $\tilde{\mathbf{F}}_n^{\rm SEE}(E_1)$ converged continuum function after n iterations. However, if we want to apply the same iterative scheme at another energy, say E_2, we can use either $\mathbf{F}_0^{\rm SME}(E_2)$ (requiring approximately the same number of n iterations) or $\tilde{\mathbf{F}}_n^{\rm SEE}(E_1)$ (requiring only $\bar{n}$ iterations) to obtain the final $\tilde{\mathbf{F}}_{\bar{n}}^{\rm SEE}(E_2)$ at energy E_2. We will show that $\bar{n}$ is much less than n and the final results converge to the same values, i.e., $\tilde{\mathbf{F}}_n^{\rm SME}(E_2) = \tilde{\mathbf{F}}_{\bar{n}}^{\rm SEE}(E_2)$. If $\tilde{\mathbf{F}}(E)$ is a slowly varying function with respect to the impact energy E, we can use a well converged scattering function at an energy E_1 to start the iteration at the next energy E_2. First, in Fig. 5.2, we show various scattering components $f_{00}(r)$ at 1 eV. The top solid curve (increasing rapidly with r) is the $\mathbf{F}_0^{\rm SME}$ (at 1 eV) (using the FEGE potential) case, while the lower solid curve is the corresponding converged result with 24 iterations which we denote as $\tilde{F}_{24}^{\rm SEE}$ (at 1 eV). The dash curve represents the $\tilde{\mathbf{F}}_{24}^{\rm SEE}$(at 0.5 eV) function at 0.5 eV. We see that the two SEE functions at 0.5 and 1 eV are very close to each other as compared to the SME curve at 1 eV. In our scheme, however, if we use the dash curve of Fig. 5.2 to start the iterations at 1 eV, we end

up with the same continumm function (lower solid curve in Fig. 5.2) with a much smaller number of iterations, $\bar{n}$. In Table 5.2, we have shown various scattering parameters with respect to SME and SEE (with different values of n and $\bar{n}$) models. Thus, by using the criterion,

$$\mathbf{F}_0^{\mathrm{SEE}}(E_p) = \tilde{\mathbf{F}}_n^{\mathrm{SEE}}(E_{p-1}), \tag{5.2}$$

to start iteration at a given energy E_p, we can save a significant amount of computer time without loosing any accuracy (see Table 5.2).

Also, the number of required iterations depends almost linearly on the size of the **K**–matrix. For example, a 16–channel problem requires 34 iterations as compared to only 24 in a 12–channel calculation (see Table 5.2). With the new optimized scheme (Eq. 5.2), as described above, only a much smaller number of iterations are required to obtain desired accuracy. Finally, in Fig. 5.2, we have shown the SEE continuum functions at several energies for the $f_{00}(r)$ case only. We see from Fig. 5.3 that the energy dependence of $f_{00}(r)$ is very weak in the inside region. At higher energies (for example at 6 eV, see Fig. 5.3), the electron functions start having more number of nodes.

A *similar iterative scheme* (Eq. 5.2) is useful at other symmetries (A_2, B_1 and B_2) of the e–H_2O collisions (not shown). In addition, when polarization effects are included, the above optimization scheme is essential to produce the final cross section data. We have examined the above iterative procedure for other systems such as the NH_3 and H_2S molecules [34].

In conclusion, we emphasize the fact that the iterative scheme to solve integro–differential coupled equations can be used more efficiently and economically if we choose a better zeroth–order function than the one based on the local exchange model to start the iterative scheme; one such way is suggested here, i.e., by taking the final continuum function at a previous energy as the starting zeroth–order function for the next energy (Eq. 5.2). This reduces the number of iterations by a significant factor (see Table 5.2). In addition, it is only the first few lower partial waves which are sensitive to the exact–exchange treatment; next higher–order partial waves can be treated in a local model–exchange approximation. The number of partial waves sensitive to the exact–exchange treatment may *increase with an increase in the impact energy.*

Table 5.1. e-H_2O A_1 symmetry K-matrix elements, $K_{\ell m,\ell' m'}$, at 1 eV in the static-exact- exchange (SEE) and static-model-exchange (SME) models using different values of ℓ_{max}. SEE (n) means n channels in the SEE case.

$K_{\ell m,\ell' m'}$	SEE(6) $\ell=3$	SME(6) $\ell=3$	SEE(9) $\ell=4$	SME(9) $\ell=4$	SEE(12) $\ell=5$	SME(12) $\ell=5$	SEE(16) $\ell=6$	SME(16) $\ell=6$	FBA
$K_{00,00}$	−0.38772	0.6737	−0.3834	1.2066	−0.3924	1.6278	−0.40834	2.9496	-
$K_{00,10}$	0.3918	0.3819	0.39165	0.37415	0.38849	0.36328	0.40489	0.32494	0.42084
$K_{00,20}$	−0.021228	0.000722	−0.02078	0.01252	−0.02094	0.019679	−0.022619	0.04024	−0.00404
$K_{10,10}$	−0.32667	−0.28888	−0.3264	−0.2885	−0.3282	−0.2880	−0.32019	−0.2858	-
$K_{10,20}$	0.20988	0.2094	0.20963	0.2089	0.20952	0.20884	0.20966	0.20801	0.19055
$K_{10,30}$	−0.004506	−0.004059	−0.004556	−0.004146	−0.004555	−0.00401	−0.004512	−0.003968	−0.001183
$K_{20,20}$	−0.06041	−0.05961	−0.06047	−0.05941	−0.06046	−0.05925	−0.06006	−0.05835	-
$K_{20,30}$	0.12633	0.1263	0.1275	0.12745	0.12751	0.12744	0.12755	0.12740	0.12475
$K_{20,40}$	-	-	−0.01016	−0.001014	−0.000973	−0.000971	−0.000968	−0.000967	−0.00104
$K_{30,30}$	−0.027798	−0.027786	−0.01262	−0.0126	−0.01253	−0.01251	0.012436	−0.0124	-
$K_{30,40}$	-	-	0.09338	0.09338	0.093925	0.093925	0.09394	0.09394	0.092979
$K_{30,50}$	-	-	-	-	−0.000426	−0.000426	−0.000405	−0.000405	−0.000343
$K_{40,40}$	-	-	−0.01326	−0.01326	−0.003681	−0.003681	−0.003698	−0.003698	-
$K_{40,50}$	-	-	-	-	0.074328	0.074328	0.074619	0.074619	0.074172
$K_{40,60}$	-	-	-	-	-	-	−0.000254	−0.000254	−0.000228
$K_{50,50}$	-	-	-	-	−0.008331	−0.008331	−0.001825	−0.001825	-
$K_{50,60}$	-	-	-	-	-	-	0.061784	0.061784	0.061715
$K_{60,60}$	-	-	-	-	-	-	−0.00584	−0.00584	-

TABLE 5.2.

K–matrix elements, $K^{A_1}_{\ell m,\ell' m'}$, eigenphase sums and partial total cross section for A_1 symmetry e–H_2O collisions at 1 eV. n is the number of iterations when $\mathbf{F}_0^{\mathrm{SME}}$ (at 1 eV) is used, while $\bar{n}$ is the corresponding number of iterations when $\tilde{\mathbf{F}}_n^{\mathrm{SEE}}$ (at E=0.5 eV) is employed to start the iteration at 1 eV. The number of channels is 9, i.e., $\ell_{\max} = 4$. For various notations see the text.

Model for $\mathbf{F}_0$	Iterations	CPU Units	$K_{00,00}$	$K_{00,10}$	$\delta_s^{A_1}$	$\sigma_t^{A_1}$
SME	-	2	1.20657	0.37415	0.44386	48.7096
$\mathbf{F}_0^{\mathrm{SME}}$(1 eV)	$n = 24$	100	−0.38338	0.39166	−0.71237	27.2794
$\mathbf{F}_{24}^{\mathrm{SEE}}$(0.5 eV)	$\bar{n} = 3$	10	−0.38438	0.39131	−0.71349	27.2818
$\mathbf{F}_{24}^{\mathrm{SEE}}$(0.5 eV)	$\bar{n} = 5$	20	−0.38333	0.39190	−0.71209	27.2818
$\mathbf{F}_{24}^{\mathrm{SEE}}$(0.5 eV)	$\bar{n} = 7$	25	−0.38353	0.39176	−0.71239	27.2805
$\mathbf{F}_0^{\mathrm{SME}}$(1 eV)*	$n = 34$	265	−0.40834	0.40489	−0.71585	26.76

*Using 16($\ell = 6$) channels

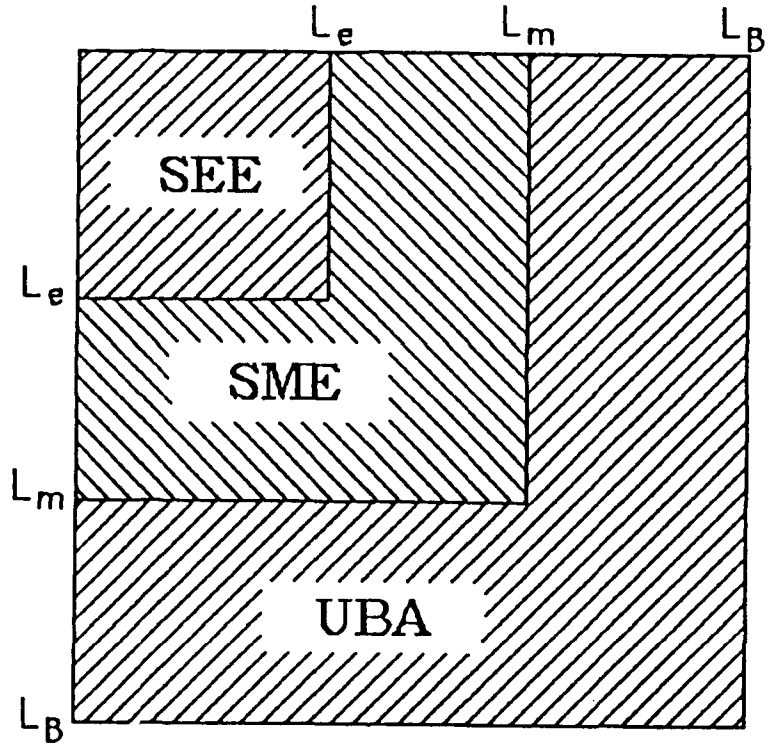

FIG. 5.1. The angular–frame–transformation (AFT) scheme in the present exact–exchange iterative procedure. The L_e, L_m and L_B are the values of ℓ_{max} in the SEE, SME and UBA models. For notations see the text.

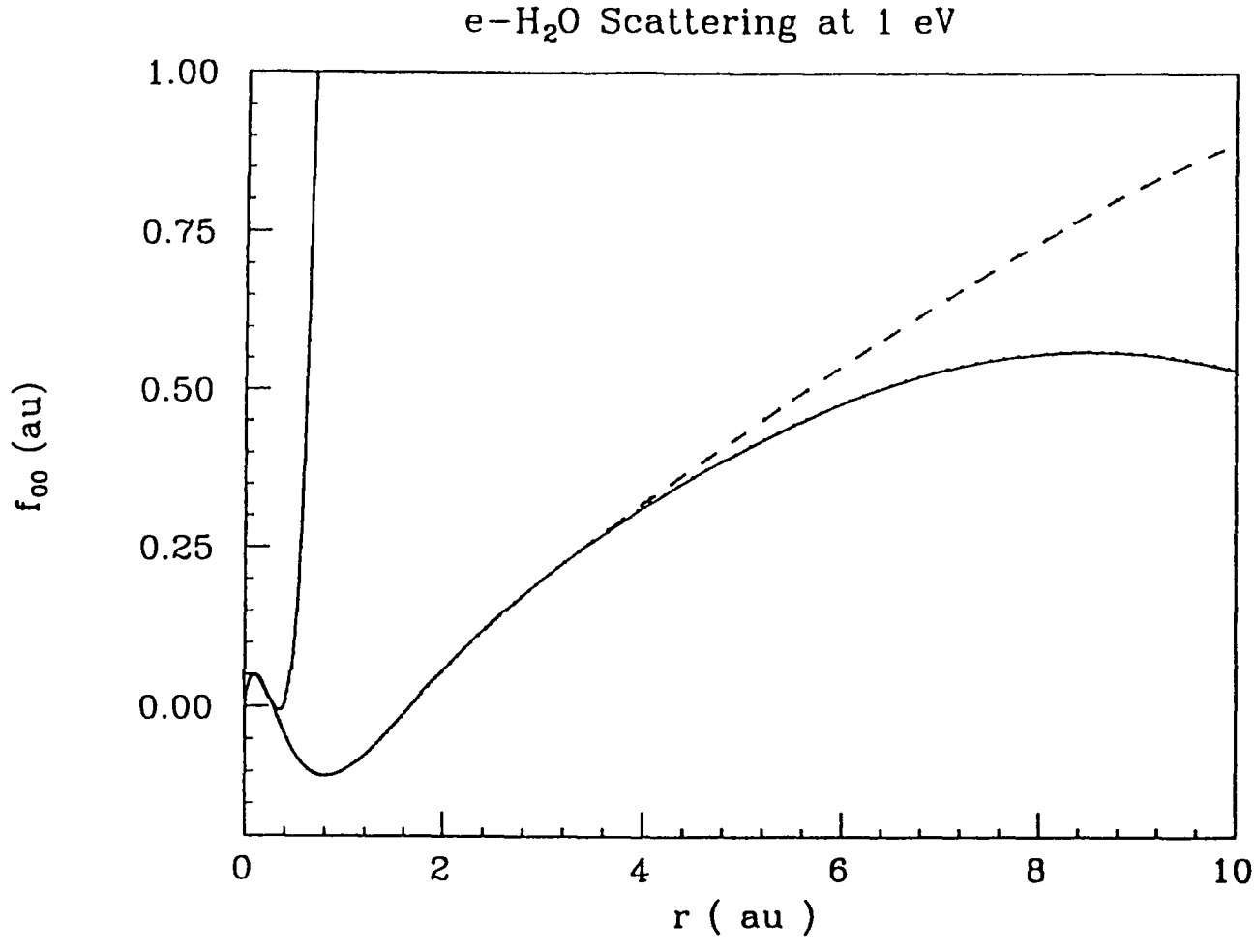

FIG. 5.2. Continuum radial function (only spherical component) of the e–H_2O A_1 symmetry collision at 1 eV. The upper solid curve is calculated in the FEGE approximation. The lower solid curve is the converged SEE function employing the upper solid curve as the starting point of the iterative calculation of Eq. 3. The dash curve represents the continuum radial function at 0.5 eV.

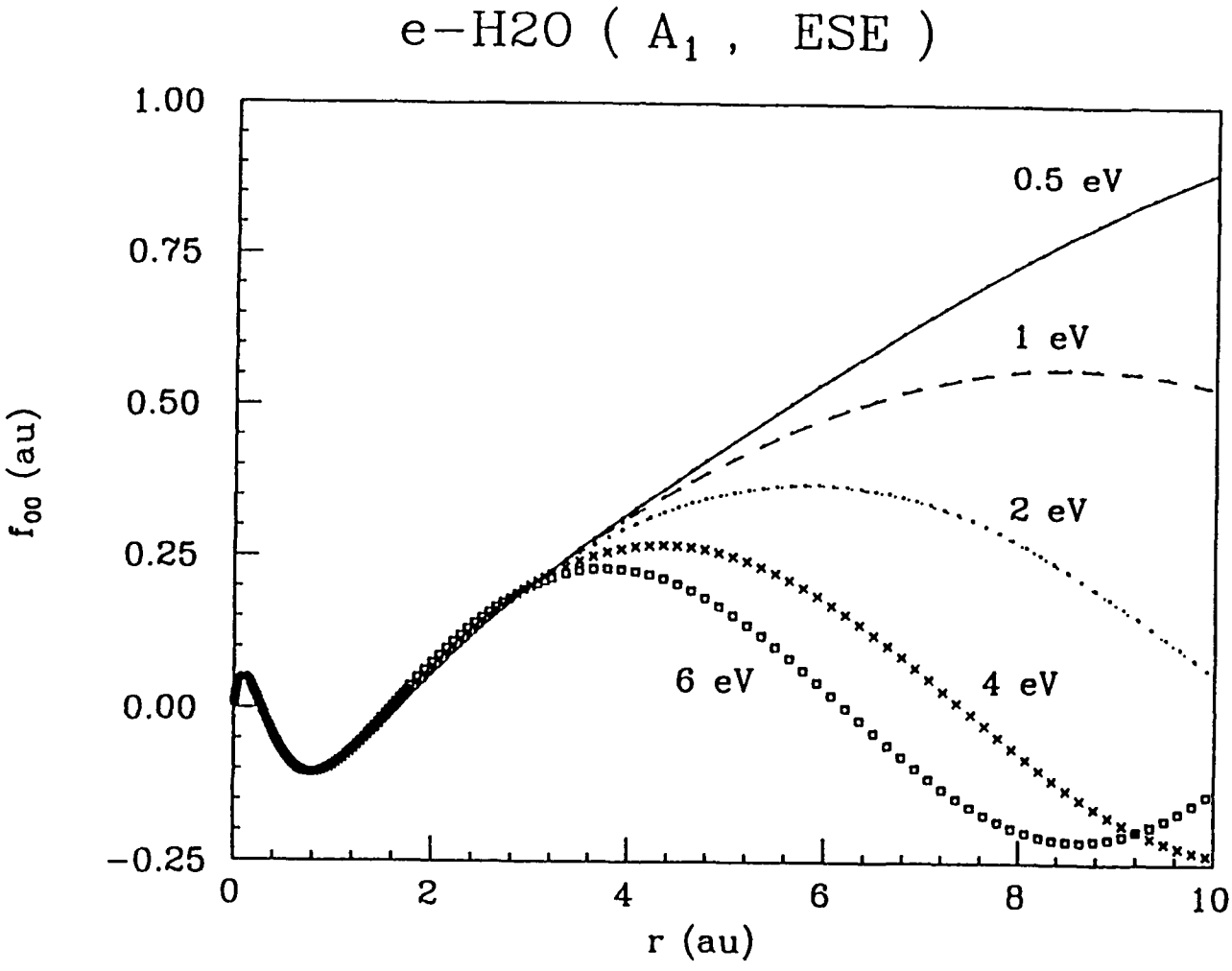

FIG. 5.3 Spherical component of the continuum radial functions for e–H_2O A_1 scattering at various energies.

5.3 Computer Codes

In order to carry out the present calculations, we used following computer codes developed by our group during more than last 15 years. All these programs are now set up on the VAX, CRAY–YMP and CRAY–2 machines at the FSU's supercomputer facilities.

1. **MOLMON** generates SCE target wavefunctions in terms of STO's. At present, this code can include $\ell_{\mathbf{max}} = 7$ in the SCE of each orbital. This code is made available to us by Professor F A Gianturco.

2. **MOPE** calculates expansion coefficient of the single center expansion of static potential and electronic density from the orbitals generated by the MOLMON program. Dr. D G Thompson wrote this code.

3. **FEGE** determines expansion coefficients of the SCE of FEGE or correlation polarization potential. This code was written by S S Salvini.

4. **ASYMP** provides rotational eigenenergies and eigenfunctions of a symmetric top molecule. The code was written by Ashok Jain, the PI.

5. **POPLE** calculates the polarization potential (see Sec. 4.3) by employing the Pople–Schoffield method. The program was written by Ashok Jain, the PI.

6. **POLY** is the main scattering code written by N Chandra, modified for polyatomic case by D G Thompson and later modified by Ashok Jain. This code calculates scattering K–matrix, eigenphase sums and partial cross sections for a particular scattering state.

7. **POLYEX** is a modified version of POLY to implement the iterative scheme. This code was developed by Paul McNaughten. Later, we modified this code to implement optimised iterative scheme and also interfacing it with the HONDO code.

8. **EROTVIB** was written by Ashok Jain. It evaluates various cross sections for asymmetric, symmetric and spherical top molecules from the K–matrix input of POLYEX code.

9. **RESON** is a small code which determines resonance parameters from the given eigenphase sums.

10. **INTERFACE** is an interfacing program between our POLYEX code and the Quantum Chemistry HONDO program. INTERFACE calculates SCE quantities from multicenter electronic density, orbital and static potential quantities. The program was written by Vi D Martino and Ashok Jain.

11. **BORN** is a general program which determines FBA quantities in the body–fixed frame of references (Born K–matrices, Unitarised Born T–matrix etc.) and cross sections (differential, integral and momentum transfer) in the space–fixed coordinate system. This program has the provision to use numerical potential (rather than the asymptotic form only). This code was written by Ashok Jain and later extended by K L Baluja.

12. **POLDEN** determines the polarised charge density of the target by employing the Pople and Shofeld method. This code was developed by Ashok Jain.

13. **VIBAVEG** calculates vibrational matrix element from the given R–dependent scattering parameter (amplitude, potential matrix, multipole moments etc.) and vibrational eigenfunctions.

14. **DERIV** is a small program which determines first or second derivative of a given R–dependent quantity (energy, multipole moments, cross sections etc.)

6. RESULTS AND DISCUSSION

6.1 Electron–CH_4 Cross Sections

The results on the e–CH_4 have been published recently [3–4]. Here we provide our most recent results on the rotationally elastic, inelastic and summed DCS integral, momentum transfer, and energy–loss cross sections in Tables 6.1–6.2. These results can be compared with recent measurements on the DCS, integral, and momentum transfer parameters. We have carried out our calculations in the Ramsauer–Townsend (RT) minimum region, in the 7–8 shape–resonance regime and also at very low energies (below 0.1 eV). No any other *ab initio* calculation has been extended to such a wide range of energy and several types of cross sections.

A large set of differential, integral and momentum transfer cross sections for any $J \rightarrow J'$ transition (with any value of initial J value to a final allowed J' value) are available in tabular form from the PI. The energy range is 0.001–20 eV. In addition, we have generated single center target basis functions for a large value of $\ell_{\max} = 20$. In the reported results (Tables 6.1 and 6.2), we have employed our earlier SCE wave function with only $\ell_{\max} = 7$. The corresponding surfaces for electronic density, static potential and individual bound orbitals are available on a radial mesh from the author of this report. The CH_4 molecule has always served a prototype molecule for testing a theoretical model for polyatomic targets. Our *ab initio* calculations with exact exchange and parameter–free correlation–polarization potential have shown that observed behavior of DCS can be described very well by theory even at very low energies.

The cross sections reported in Tables 6.1 and 6.2 are determined from our theory described in the previous sections. In brief, exchange correlation is implemented exactly and polarization effects are included approximately via a local real potential based on the method of Pople and Shofield [23] and the non–penetrating criterion of Temkin [24], in which the incoming electron is not allowed to penetrate the target charge cloud. In this non–empirical calculation, our results at very low energies (RT minimum region) compare very well with experiment. In addition, our value of -2.9 au for the scattering length for the e–CH_4 system compares well with the experimental value of -2.48 [35].

TABLE 6.1(a).

Differential cross sections for the e–CH_4 rotationally elastic ($0 \rightarrow 0$), inelastic ($0 \rightarrow 3$ and $0 \rightarrow 4$) and summed processes. All numbers are in units of 10^{-16} cm^2. A number like 1.78-6 means 1.78×10^{-6}.

	0.5 eV				1.0 eV			
Angle (deg)	$0 \rightarrow 0$	$0 \rightarrow 3$	$0 \rightarrow 4$	total	$0 \rightarrow 0$	$0 \rightarrow 3$	$0 \rightarrow 4$	total
0	0.758	0.0	1.78-6	0.758	0.534	0.0	3.56-5	0.534
5	0.734	1.23-6	1.48-6	0.734	0.507	7.43-6	3.76-5	0.507
10	0.668	4.78-6	9.28-7	0.668	0.433	2.90-5	4.38-5	0.433
20	0.456	1.71-5	2.46-6	0.456	0.217	1.05-4	7.15-5	0.217
30	0.240	3.23-5	1.11-5	0.240	4.87-2	2.04-4	1.14-4	4.91-2
40	9.50-2	4.57-5	2.13-5	0.095	4.32-3	3.03-4	1.48-4	4.79-3
50	2.40-2	5.61-5	2.31-5	0.024	4.88-2	3.96-4	1.46-4	4.93-2
60	1.69-3	6.59-5	1.78-5	1.78-3	0.119	4.86-4	1.16-4	0.119
65	9.61-5	7.21-5	1.52-5	1.91-4	0.152	5.30-4	1.02-4	0.152
70	2.38-3	8.04-5	1.36-5	2.48-3	0.181	5.72-4	9.17-5	0.181
80	1.42-2	1.05-4	1.18-5	1.43-2	0.223	6.47-2	8.89-5	0.224
90	3.03-2	1.44-4	1.27-5	3.05-2	0.242	6.93-4	1.12-4	0.243
100	4.50-2	1.96-4	2.18-5	4.52-2	0.235	6.95-4	1.60-4	0.236
110	5.49-2	2.58-4	3.35-5	5.52-2	0.206	6.50-4	2.04-4	0.206
120	6.03-2	3.23-4	3.52-5	6.07-2	0.166	5.68-4	2.10-4	0.167
130	6.29-2	3.87-4	3.22-5	6.33-2	0.127	4.67-4	1.97-4	0.127
140	6.34-2	4.44-4	3.49-5	6.39-2	9.31-2	3.77-4	2.14-4	9.37-2
150	6.13-2	4.91-4	4.42-5	6.18-2	6.51-2	3.03-4	2.84-4	6.57-2
160	5.68-2	5.25-4	7.26-5	5.74-2	4.39-2	2.54-4	4.26-4	4.46-2
170	5.22-2	5.46-4	1.24-4	5.29-2	3.10-2	2.28-4	6.11-4	3.18-2
180	5.03-2	5.53-4	1.52-4	5.10-2	2.68-2	2.20-4	7.03-4	2.77-2

TABLE 6.1(b).

Differential cross sections for the e–CH_4 rotationally elastic ($0 \rightarrow 0$), inelastic ($0 \rightarrow 3$ and $0 \rightarrow 4$) and summed processes. All numbers are in units of 10^{-16} cm^2. A number like 1.78-6 means 1.78×10^{-6}.

	3.0 eV				5.0 eV			
Angle (deg)	$0 \rightarrow 0$	$0 \rightarrow 3$	$0 \rightarrow 4$	total	$0 \rightarrow 0$	$0 \rightarrow 3$	$0 \rightarrow 4$	total
0	1.31	0.0	1.09-2	1.32	5.53	0.0	8.63-2	5.61
5	1.24	6.08-5	1.09-2	1.25	5.33	1.86-4	8.62-2	5.42
10	1.05	2.40-4	1.10-2	1.06	4.78	7.31-4	8.58-2	4.87
15	0.792	5.28-4	1.11-2	0.804	4.00	1.60-3	8.52-2	4.09
20	0.539	9.18-4	1.11-2	0.551	3.14	2.78-3	8.42-2	3.23
30	0.258	2.01-3	1.11-2	0.271	1.74	6.07-3	8.13-2	1.82
40	0.387	3.59-3	1.07-2	0.401	1.17	1.09-2	7.67-2	1.26
50	0.749	5.67-3	9.83-3	0.765	1.30	1.72-2	7.07-2	1.39
60	1.09	7.94-3	8.66-3	1.11	1.67	2.42-2	6.44-2	1.76
70	1.28	9.82-3	7.68-3	1.29	1.95	3.00-2	5.89-2	2.03
80	1.27	1.08-2	7.21-3	1.22	1.94	3.33-2	5.55-2	2.03
90	1.09	1.06-2	7.31-3	1.11	1.59	3.34-2	5.44-2	1.68
100	0.775	9.76-3	7.79-3	0.792	0.985	3.14-2	5.51-2	1.07
110	0.430	8.81-3	8.27-3	0.447	0.379	2.95-2	5.68-2	0.465
120	0.176	8.54-3	8.50-3	0.193	7.74-2	3.06-2	5.87-2	0.167
130	8.99-2	9.58-3	8.61-3	0.108	0.282	3.82-2	6.08-2	0.382
140	0.181	1.21-2	9.04-3	0.203	1.01	5.38-2	6.38-2	1.13
150	0.412	1.59-2	1.01-2	0.438	2.13	7.59-2	6.80-2	2.28
160	0.707	1.99-2	1.17-2	0.880	3.36	9.94-2	7.31-2	3.54
170	0.959	2.31-2	1.34-2	0.996	4.34	0.117	7.75-2	4.53
180	1.06	2.43-2	1.42-2	1.10	4.71	0.124	7.93-2	4.92

TABLE 6.1(c).

Differential cross sections for the e–CH_4 rotationally elastic ($0 \rightarrow 0$), inelastic ($0 \rightarrow 3$ and $0 \rightarrow 4$) and summed processes. All numbers are in units of 10^{-16} cm^2. A number like 1.78-6 means 1.78×10^{-6}.

	7.5 eV				10.0 eV			
Angle(deg)	$0 \rightarrow 0$	$0 \rightarrow 3$	$0 \rightarrow 4$	total	$0 \rightarrow 0$	$0 \rightarrow 3$	$0 \rightarrow 4$	total
0	11.86	0.0	0.191	12.05	14.30	0.0	0.174	14.48
5	11.53	7.84-4	0.191	11.72	13.93	1.62-3	0.174	14.10
10	10.61	3.06-3	0.190	10.80	12.87	6.32-3	0.173	13.05
15	9.26	6.62-3	0.188	9.45	11.33	1.37-2	0.172	11.51
20	7.70	1.12-2	0.185	7.89	9.53	2.31-2	0.170	9.73
30	4.77	2.22-2	0.178	4.97	6.09	4.51-2	0.166	6.30
40	2.84	3.44-2	0.170	3.05	3.63	6.73-2	0.161	3.86
50	1.94	4.64-2	0.160	2.14	2.19	8.51-2	0.156	2.43
60	1.66	5.63-2	0.151	1.87	1.45	9.52-2	0.153	1.70
70	1.63	6.22-2	0.143	1.83	1.12	9.55-2	0.149	1.37
80	1.55	6.23-2	0.137	1.75	0.955	8.62-2	0.146	1.19
90	1.22	5.65-2	0.133	1.41	0.728	6.92-2	0.142	0.939
100	0.672	4.68-2	0.132	0.85	0.391	4.87-2	0.138	0.579
110	0.152	3.78-2	0.134	0.325	0.103	3.17-2	0.135	0.272
120	2.01-2	3.68-2	0.137	0.195	0.107	2.68-2	0.135	0.271
130	0.525	5.11-2	0.142	0.719	0.576	4.15-2	0.137	0.757
140	1.70	8.37-2	0.148	1.94	1.54	7.83-2	0.141	1.76
150	3.37	0.131	0.153	3.65	2.85	0.132	0.144	3.13
160	5.14	0.181	0.158	5.48	4.24	0.188	0.144	5.20
170	6.51	0.219	0.160	6.89	5.32	0.231	0.142	5.69
180	7.03	0.233	0.161	7.43	5.72	0.248	0.141	6.12

TABLE 6.2.

Rotational excitation cross sections for the e–CH_4 system (10^{-16} cm^2) in the ESEP model. A number like 6.57-5 means 6.57×10^{-5}.

	σ_t				σ_m			
Energy(eV)	$0 \rightarrow 0$	$0 \rightarrow 3$	$0 \rightarrow 4$	total	$0 \rightarrow 0$	$0 \rightarrow 3$	$0 \rightarrow 4$	total
0.1	4.46	6.57-5	3.26-5	4.46	2.68	1.04-3	3.95-5	2.68
0.2	1.95	3.91-4	7.22-5	1.95	6.37-1	6.12-4	8.87-5	6.38-1
0.3	1.143	9.79-3	1.20-4	1.144	2.76-1	1.50-3	1.52-4	2.78-1
0.4	0.91	1.73-3	1.97-4	0.91	3.76-1	2.57-3	2.54-4	3.79-1
0.5	0.91	2.52-3	3.20-4	0.91	6.11-1	3.63-3	4.15-4	6.15-1
0.6	1.02	3.30-3	4.91-4	1.025	8.81-1	4.53-3	6.37-4	8.86-1
0.8	1.41	4.70-3	1.07-3	1.42	1.41	5.71-3	1.36-3	1.417
1.0	1.90	6.14-3	2.09-3	1.91	1.89	6.44-3	2.57-3	1.90
2.0	4.94	3.26-2	2.28-2	4.99	4.24	3.37-2	2.42-2	4.30
3.0	8.73	0.115	0.112	8.96	7.55	0.139	0.111	7.80
4.0	13.35	0.252	0.355	13.96	11.92	0.322	0.344	12.58
5.0	18.29	0.420	0.799	19.51	16.34	0.548	0.772	17.66
6.0	22.36	0.578	1.329	24.27	19.31	0.747	1.283	21.35
7.5	25.28	0.738	1.856	27.88	20.02	0.901	1.795	22.73
10.0	24.81	0.903	1.840	27.58	16.75	0.968	1.778	19.53
15.0	20.83	1.189	1.20	23.28	10.81	1.086	1.114	13.10
20.0	17.60	1.297	0.850	19.85	7.57	1.119	0.729	9.56

6.2 Electron–SiH_4 Cross Sections

Here we discuss the low energy electron collisional cross sections from silane molecules in the exact–static–exchange plus polarization (ESEP) model. For comparison purpose, we will also include static–model–exchange plus polarization (SMEP) results; this comparison will give us an idea of the importance of exchange effects in this low energy region. The results without polarization (ESE) will also be included in the following discussion.

6.2.1. Elastic (Rotationally Summed) Cross Sections

The electron–silane cross sections are very important from the point of view of plasma physics [36].There are several experimental [36–45] and theoretical studies [46-51] on the low energy electron interactions with SiH_4. Similar to CH_4 case, the e–SiH_4 low energy cross sections are characterised by RT minimum below 1 eV and a shape resonance feature around 2–4 eV. Very recently, low energy DCS have been measured by Tanaka *et al.* [45].

We first discuss the qualitative features of low energy e–SiH_4 cross sections such as the RT minimum below 1 eV and a 3–4 eV shape resonance phenomenon. Figs. 6.2.1 and 6.2.2 illustrate the eigenphase sums for various scattering symmetries in the 0.1–20 eV region. It is clear from Fig. 6.2.1 that the present ESEP (solid curve) is responsible for (nearly) the correct position of the minimum (around 0.25 eV in a recent swarm study of Kurachi and Nakamura, Ref. 43) because of the A_1 scattering symmetry. Note that our earlier SMEP (static, FEGE and the JT polarisation potentials) results (Jain and Thompson, Ref. 46) or the present ESE (without polarization) curves are incorrect in this low energy region. The value of the position of this minimum as obtained by Yuan [50] in the spherical approximation is quite low (around 0.11 eV). Other calculations, where exchange is treated via a model local potential (Gianturco *et al* [48]; Jain *et al.* [47]), do not give reliable results in this rather low energy region. In Fig. 6.2.2, we have shown the eigenphase sums for the T_2 and E symmetries above 1 eV. Also shown in this figure is the SMEP curve for the T_2 state. The ESEP curve clearly exihibits a shape resonance phenomenon around 3.75 eV; this structure is due to the d–wave of the incoming electron's partial waves. Therefore, the E symmetry (which also have a d-wave component) also exihibits a weak shape resonance feature at about 4 eV. As we will see later, the ESEP curve is more realistic compared to our previous model exchange (FEGE) calculation (the dash curve of Fig. 6.2.2 is due to Jain and Thompson [46]).

The corresponding behaviour of the ESEP partial cross sections in various scattering states is illustrated in Fig. 6.2.3 for all the dominating states (A_1, E and T_2) below (curve 6.2.3(a)) and above (curve 6.2.3(b)) 1 eV impact energy. Here we see a visual effect of the minimum and the maximum in the cross sections for various scattering states. In these figures (6.2.3(a) and 6.2.3(b)), we have also included the SMEP results of Jain and Thompson [46] for the A_1 and T_2 states for comparison purpose.

We now discuss our rotationally summed (vibrationally and electronically elastic) differential cross sections in the energy range from 1.8 to 20 eV, where recent absolute measured values are available (Tanaka *et al* [45]). These results are depicted in Figs. 6.2.4(a) through 6.2.4(j) along with the experimental data of Tanaka *et al.* For comparison purpose, we also show our ESE results (dash curves in Figs. 6.2.4(a)-6.2.4(j)) where polarization effects are switched off. This comparison (between solid and dash curves) gives us an idea about the importance of polarization effects in this energy range for various angular regions. We can clearly see that the polarization interaction changes the shape (and magnitude too) of the DCS at all energies considered here. It is quite clear from these Figs. (6.2.4(a)-6.2.4(j)) that the ESEP curves agree much better with the experimental data as compared to the ESE model. We also notice that the polarization effects are more important in the resonance region (see the DCS at 3, 4, and 5 eV in Figs. 6.2.4(d), 6.2.4(e), and 6.2.4(f) respectively), where the structure in the DCS reflects the d-wave dominance. This is expected since polarization interaction influences the shape-resonance region considerably. In general, the agreement with experimental data is reasonable. The dip at about 55^0 observed at 1.8 and 2.15 eV by Tanaka *et al.* is shifted in our results towards lower angle by about 10^0 difference. The second dip occuring in our DCS around 130^0 at 1.8 and 2.15 eV, seems to be shifted in the same fashion as the lower angle dip with respect to experimental data (however, the measured values are not available above 130^0 angle).

At somewhat higher energies ($E \geq 3$ eV), the two dips in the DCS are still visible, while such a structure in the measured angular functions is quite weak. It may be interesting to compare our DCS with another set of absolute experimental data (not available right now). The present predicted DCS values may be quite useful for normalizing purpose in future measurements. No other theoretical calculations are available on the DCS for the e-SiH_4 collisions in this energy range. We have provide our ESEP DCS values in tabular form in Tables 6.2.1 and 6.2.2.

The integral cross sections (total, σ_t; momentum transfer, σ_m; viscosity, σ_v and energy-loss, σ_l) are shown in Figs. 6.2.5–.7 in the whole energy region considered here. First we discuss our low energy (below 1 eV) integral and momentum transfer cross sections shown in Figs. 6.2.5(a) and 6 (see the inset) respectively. Our value of the cross section near the RT minimum is about 2.8×10^{-16} cm^2 for the σ_t and 0.4×10^{-16} cm^2 for the σ_m. The swarm data of Kurachi and Nakamura [43] gives a minimum value of about 1.1×10^{-16} cm^2 in their σ_m curve, while Hayashi [44] estimates this minimum value to be 0.5×10^{-16} cm^2 . Finally, we can conclude from Figs. 6.2.5(a) and 6 that the agreement between present theory (ESEP model) and experimental results is rather encouraging keeping in mind that this low energy region is quite difficult to study both in theory and experiment.

Next we show our σ_t and σ_m values in the 1–20 eV region in Figs. 6.2.5(b) and 6 respectively. The experimental data are taken from Mori *et al.* [40] and Wan *et al.* [37]. There is significant discrepancy between the two sets of measured values. Our present ESEP curve seems to be in fair agreement with recent measurements of Wan et al. The position of the shape resonance in ESEP theory (around 3.75 eV) and experiment (around 3.1 eV) differs about 20%, while the magnitude of the cross sections in this energy region also has significant discrepancy; for example, the theoretical (ESEP) peak value of the σ_t is about 20% higher than the measured value of Wan *et al.*. A good agreement above 5 eV between the ESE curve and experimental points (crosses) is definitely fortuitous. Note that the inclusion of polarization effects shifts the shape resonance position from about 6.5 eV to about 3.75 eV and increases its magnitude by about 45%. Thus, the importance of polarization interaction in this energy region can not be overlooked.

In Fig. 6.2.6, we have plotted our σ_m cross sections at all energies considered here. The swarm points are taken from Kurachi and Nakamura [43] and Ohmori *et al.* [42]. We see significant discrepancy bewteen theory and experiment; however, there seems to be agreement in the general trend of the cross sections as a function of impact energy. In the resonance energy region, our calculations are much higher than the swarm data. The accuracy of the swarm analysis above 1 eV may be questionable. We also realize that a better polarization potential may be required in the present energy region. The momentum transfer cross sections are dominated by large angle scattering, therefore, there may be other reasons too for the observed discrepancy between present theory and swarm results. Finally, Fig. 6.2.7 illustrates the σ_v values along with energy-loss cross sections. The dominance of the 3–4 eV feature is seen in these curves too (Fig. 6.2.7).

6.2.2 Rotationally Elastic and Inelastic Cross Sections

At very low energies, the energy loss of the incoming projectile because of rotational channel, is a very important mechanism in e-molecule collisions. It is now possible to measure indirectly the rotational excitation cross sections for the electron-molecule system (Müller *et al.* [52]). With this possibility in mind, we discuss our rotationally elastic and inelastic cross sections. First, we present our rotationally elastic and inelastic differential cross sections in Figs. 6.2.8 (a), (b), (c), (d), (e), and (f) at 0.5, 3, 5, 10, 15, and 20 eV respectively. As expected, the elastic $0 \rightarrow 0$ channel dominates all other inelastic processes at all angles except at those angles where a deep minimum occurs in the $0 \rightarrow 0$ DCS. Also shown in these figures are the energy–loss DCS (crosses) summed over all final rotational states. From qualitative point of view, the general shape of rotationally inelastic DCS for the e-SiH_4 system is quite similar to the corresponding CH_4 curves (see McNaughten *et al.* [3]). The $0 \rightarrow 4$ transition depends weakly on the scattering angle, while the $0 \rightarrow 3$ one has considerable angular dependence. The $0 \rightarrow 6$ cross sections are generally smaller; however, as the energy is increased, they become larger than the other transitions at certain scattering angles. The total energy–loss DCS are almost flat with respect to angular variation. It is also clear from these figures that a spherical approximation may not be an appropriate model for the total DCS in this energy range. We do not have any other data with which to compare these results of Figs. 6.2.8 (a)–6.2.8 (f).

We will see an effect of polarization potential on the rotational excitation process. Symmetry of the polarization term (there exists only the spherical, $\ell = 0$, term) for the T_d point group, the first Born approximation (FBA) will give zero cross section from the polarization potential term only. In the present calculation, we, however, see a substantial difference in the DCS with and without polarisation effects. In Figs. 6.2.9 and .10, we have shown a comparison of ESE and ESEP DCS for all three transitions ($0 \rightarrow 3$, $0 \rightarrow 4$ and $0 \rightarrow 6$) at 5 eV and 10 eV respectively. In general, the ESEP cross sections are higher than the corresponding ESE values and, in addition, exihibit more features. These figures (6.2.9 and .10) demonstrate that a polarised target is more efficient to excite its rotational modes through the angular momentum transfer from the projectile. We will see later the same comparison for integral cross sections at all energies considered here.

We now discuss the integral values of various rotational excitation cross sections. In Figs. 6.2.11–.14, we have shown our integral (solid lines) and momentum transfer (dash

lines) values for all the four cases, i.e., $\sigma^{00}_{t,m}$, $\sigma^{03}_{t,m}$, $\sigma^{04}_{t,m}$ and $\sigma^{06}_{t,m}$. As expected, the pure elastic process has all the main features (RT minimum and the 3–4 eV shape–resonance) of the total scattering process. The rotational channels are small, but exihibit interesting features in the energy distribution of their cross sections. For example, the $0 \rightarrow 3$ curves in Fig. 6.2.12, have enhancement in the cross sections around 8 eV, while the 3–4 eV region shows a weak structure (remember there is a 3–4 eV shape resonance here in the elastic and total cross sections). The $0 \rightarrow 4$ cross sections are, however, enhanced in the 3–4 eV region. it is interesting to notice that this structure is produced mainly because of polarisation effect (see the crosses in Fig. 6.2.13, which represent the ESE σ^{04}_{t} values). Finally, the $0 \rightarrow 6$ cross sections (Fig. 6.2.14) are also characterised by an enhancement around 10 eV. Here also, we see a significant change in the inelastic cross sections when polarisation effects are included (see the crosses in Fig. 6.2.14). In the inset of Fig. 6.2.14, we have shown low–energy (below 1 eV) $\sigma^{06}_{t,m}$ results with and without polarisation effects. Some strange features in the ESEP curves around 1 eV are seen without any explanation at this time.

Finally, we want to show our integrated energy–loss cross sections in all the three ($\Delta J = 3, 4, 6$) transitions with and without polarisation effects. Fig. 6.2.15 depicts the ESEP σ^{03}_{l} (solid line), σ^{04}_{l} (dash line) and σ^{06}_{l} (dotted line) values, while Fig. 6.2.16 shows the same cross sections in the ESE model. We see clearly that the inclusion of polarisation effect changes the behaviour of the energy–loss cross sections with respect to the projectile energy. At higher energies ($E \geq 15$ eV), the $0 \rightarrow 6$ transition dominates over other lower order rotational excitations. The $0 \rightarrow 4$ cross sections are always higher than the $0 \rightarrow 3$ ones except at lower energies (below 2 eV), where the $0 \rightarrow 3$ transition dominates over all higher excitations. The total energy–loss or the stopping cross sections, shown earlier in Fig. 6.2.7, are independent of initial J value of rotational state of the target. This agrees with a general theorem (per Shimamura [9–15]) that the stopping cross sections, when summed over all final rotational states, are independent of the initial rotational state of the molecule in a situation where the adiabatic–nuclei–rotation approximation is valid. We have checked the σ_l values with several initial J values and found that the above theorem is correct [16]. A detailed picture of the gas temperature dependence on the collisional parameters is presented in Section 7. Our cross sections for rotationally elastic and inelastic channels may be useful in extracting experimental DCS from their energy–broadened peaks Because of rotational excitation.

6.2.3 Cross Sections below 0.1 eV

We have extended our calculations at further lower energies towards the zero-energy limit. For example, at 0.001, 0.0025, 0.005, 0.01, 0.025, and 0.05 eV energies the values of the $\sigma_t(\sigma_m)$ are (in units of 10^{-16} cm^2) 47.82 (46.45), 42.53 (40.4), 37.42 (34.64), 30.88 (27.63), 20.68 (16.63), and 12.83 (8.58) respectively. At 0.01 eV, the σ_m values given by various swarm studies are 56.0 (Hayashi [44]), 66.0 (Ohmori *et al.* [42]), and 32.0 (Kurachi and Nakamura [43]). It is rather frustating to see such a large discrepancy between these swarm values for the σ_m value at this low energy. We plan to use our ESEP σ_m values in the swarm analysis. The value of scattering length is estimated to be -4.2 au in our present ESEP calculation.

6.2.4 Polarization Approximations in e–SiH_4 Collisions

It is now a well established fact that in low energy regime, the use of model potentials for both the exchange and polarization forces is rather misleading because to make theory and experiment closer, these interactions do compensate for each other. In the situation where exchange is included exactly, In this sub section, we made a relative comparison with our SEP(JT) results (previous 6.2 Sections) with another model SEP(CP) calculation. Here the SEP (JT) model means the use of Jain and Thompson [22] potential along with our iterative ESE approach, while the SEP (CP) employs correlation-polarization [25] model.

A comparison of the present nonadjustable and energy-independent JT and CP potentials is given in Fig. 6.2.17. we see that the SEP(JT) model is stronger than the SEP(CP) one in the 0.5–4 au radial region. In addition, near the origin, the JT potential has the correct form. It was observed by Jain and Thompson [22] that when the JT approximation is employed along with the OFEGE model (free-electron-gas exchange along with orthogonalization procedure [21]), the position of the RT minimum occurs at much lower energy (at 0.08 eV compared to the experimental value around 0.25 eV); this indicates that the JT is a weak potential when employed along with the OFEGE model [22].

Fig. 6.2.18 displays our σ_t values in both the SEP(JT) (solid line) and SEP(CP) (lower dash curve) models along with the experimental data of Wan *et al.* [36] (crosses). This figure also shows our SEE results (multiplied by a factor of three) without polarization

(upper dash curve). No other close–coupling calculation where exchange is treated exactly are available below 1 eV. Polarization effects are more crucial below 1 eV than above this energy. We see from Fig. 6.2.18 that the ESE cross sections without polarization effects are too large. Fig. 6.2.18 clearly shows that the SEP(JT) curve, predicting a RT structure around 0.25 eV, is more favourable. Although the measured values of Wan *et al.* do not seem to show any RT minimum; however, its existence is clearly visible in their σ_t curve around the same energy of 0.25 eV (see Fig. 5 of Ref. 37). The existence of the RT minimum is also confirmed in several swarm type studies by several investigators [42-44].

Fig. 6.2.19 illustrates our σ_m results in both the SEP(JT) and SEP(CP) models along with swarm data [42-43]. The experimental σ_m cross sections (Fig. 6.2.19) exihibit the RT minimum around 0.25 eV, while our SEP(JT) (solid line) predicts this minimum around 0.2 eV. The SEP(CP) σ_m results (dashed curve in Fig. 6.2.19) do not show any RT effect. In the σ_t curves of Fig. 6.2.18, the corresponding positions of the RT minimum in SEP(JT) and SEP(CP) models occur respectively at 0.16 and 0.25 eV. In general, σ_m minimum occurs at lower energy than the corresponding minimum in the σ_t cross sections. Even the magnitude of σ_m results in the SEP(JT) model agrees very well with the swarm results (Fig. 6.2.19). On the other hand, the SEP(CP) σ_m are not in agreement even qualitatively with the measured values.

In Fig.6.2.20, we have shown our σ_t values at 1–15 eV in both the models alongwith measured data. Again we see that the SEP(JT) model is superior over the SEP(CP) one. In particular, the position of the shape–resonance in the SEP(JT) case is in better agreement with the experiment as compared to the SEP(CP) model. The discrepancy between experimental data and present SEP(JT) calculations suggests that a realistic polarization potential may be even stronger than the present JT approximation. A full polarised–orbital type calculation is required in order to test this hypothesis.

The DCS present a more stringent test of any theoretical model when compared with experiment. The two models, i.e., SEP(JT) and SEP(CP), differs significantly when compared at the DCS level. Fig. 6.2.21 displays the angular functions at 0.2, 0.5, 1 and 3 eV in both the models along with experimental data (only at 3 eV). There are no experimental data at and below 1 eV. The DCS at 0.2 and 0.5 eV in Fig. 6.2.21 present distinct features in the DCS. At 0.2 eV, the SEP(JT) model dip occurs at 100^0 as compared to 75^0 in the SEP(CP) case. This difference of 25^0 in the positions of minima in the DCS at 0.2 eV reflects the sensitivity of low energy scattering with respect to polarization effects. At 0.5

eV (Fig. 6.2.21), the difference in the positions of the minima in both the models is about 10^0. Note that in case of e–CH_4 scattering [5] a similar distinction is observed at 0.5 eV between the SEP(JT) and SEP(CP) models. The experimental DCS at 0.5 eV for e–CH_4 scattering agrees with the SEP(JT) model. We, therefore, expect that our SEP(JT) curve (in Fig. 6.2.21 at 0.2 and 0.5) is more realistic and reliable than the corresponding data in the SEP(CP) model. At 1 eV (Fig. 6.2.21), there is still some difference between the two models, however, the qualitative features are quite similar. We emphasize here that the significant discrepancy between the two polarization potentials is to be found below 1 eV.

Let us examine our higher energy DCS where experimental data are available for comparison. At 3 eV (Fig. 6.2.21), both the theoretical models predict similar dip structure, while we see significant difference in the forward and backward directions. We can see from 3eV DCS that the SEP(JT) potential is stronger than the SEP(CP) one. Both the models have considerable discrepancy with the experimental DCS [45]. One reason of this discrepancy may the inadequacy of present polarization models. On the other hand, the accuracy of measured data is not clear since no other experimental studies are available at this time.

Finally, our SEP(JT) model appears to be better than the SEP(CP) one, in particular in the RT minimum region. This conclusion is consistent with our similar investigation on the e–CH_4 system[5]. However, this conclusion will further be supported if differential measurements are available for the e–SiH_4 case. There is plenty of room to improve upon the JT potential by actually carrying out a full polarised-orbital calculation for the e–SiH_4 system. Our present JT potential is obtained by employing a less accurate Pople and Schofield method [23] in which all the orbitals are distorted equally. Nevertheless, by employing a better JT type polarization potential the basic conclusions of this paper will remain valid. It would be quite interesting if more experiments are performed on the DCS quantities, particularly below 3 eV.

TABLE 6.2.1.

Elastic (rotationally summed) cross sections (DCS, σ_t, σ_m and σ_v) for the e–SiH_4 system (10^{-16} cm^2) in the ESEP model.

	Energy(eV)							
θ (deg)	0.1	0.2	0.4	0.6	0.8	1.0	1.8	2.15
0	2.67	2.337	2.083	2.009	2.105	2.224	6.121	9.891
5	2.643	2.293	2.025	1.940	2.023	2.133	5.882	9.540
10	2.538	2.167	1.862	1.747	1.793	1.878	5.212	8.551
15	2.382	1.974	1.616	1.460	1.458	1.508	4.236	7.098
20	2.186	1.735	1.323	1.127	1.075	1.088	3.128	5.425
30	1.739	1.215	0.732	0.499	0.394	0.365	1.215	2.409
40	1.314	0.761	0.299	0.117	0.0542	0.0544	0.409	0.895
50	0.972	0.439	0.076	0.0077	0.0566	0.149	0.714	1.012
60	0.720	0.238	0.0049	0.0618	0.232	0.437	1.539	2.005
70	0.536	0.119	0.0124	0.170	0.428	0.722	2.290	3.017
80	0.395	0.0496	0.0544	0.279	0.577	0.916	2.650	3.522
90	0.283	0.0128	0.113	0.372	0.668	0.997	2.544	3.339
100	0.196	0.0005	0.176	0.439	0.694	0.963	2.032	2.547
110	0.132	0.0056	0.231	0.465	0.647	0.818	1.286	1.453
120	0.090	0.0189	0.263	0.443	0.537	0.599	0.594	0.557
130	0.0628	0.0332	0.271	0.385	0.398	0.371	0.264	0.371
140	0.0453	0.0458	0.266	318	0.270	0.198	0.462	1.132
150	0.0333	0.0572	0.258	0.263	0.180	0.103	1.096	2.639
160	0.0251	0.0677	0.255	0.228	0.129	0.071	1.880	4.352
170	0.0202	0.0759	0.257	0.211	0.105	0.067	2.497	5.667
180	0.0185	0.0791	0.258	0.206	0.0978	0.069	2.727	6.155
σ_t	6.564	3.246	3.143	4.289	5.717	7.407	19.75	29.25
σ_m	2.823	0.921	2.521	4.169	5.478	6.867	17.56	26.74
σ_v	3.374	1.097	1.330	2.592	4.051	5.657	13.78	18.39

Table 6.2.2

Elastic (rotationally summed) cross sections (DCS, σ_t, σ_m and σ_v) for the e–SiH_4 system (10^{-16} cm^2) in the ESEP model.

	Energy(eV)							
θ (deg)	2.65	3.0	4.0	5.0	7.5	10.0	15.0	20.0
0	17.43	22.73	30.01	30.56	32.04	35.81	40.93	38.48
5	16.90	22.09	29.29	29.88	31.27	34.82	39.57	37.08
10	15.37	20.27	27.27	27.96	29.07	32.02	35.76	33.20
15	13.11	17.54	24.20	25.05	25.78	27.88	30.21	27.57
20	10.45	14.29	20.48	21.51	21.89	23.05	23.87	21.23
30	5.37	7.906	12.78	14.10	14.09	13.77	12.35	10.08
40	2.275	3.629	6.795	8.044	8.127	7.284	5.361	3.826
50	1.608	2.146	3.496	4.187	4.367	3.707	2.390	1.578
60	2.498	2.648	2.511	2.365	2.286	1.932	1.316	0.933
70	3.751	3.844	2.878	2.018	1.445	1.233	0.974	0.759
80	4.475	4.646	3.501	2.338	1.428	1.228	1.033	0.857
90	4.242	4.437	3.479	2.453	1.632	1.451	1.186	0.983
100	3.096	3.180	2.498	1.891	1.570	1.504	1.170	0.908
110	1.551	1.480	1.066	0.921	1.225	1.337	0.991	0.680
120	4.724	0.405	0.308	0.413	0.965	1.139	0.783	0.457
130	7.194	1.009	1.367	1.289	1.197	1.079	0.600	0.297
140	2.656	3.731	4.724	3.964	2.107	1.216	0.439	0.192
150	5.885	8.064	9.860	8.075	3.612	1.565	0.346	0.152
160	9.412	12.75	15.40	12.56	5.372	2.087	0.381	0.198
170	12.10	16.32	19.65	16.06	6.826	2.600	0.505	0.297
180	13.09	17.64	21.23	17.37	7.395	2.819	0.574	0.349
σ_t	45.89	56.06	64.87	60.08	50.16	45.17	37.94	30.85
σ_m	42.81	52.03	55.98	46.46	29.15	20.95	12.84	9.04
σ_v	24.67	27.36	26.39	22.75	19.23	17.21	13.07	9.85

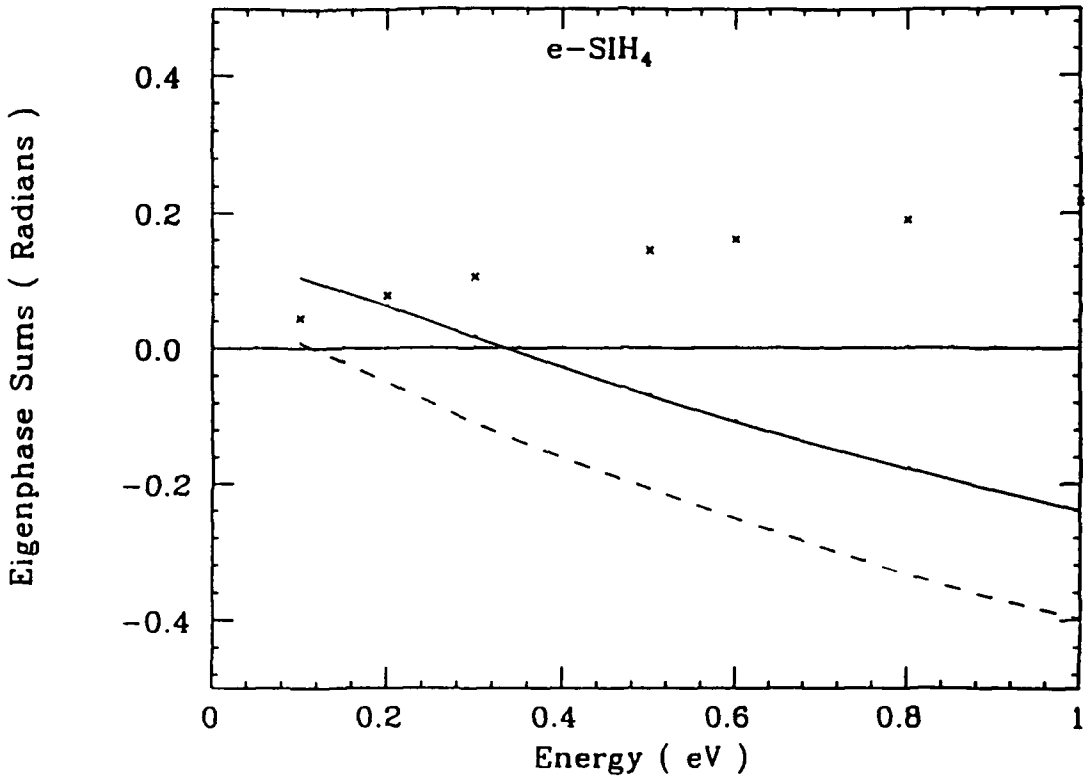

Fig. 6.2.1. Eigenphase sums for the e–SiH_4 collisions in A_1 symmetry in the present ESEP (solid curve) and ESE (crosses) models. The dash curve is the SMEP calculation of Jain and Thompson (1987). For various notations, see the text.

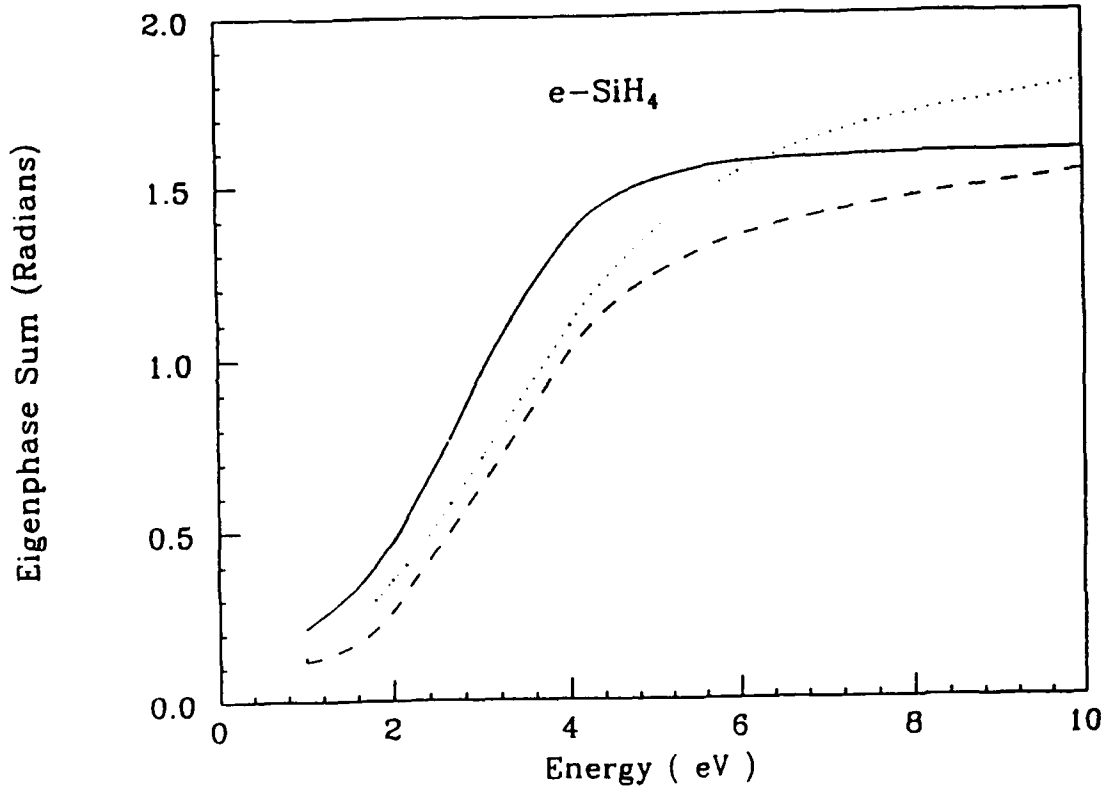

Fig. 6.2.2. Eigenphase sums for the e-SiH_4 collision in the T_2 (solid curve) and E (dotted curve) symmetries by using the present ESEP model. The dash curve represents the SMEP values of Jain and Thompson (1987) for T_2 state.

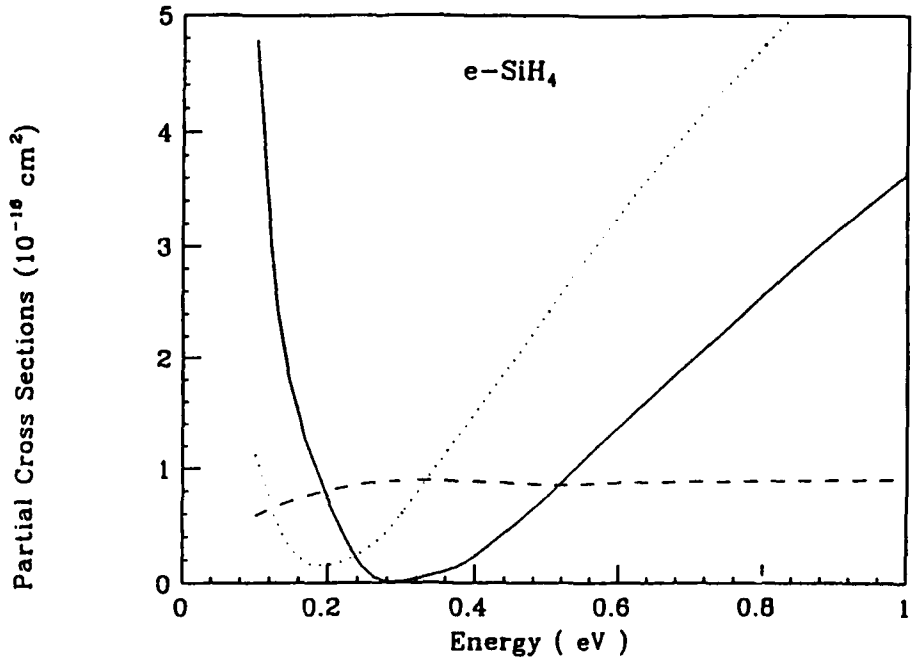

Fig. 6.2.3(a). Partial cross sections at 0–1 eV energy range for the e–SiH_4 system in A_1 (solid curve) and T_2 (dash curve) scattering states. The dotted curve represents the SMEP calculations of Jain and Thompson (1987) for A_1 representation.

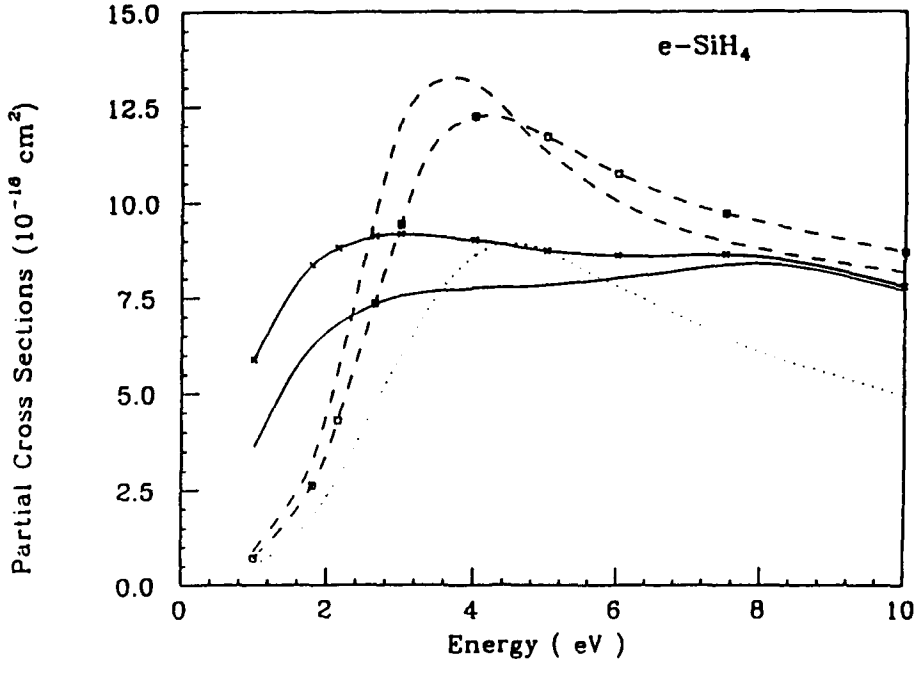

Fig. 6.2.3(b). Same legend as in Fig. 6.2.3(a) but in the 1–20 eV region. The solid and dash curves marked with crosses (A_1 state) and squares (T_2 state) are the corresponding results of Jain and Thompson (1987). The dotted line is our ESEP calculation for the E symmetry.

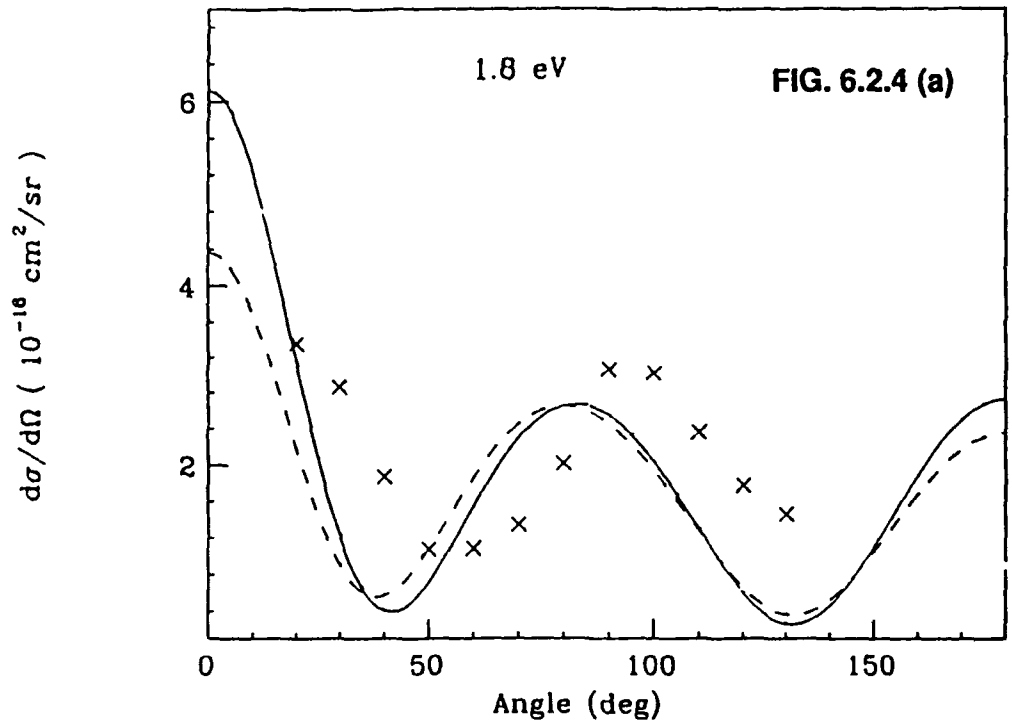

Fig. 6.2.4(a). Rotationally summed (vibrationally elastic) differential cross sections for the e-SiH_4 collisions at 1.8 eV. Theory; solid curve, present ESEP model; dash curve, present ESE model. Experiment: crosses, Tanaka et al (1990).

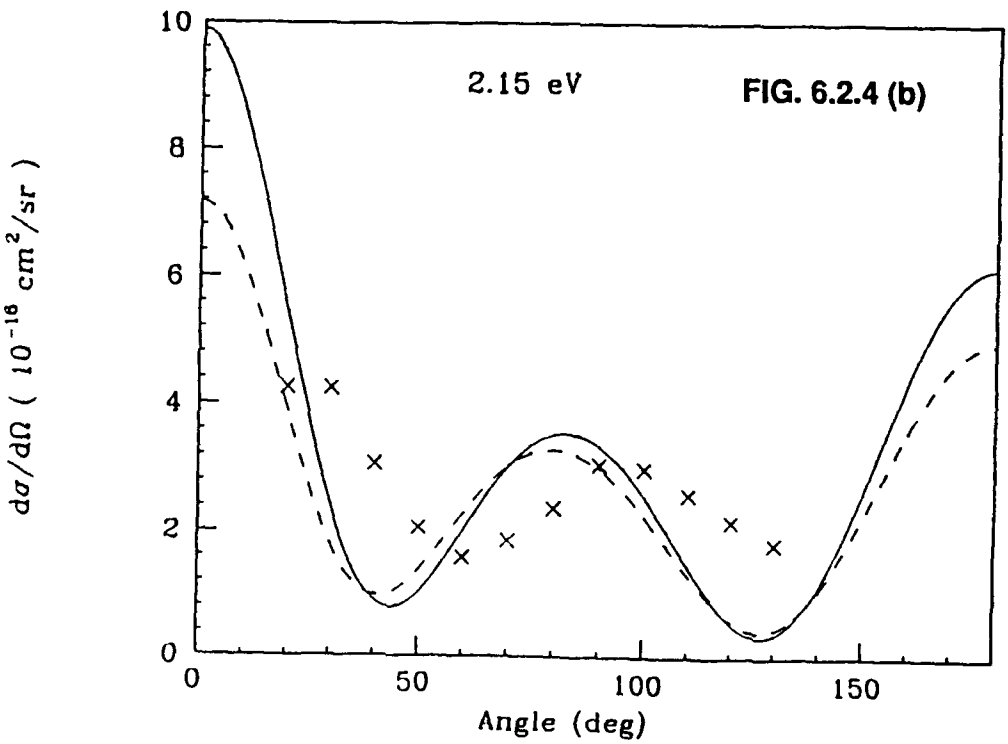

Fig. 6.2.4(b). Rotationally summed (vibrationally elastic) differential cross sections for the e-SiH_4 collisions at 2.15 eV. Theory; solid curve, present ESEP model; dash curve, present ESE model. Experiment: crosses, Tanaka et al (1990).

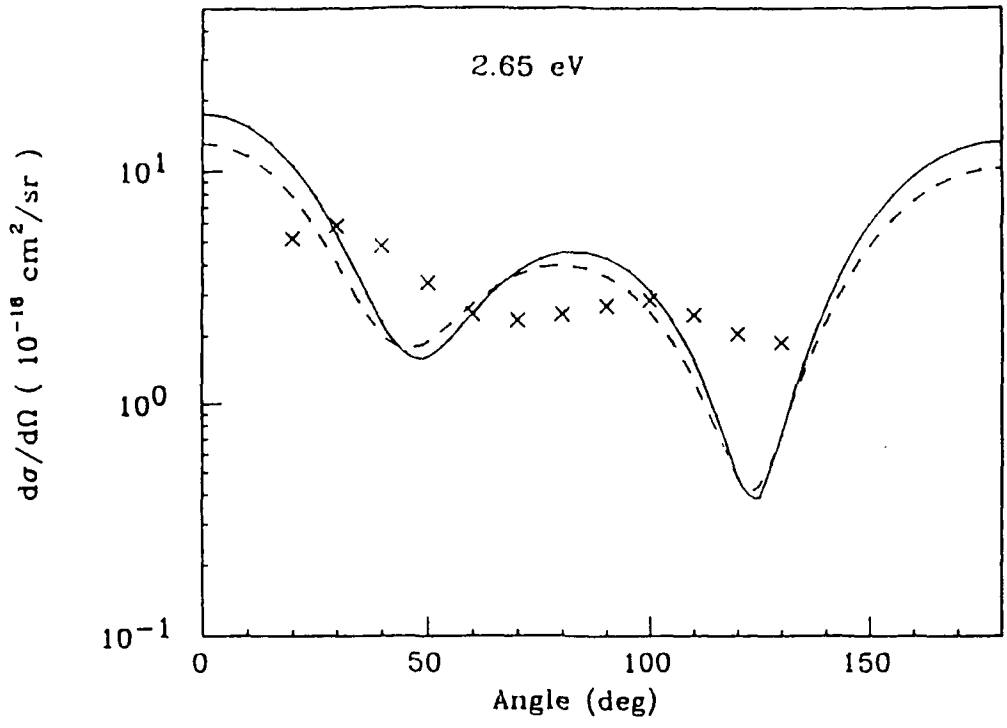

Fig. 6.2.4(c). Rotationally summed (vibrationally elastic) differential cross sections for the e-SiH_4 collisions at 2.65 eV. Theory; solid curve, present ESEP model; dash curve, present ESE model. Experiment: crosses, Tanaka et al (1990).

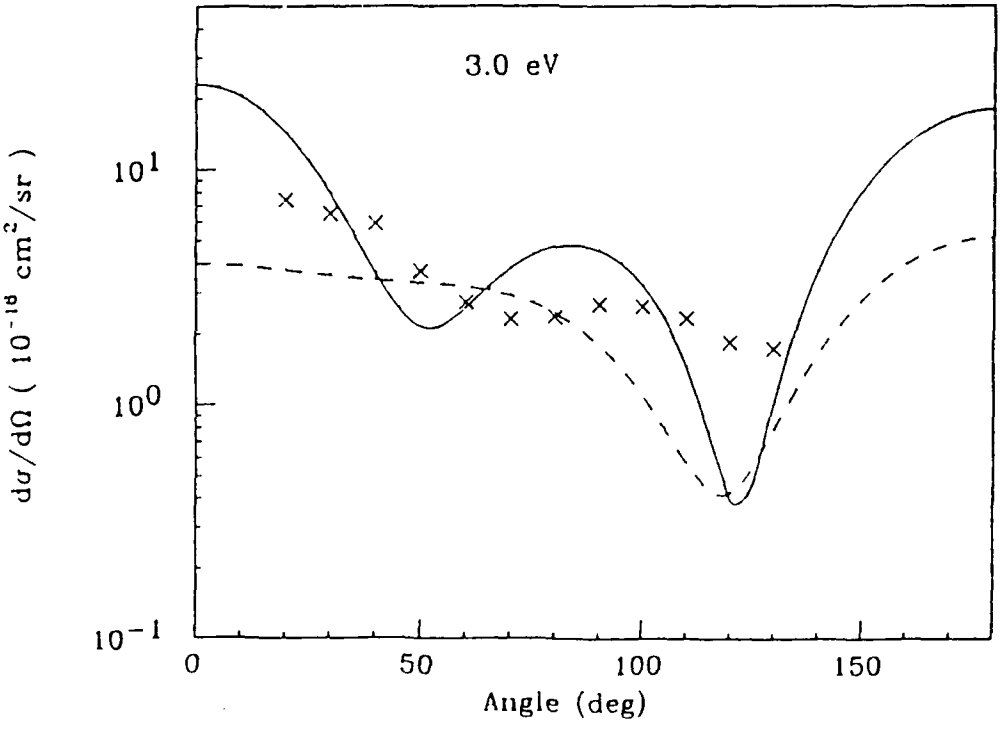

Fig. 6.2.4(d). Rotationally summed (vibrationally elastic) differential cross sections for the e-SiH_4 collisions at 3.0 eV. Theory; solid curve, present ESEP model; dash curve, present ESE model. Experiment: crosses, Tanaka et al (1990).

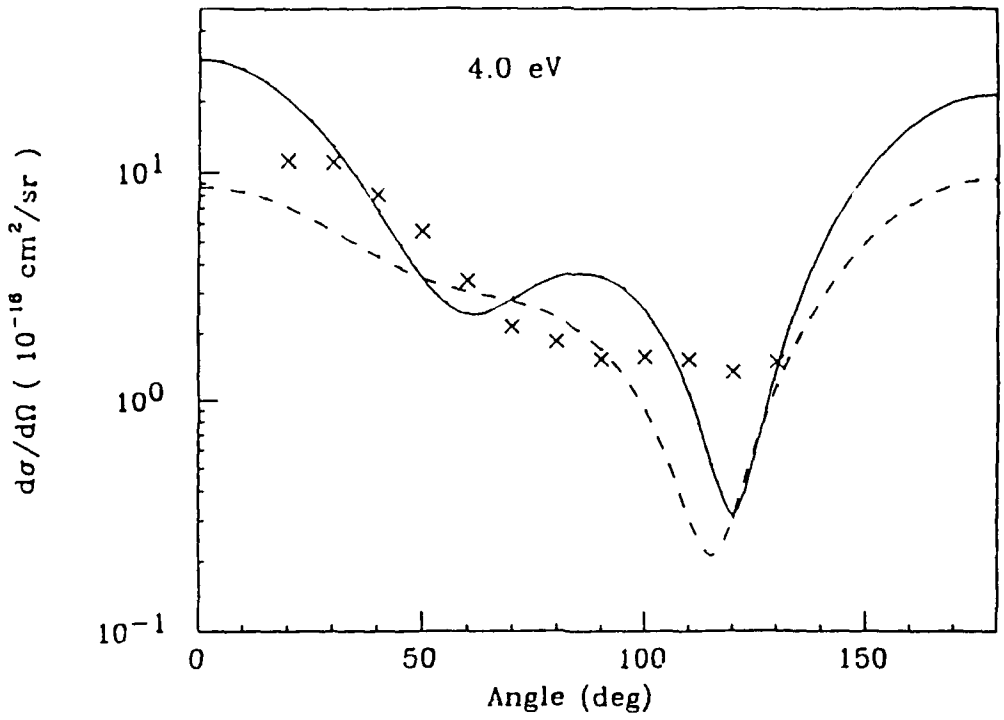

Fig. 6.2.4(e). Rotationally summed (vibrationally elastic) differential cross sections for the e-SiH_4 collisions at 4.0 eV. Theory; solid curve, present ESEP model; dash curve, present ESE model. Experiment: crosses, Tanaka et al (1990).

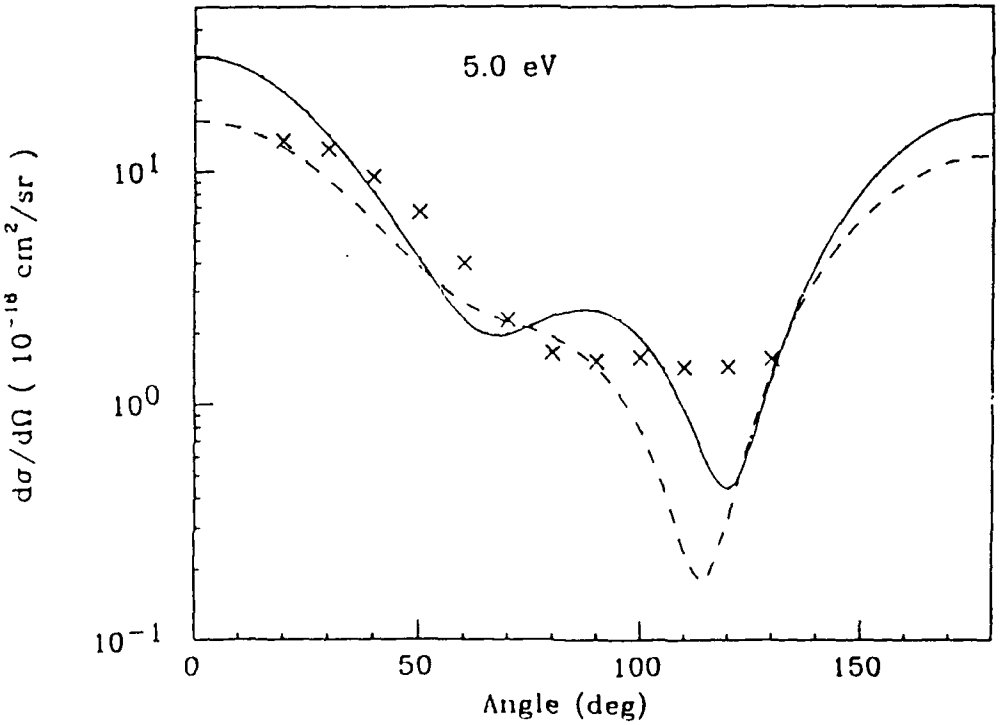

Fig. 6.2.4(f). Rotationally summed (vibrationally elastic) differential cross sections for the e-SiH_4 collisions at 5.0 eV. Theory; solid curve, present ESEP model; dash curve, present ESE model. Experiment: crosses, Tanaka et al (1990).

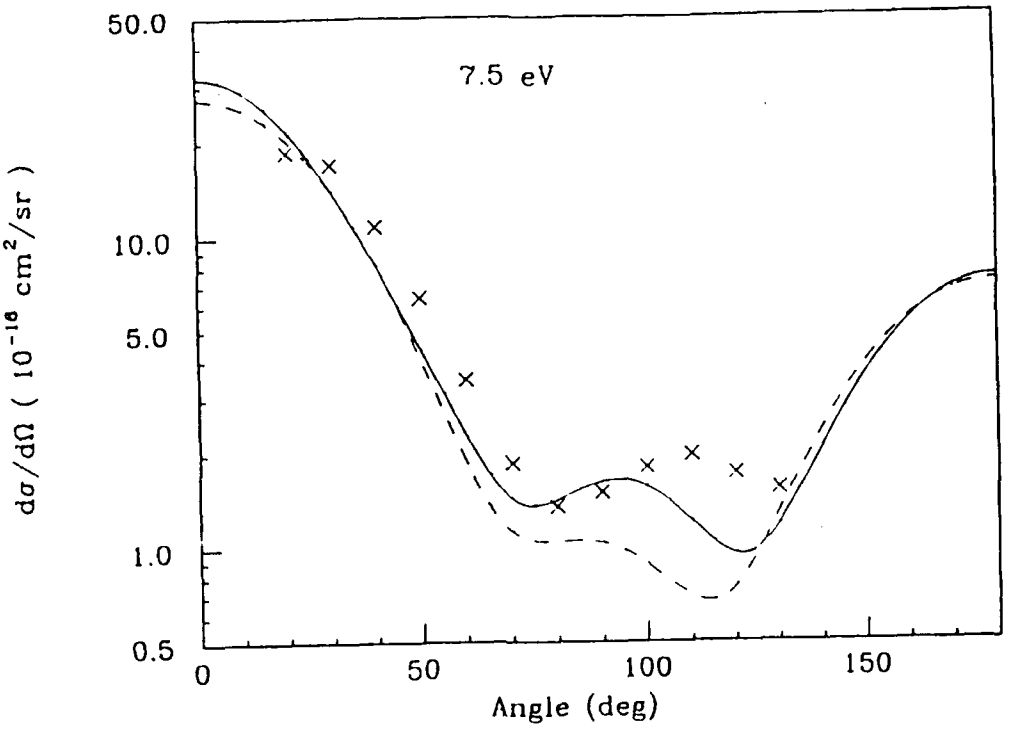

Fig. 6.2.4(g). Rotationally summed (vibrationally elastic) differential cross sections for the e-SiH_4 collisions at 7.5 eV. Theory; solid curve, present ESEP model; dash curve, present ESE model. Experiment: crosses, Tanaka et al (1990).

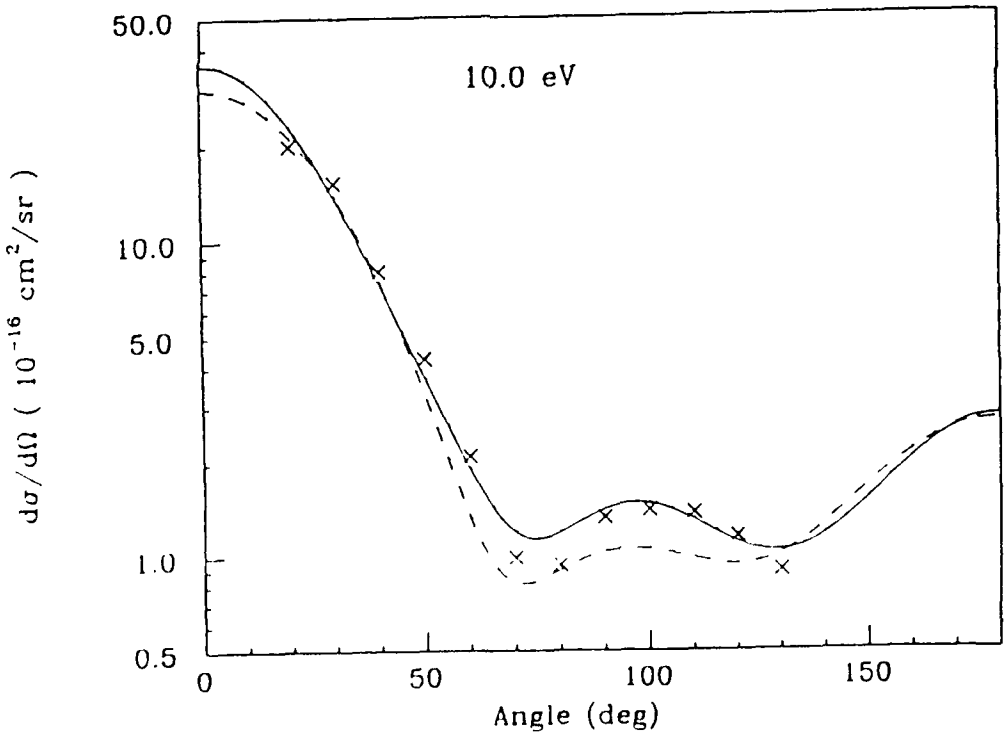

Fig. 6.2.4(h). Rotationally summed (vibrationally elastic) differential cross sections for the e SiH_4 collisions at 10 eV. Theory, solid curve, present ESEP model; dash curve, present ESE model. Experiment: crosses, Tanaka et al (1990).

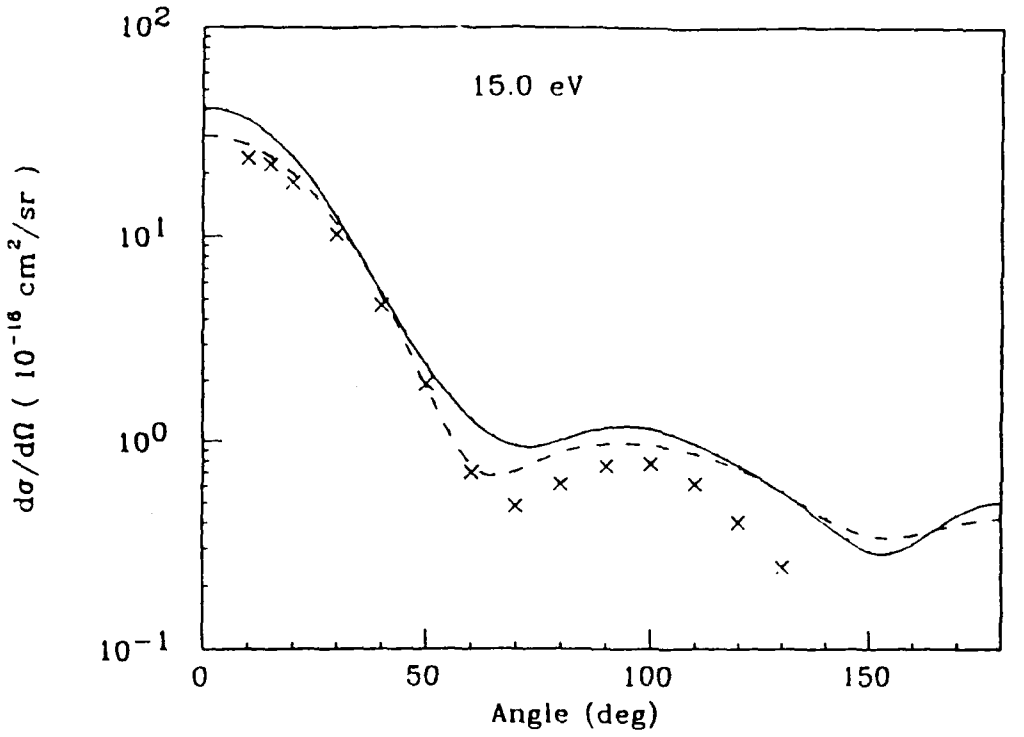

Fig. 6.2.4(i). Rotationally summed (vibrationally elastic) differential cross sections for the e-SiH_4 collisions at 15 eV. Theory; solid curve, present ESEP model; dash curve, present ESE model. Experiment: crosses, Tanaka et al (1990).

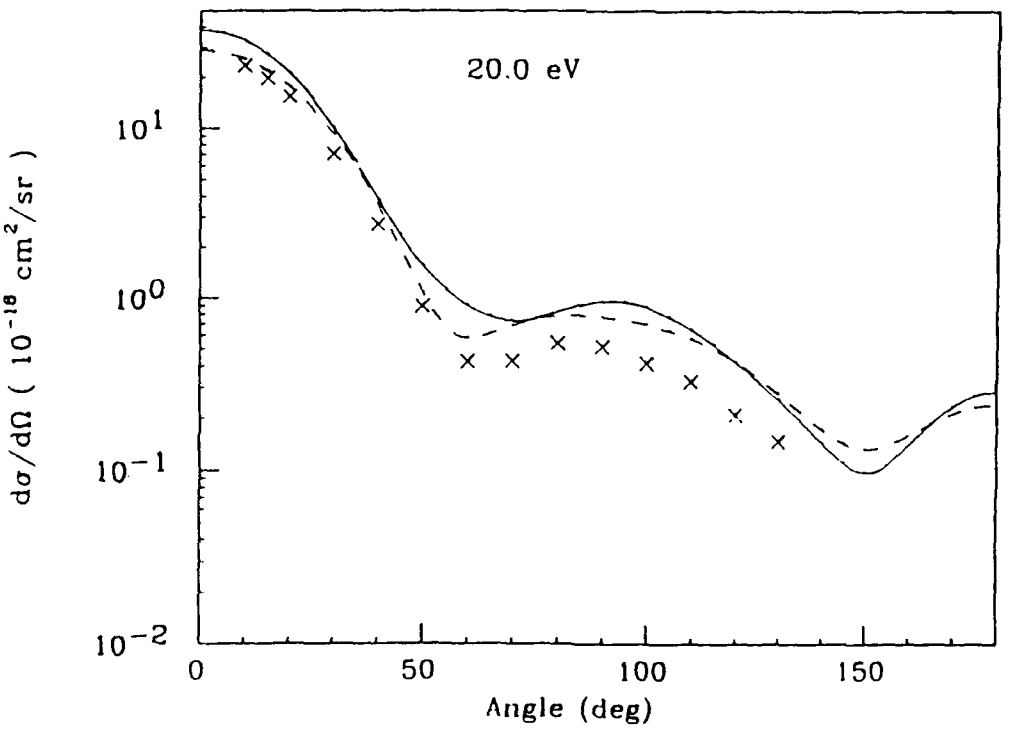

Fig. 6.2.4(j). Rotationally summed (vibrationally elastic) differential cross sections for the e-SiH_4 collisions at 20 eV. Theory; solid curve, present ESEP model; dash curve, present ESE model. Experiment: crosses, Tanaka et al (1990).

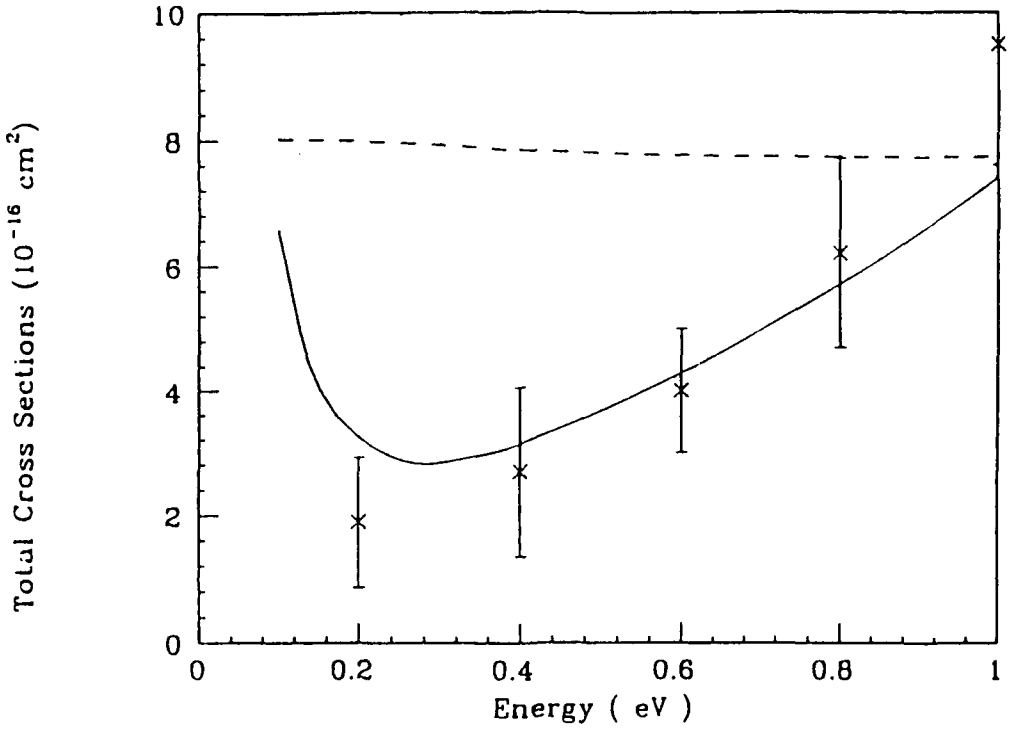

Fig. 6.2.5(a). Total integral (rotationally summed, vibrationally elastic) cross section for the e-SiH_4 system in the 0.1–1 eV energy range. Solid line, present ESEP; dash line, present ESE (multiplied by a factor of three). The experimental points (crosses) are taken from Wan *et al.* (1989).

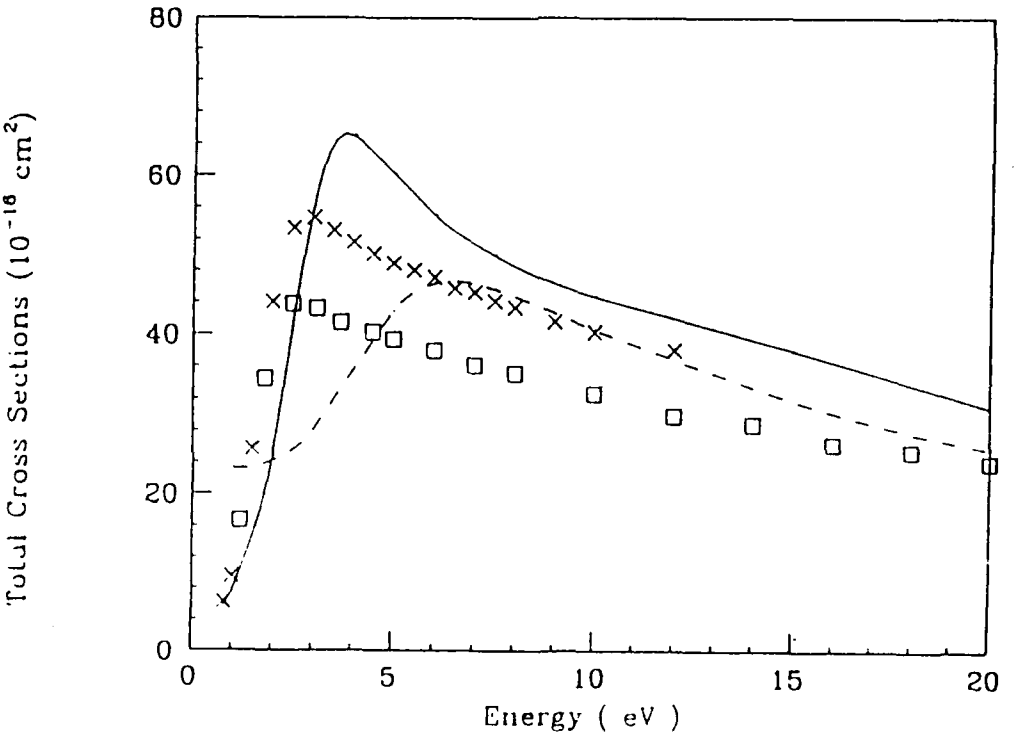

Fig. 6.2.5(b). Total integral (rotationally summed, vibrationally elastic) cross section for the e-SiH_4 system in the 1–20 eV energy range. Solid line, present ESEP; dash line, present ESE (multiplied by a factor of three). The experimental points (crosses) are taken from Wan *et al.* (1989) and Sucoka and Mori (1985) (squares).

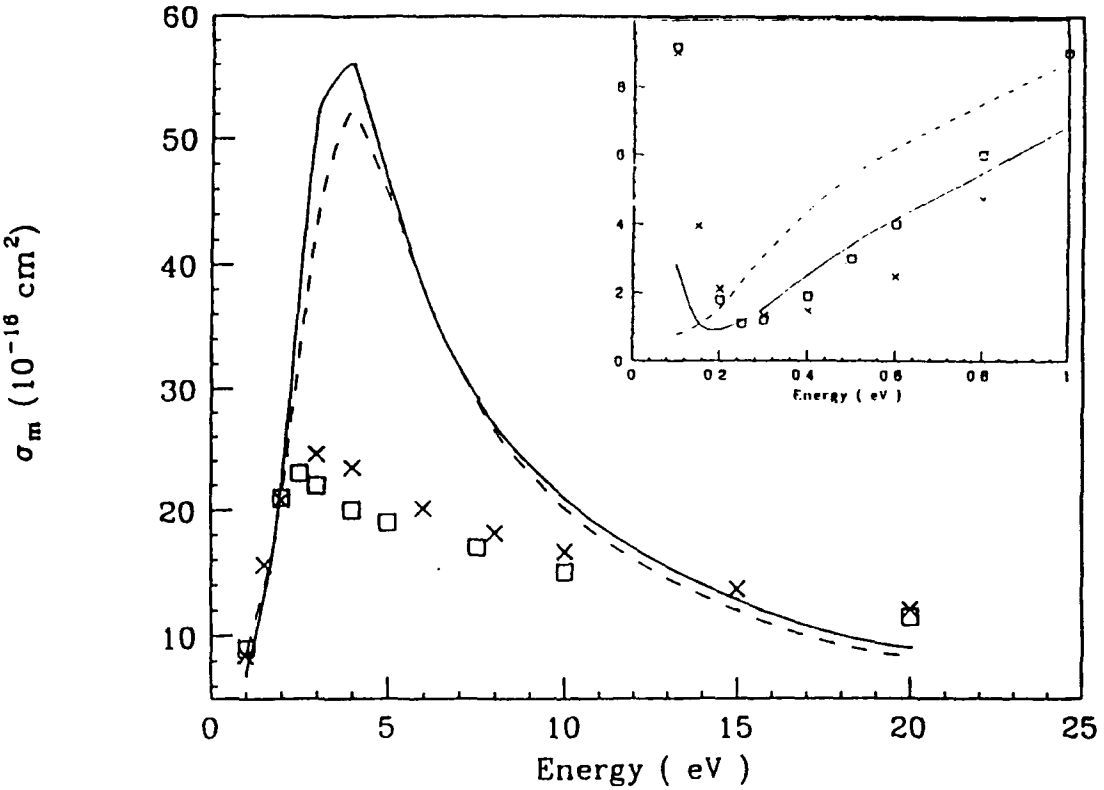

Fig. 6.2.6. Momentum transfer cross sections for the e-SiH_4 collisions in the present ESEP (solid curve) and ESE (dash curve) models. In the inset, we have shown more clearly the results al low (below 1 eV) energies. The experimental points are taken from Kurachi and Nakamura (1989) (squares) and Ohmori *et al.* (1986) (crosses).

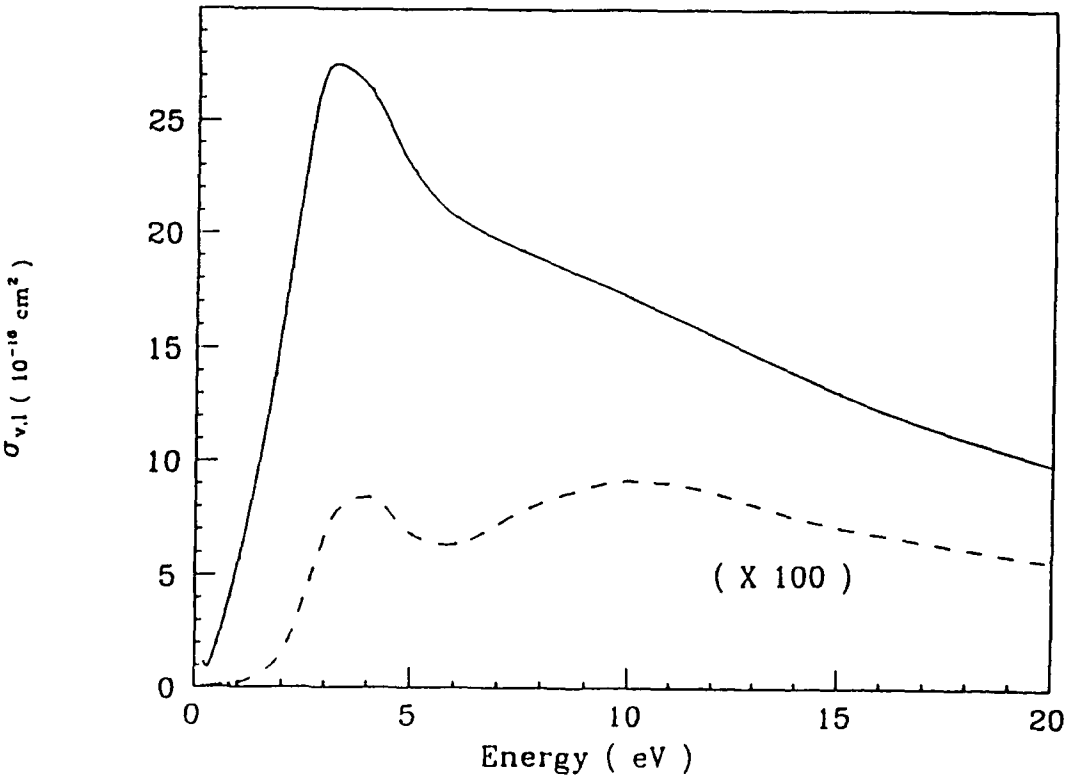

Fig. 6.2.7. Viscosity, σ_v, (solid curve) and energy-loss, σ_l, (dash curve) cross sections for the e-SiH_4 collision in the whole energy (0.2-20 eV) range. Note that the energy-loss numbers are multiplied by a factor of 100.

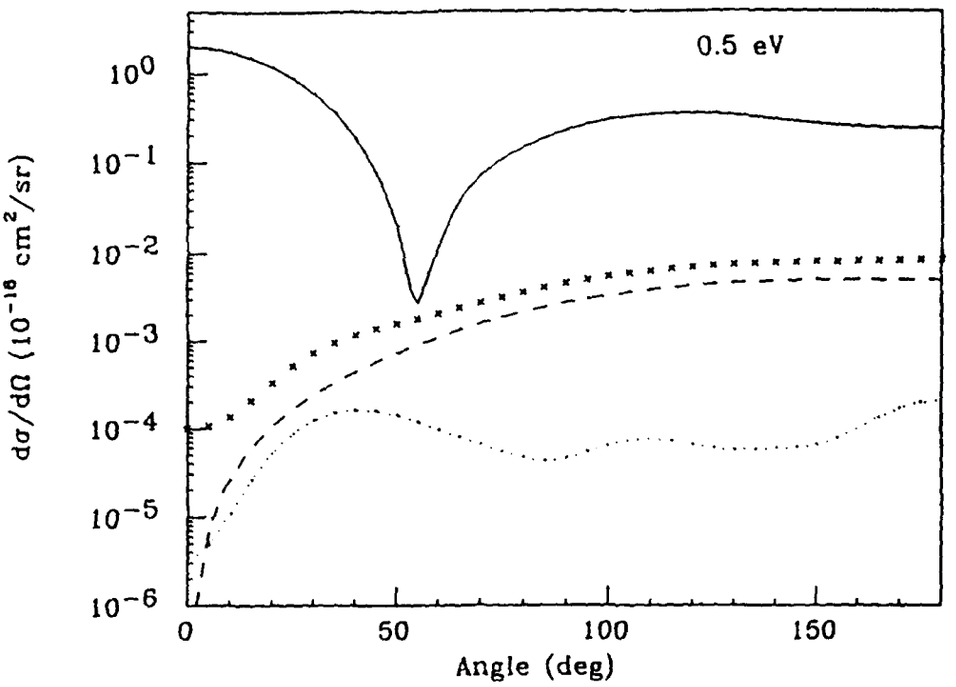

Fig. 6.2.8(a). Rotationally elastic and inelastic differential cross sections for the e-SiH_4 scattering in the ESEP model at 0.5 eV. Solid line, $0 \rightarrow 0$; dash line, $0 \rightarrow 3$; dotted line, $0 \rightarrow 4$; squares, $0 \rightarrow 6$; crosses, energy-loss (rotationally summed) differential cross sections.

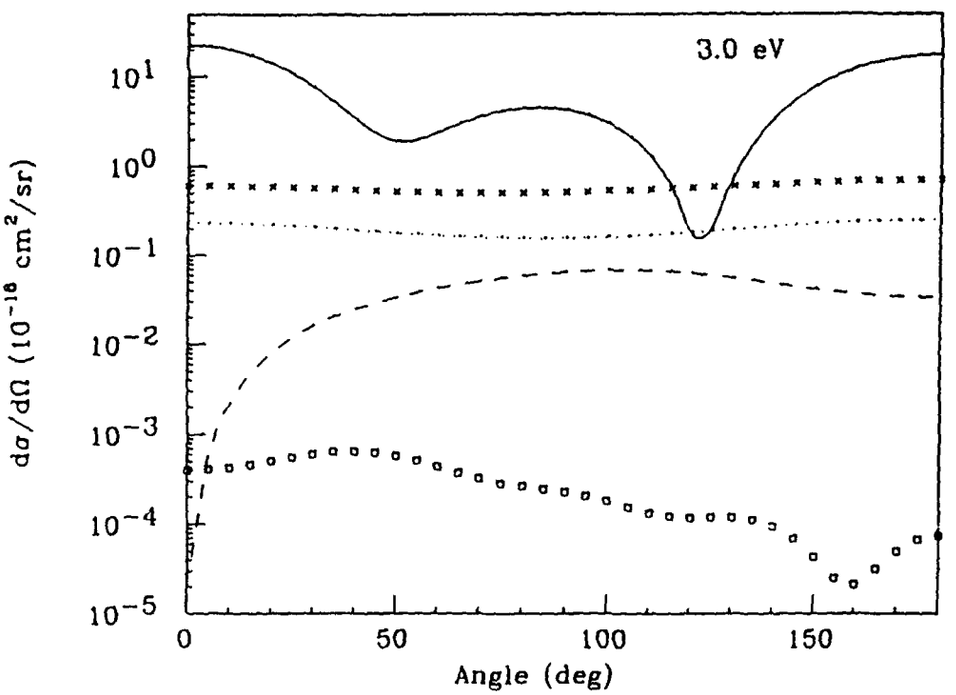

Fig. 6.2.8(b). Rotationally elastic and inelastic differential cross sections for the e-SiH_4 scattering in the ESEP model at 3 eV. Solid line, $0 \rightarrow 0$; dash line, $0 \rightarrow 3$; dotted line, $0 \rightarrow 4$; squares, $0 \rightarrow 6$; crosses, energy-loss (rotationally summed) differential cross sections.

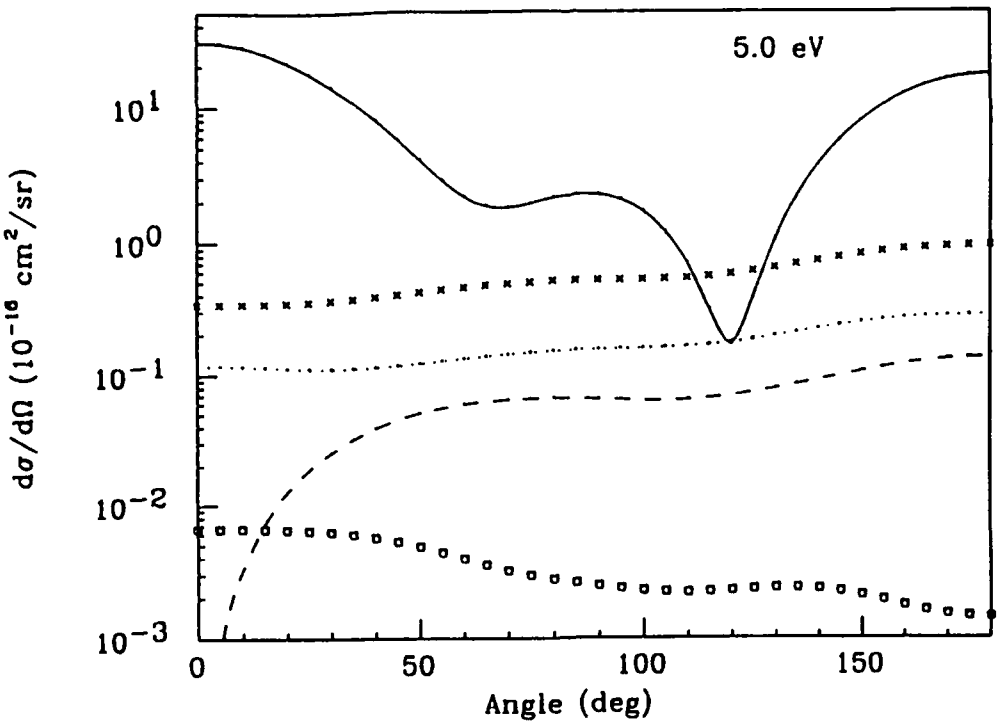

Fig. 6.2.8(c). Rotationally elastic and inelastic differential cross sections for the e–SiH_4 scattering in the ESEP model at 5 eV. Solid line, $0 \rightarrow 0$; dash line, $0 \rightarrow 3$; dotted line, $0 \rightarrow 4$; squares, $0 \rightarrow 6$; crosses, energy-loss (rotationally summed) differential cross sections.

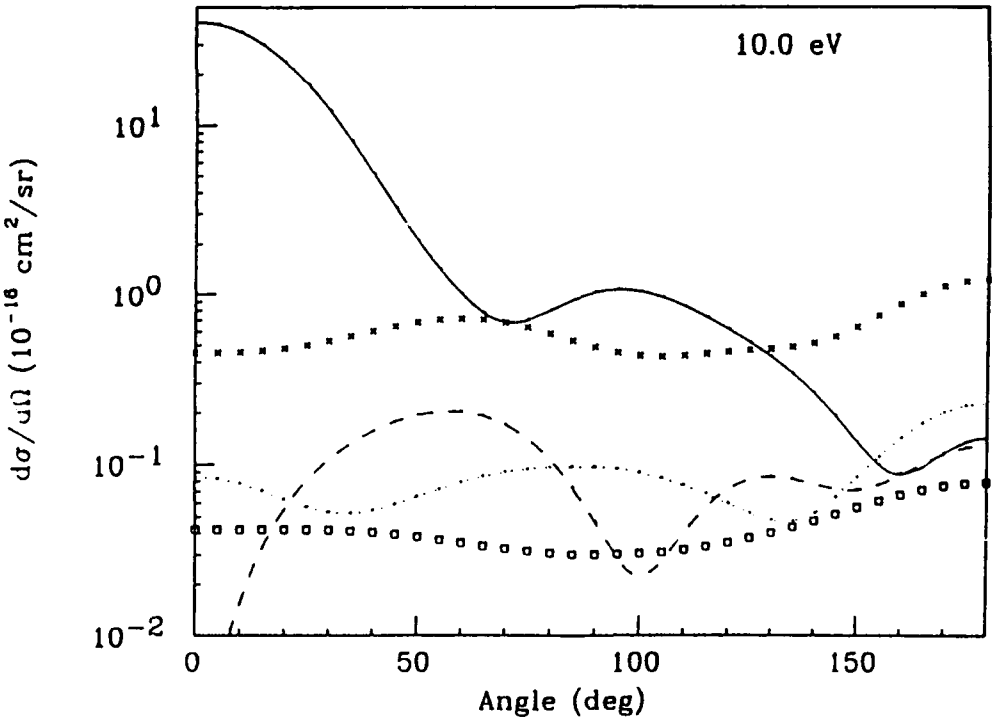

Fig. 6.2.8(d). Rotationally elastic and inelastic differential cross sections for the e–SiH_4 scattering in the ESEP model at 10 eV. Solid line, $0 \rightarrow 0$; dash line, $0 \rightarrow 3$; dotted line, $0 \rightarrow 4$; squares, $0 \rightarrow 6$; crosses, energy-loss (rotationally summed) differential cross sections.

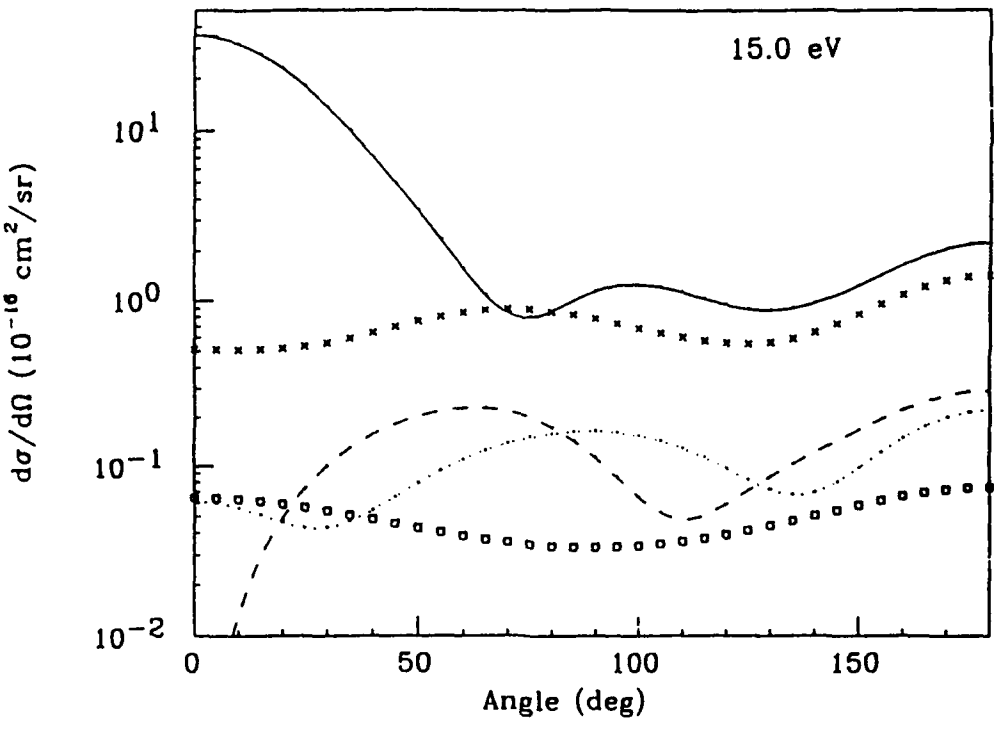

Fig.6.2.8(e). Rotationally elastic and inelastic differential cross sections for the e-SiH_4 scattering in the ESEP model at 15 eV. Solid line, 0 → 0; dash line, 0 → 3; dotted line, 0 → 4; squares, 0 → 6; crosses, energy-loss (rotationally summed) differential cross sections.

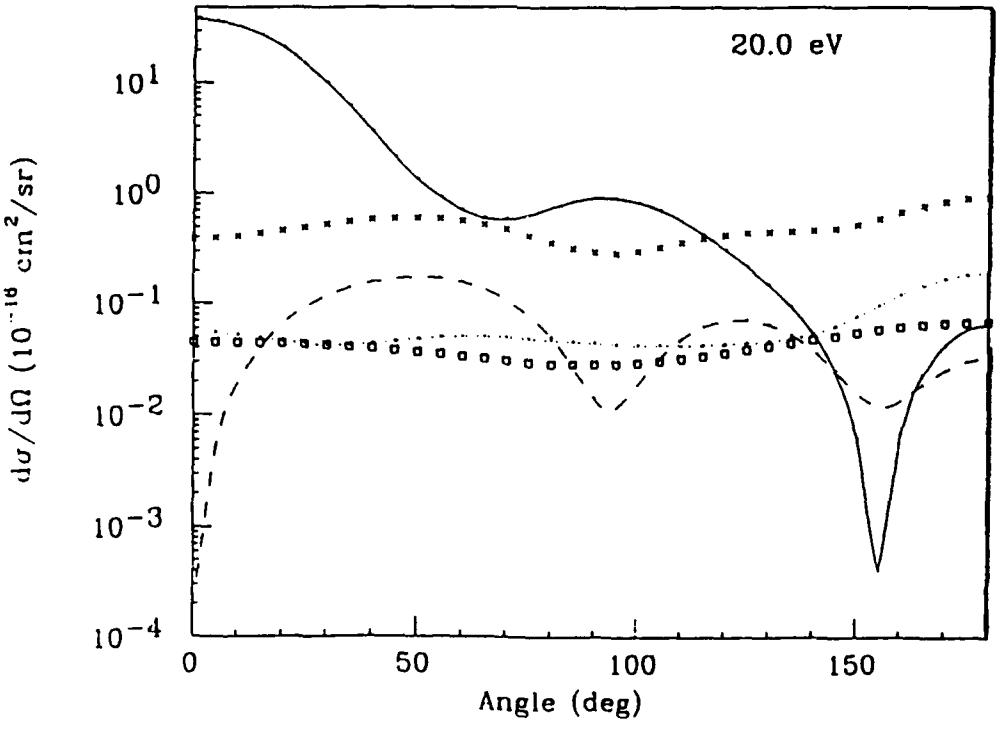

Fig. 6.2.8(f). Rotationally elastic and inelastic differential cross sections for the e-SiH_4 scattering in the ESEP model at 20 eV. Solid line, 0 → 0; dash line, 0 → 3; dotted line, 0 → 4; squares, 0 → 6; crosses, energy-loss (rotationally summed) differential cross sections.

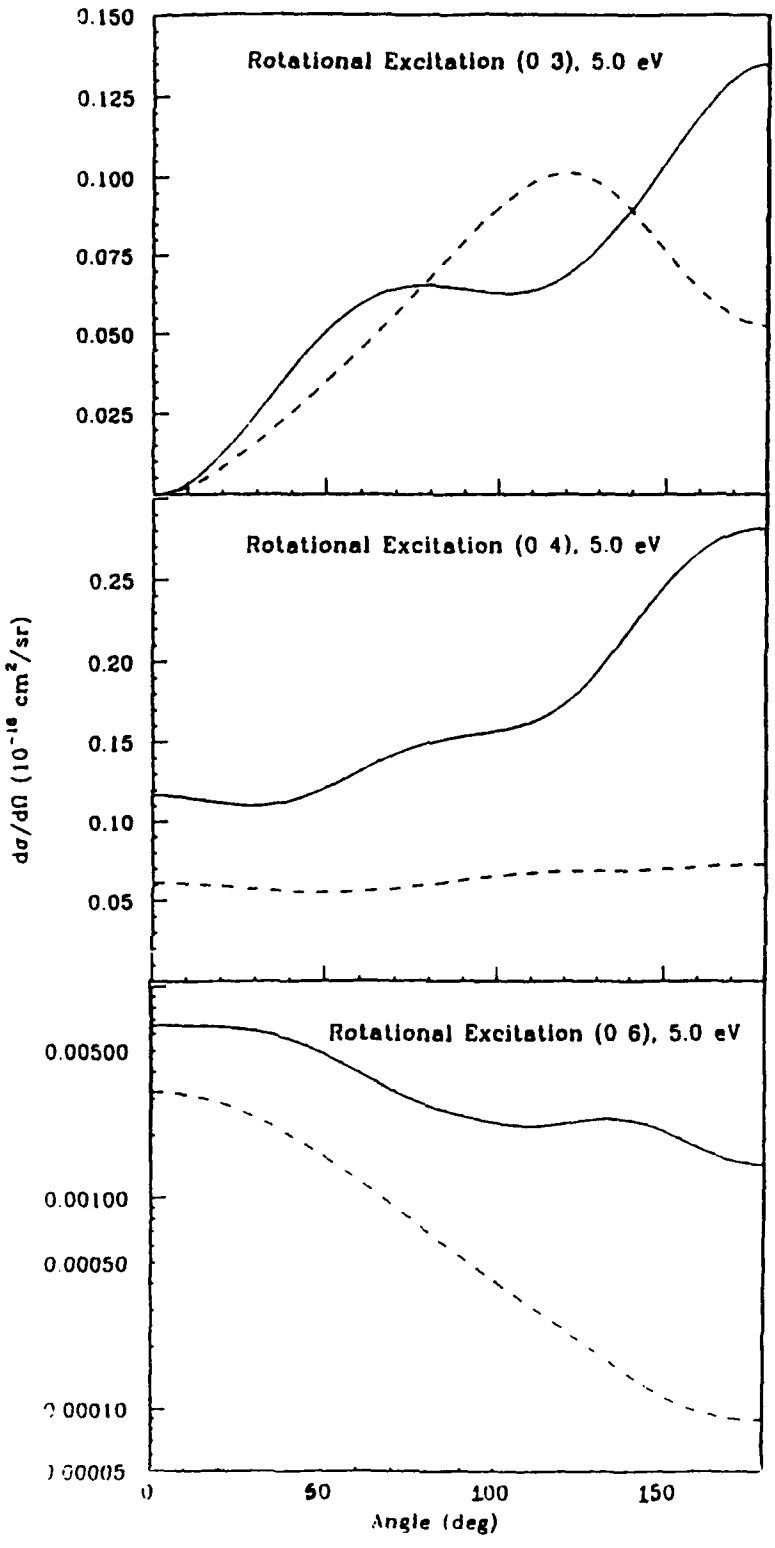

Fig. 6.2.9. Differential cross sections for rotationally inelastic transitions with (solid lines, ESEP model) and without (dash lines, ESE model) polarisation effect at 5 eV.

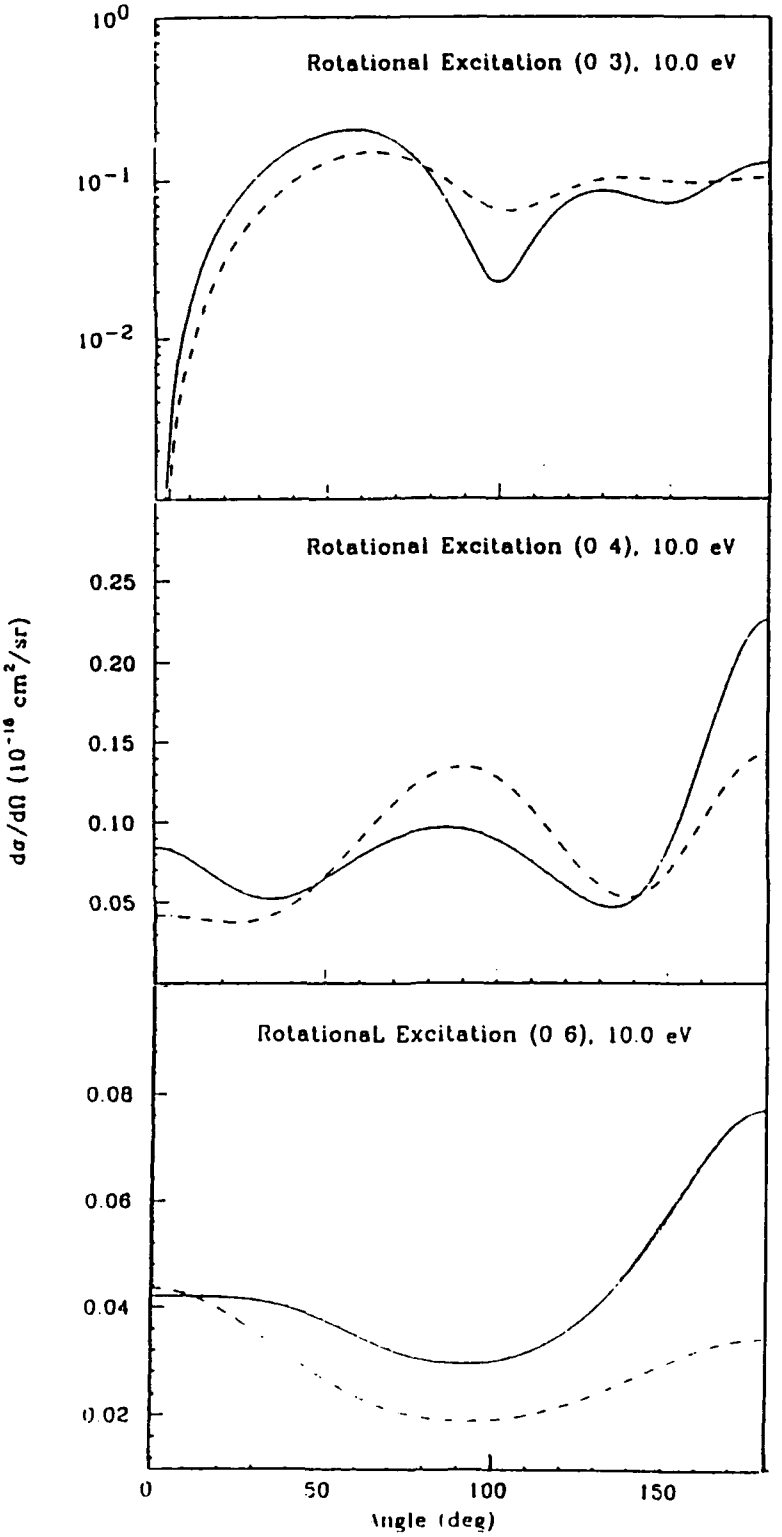

Fig. 6.2.10. Differential cross sections for rotationally inelastic transitions with (solid lines, ESEP model) and without (dash lines, ESE model) polarisation effect at 10 eV.

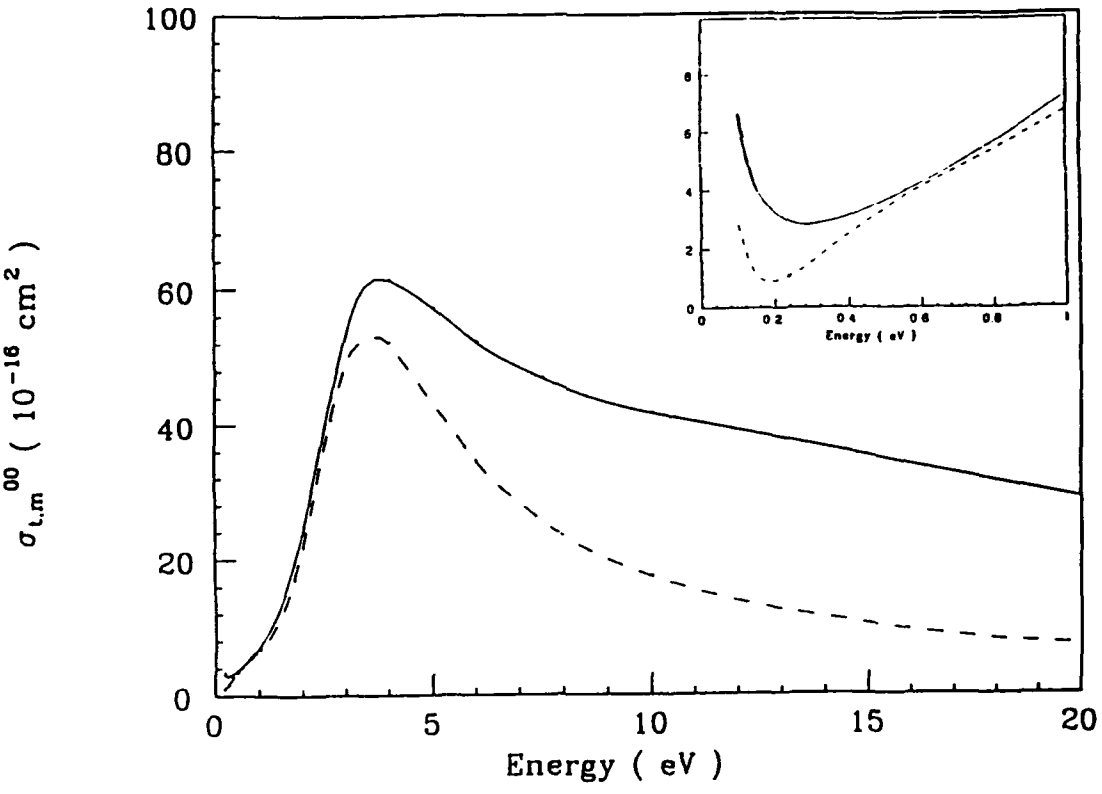

Fig. 6.2.11. σ_t^{00} (solid line) and σ_m^{00} (dash line) cross sections for the e–SiH_4 collisions in the ESEP model. In the inset, we have shown more clearly the low-energy (below 1 eV) data.

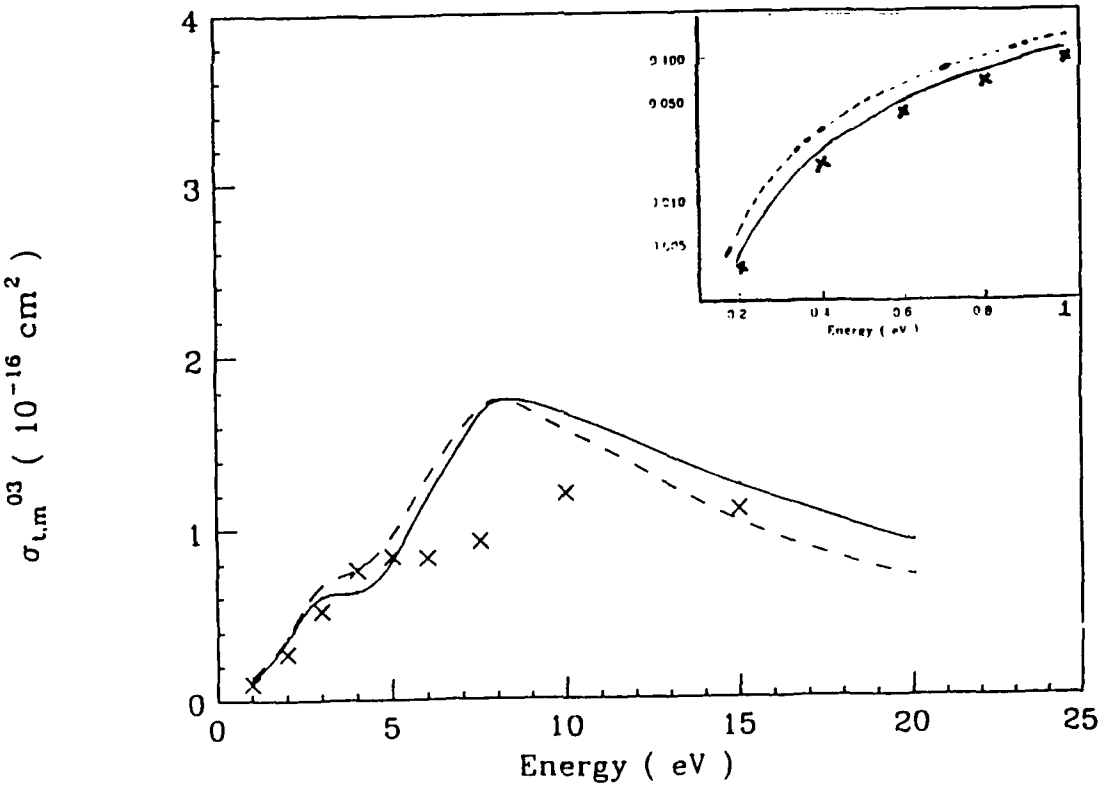

Fig. 6.2.12. σ_t^{03} (solid line) and σ_m^{03} (dash line) cross sections for the e–SiH_4 collisions in the ESEP model. In the inset, we have shown more clearly the low-energy (below 1 eV) data. The crosses are the σ_t^{03} values in the ESE model.

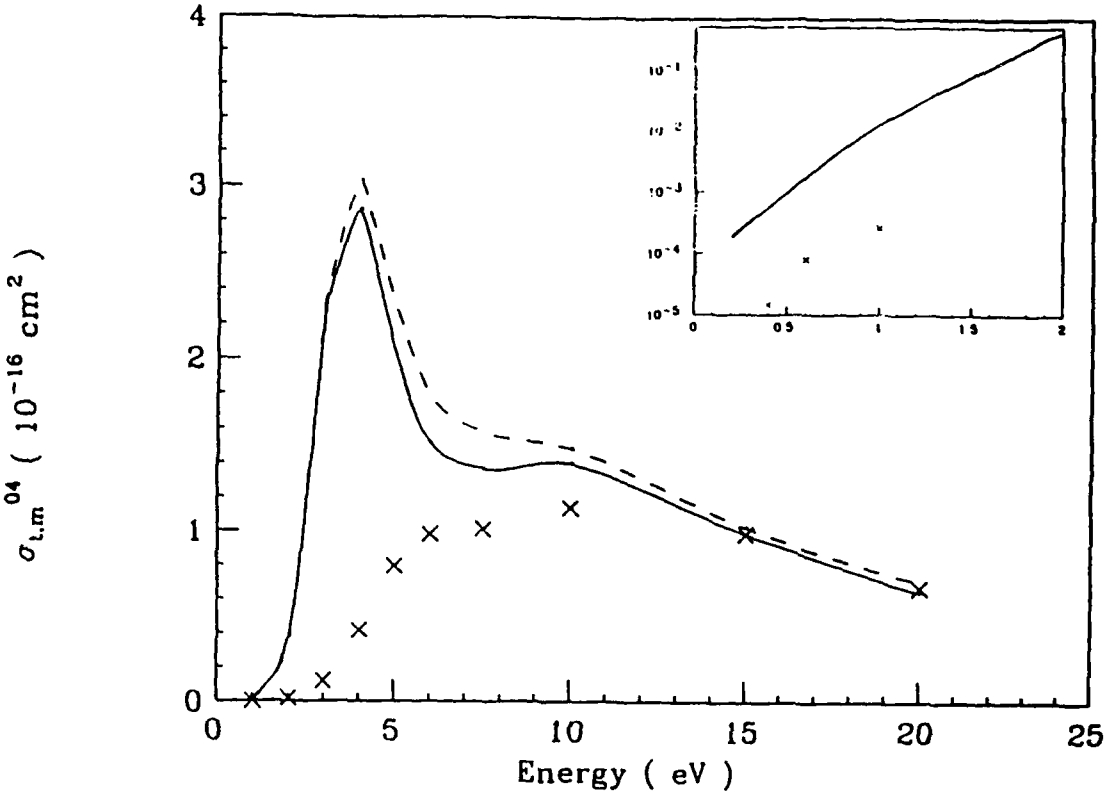

Fig. 6.2.13. σ_t^{04} (solid line) and σ_m^{04} (dash line) cross sections for the e–SiH_4 collisions in the ESEP model. In the inset, we have shown more clearly the low-energy (below 1 eV) data. The crosses are the σ_t^{03} values in the ESE model.

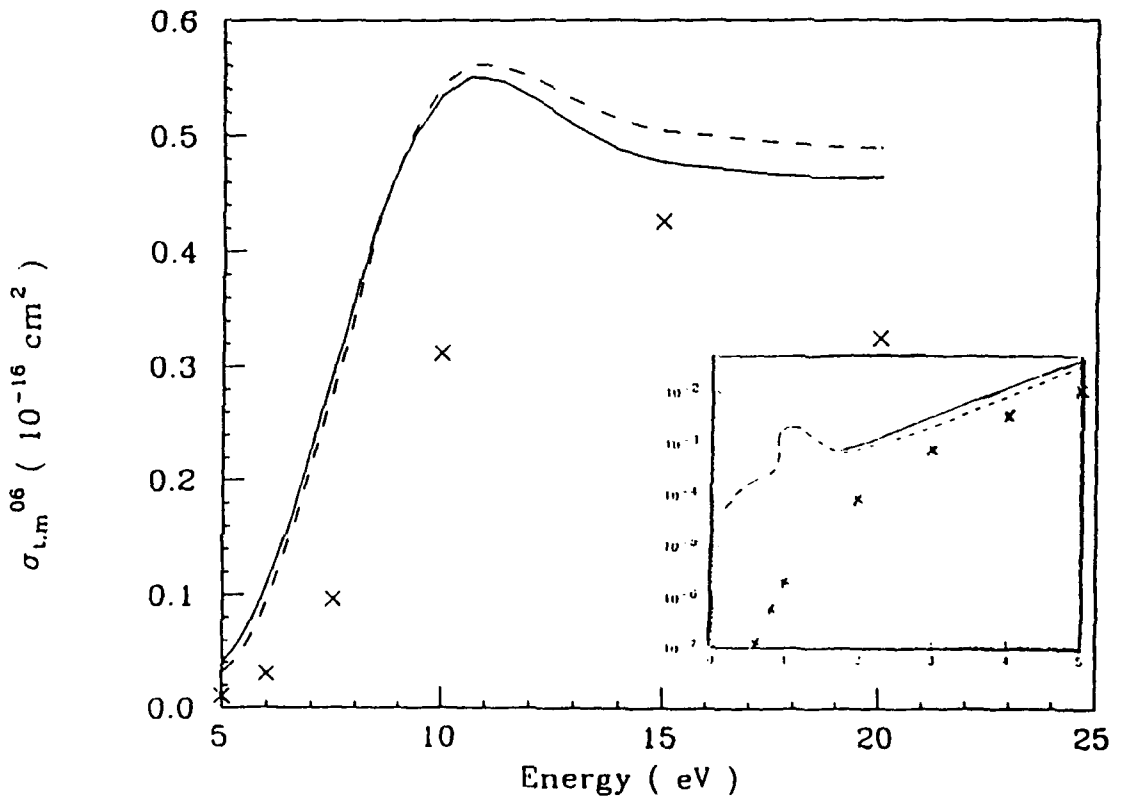

Fig. 6.2.14. σ_t^{06} (solid line) and σ_m^{06} (dash line) cross sections for the e–SiH_4 collisions in the ESEP model. In the inset, we have shown more clearly the low-energy (below 1 eV) data. The crosses are the σ_t^{03} values in the ESE model.

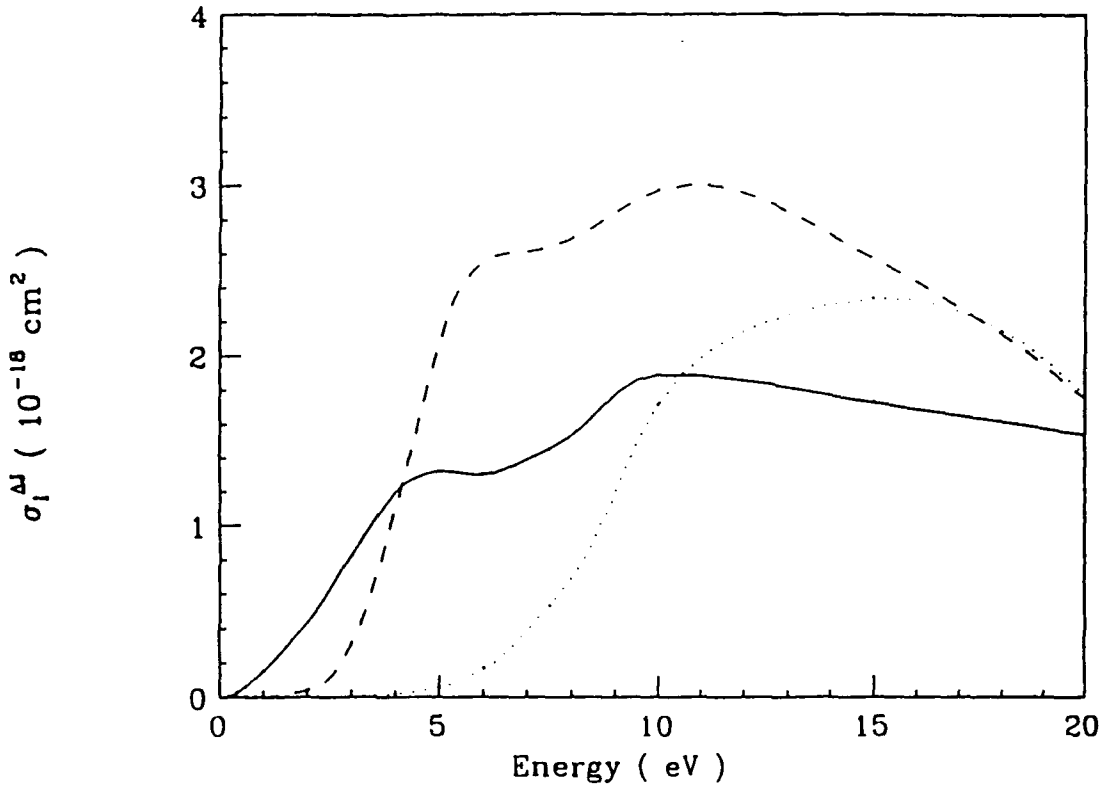

Fig. 6.2.15. Energy-loss (integral) cross sections for various rotational transitions for the e–SiH_4 scattering in the ESEP model as a function of impact energy. Solid lines, $0 \rightarrow 3$; dash lines, $0 \rightarrow 4$; dotted lines, $0 \rightarrow 6$.

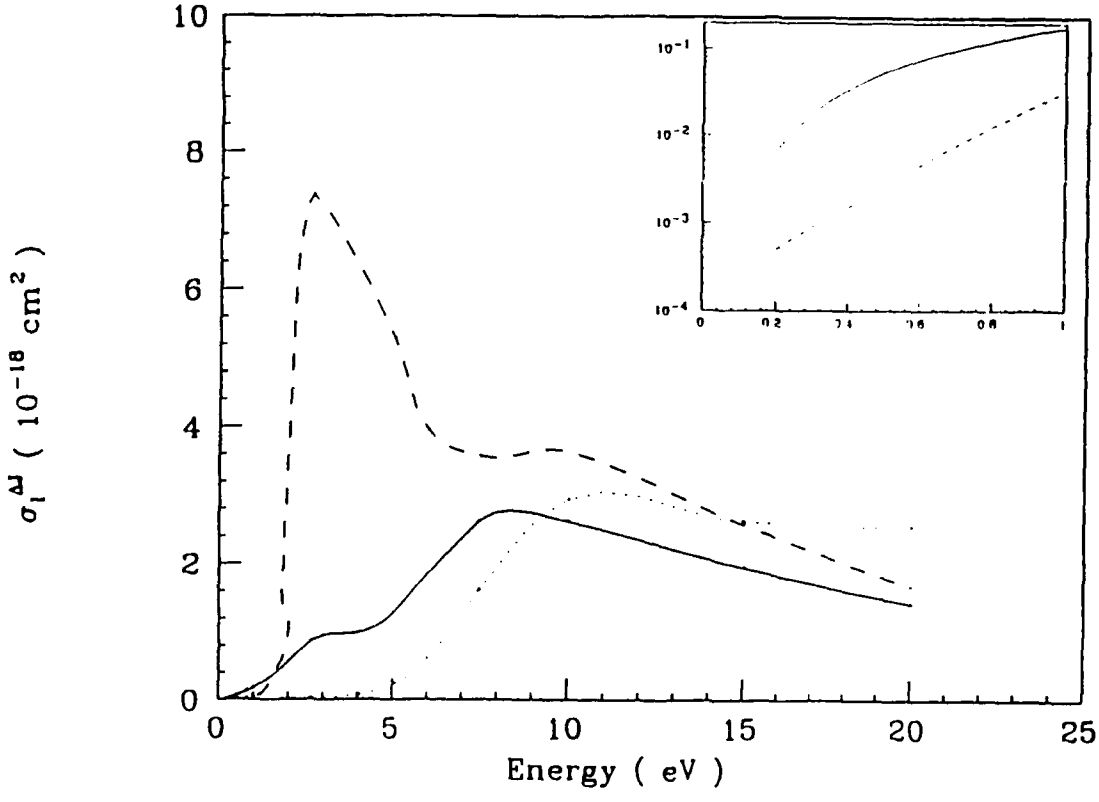

Fig. 6.2.16. Energy-loss (integral) cross sections for various rotational transitions for the e–SiH_4 scattering in the ESE model as a function of impact energy. Solid lines, $0 \rightarrow 3$; dash lines, $0 \rightarrow 4$; dotted lines, $0 \rightarrow 6$.

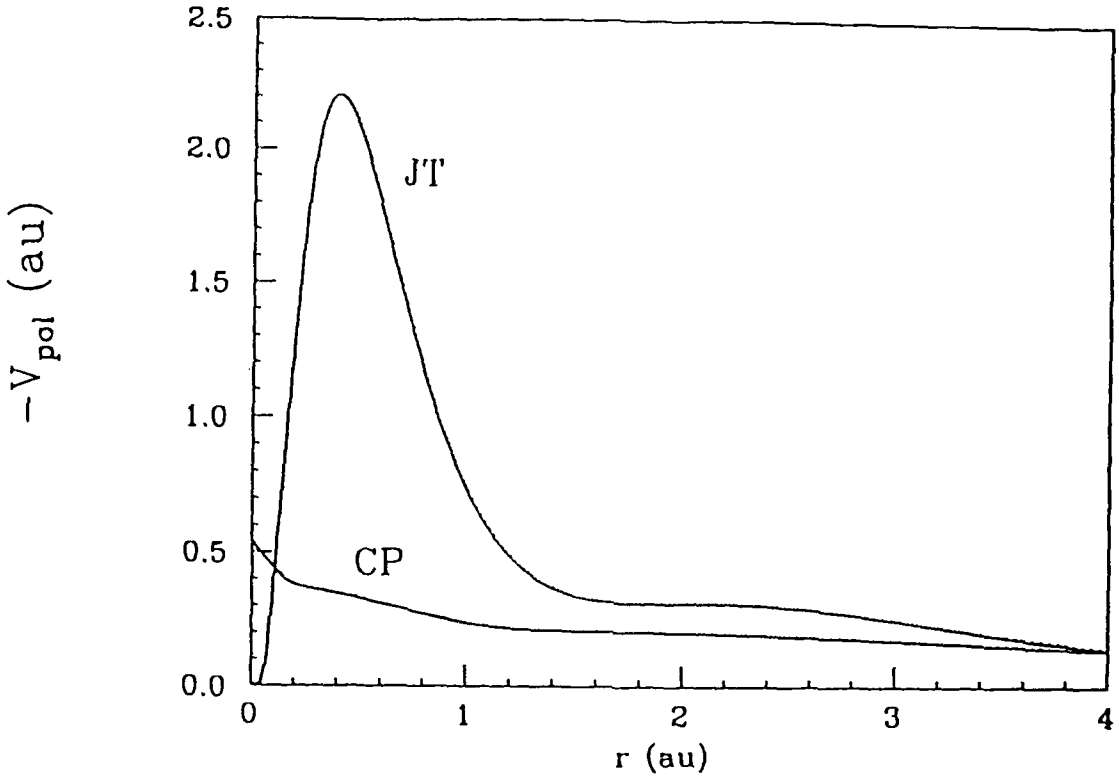

Fig. 6.2.17. Nonadjustable polarization potentials for the e–SiH_4 system in the JT and CP approximations as a function of radial distance r in atomic units. Note that each potential is multiplied by a factor of $\sqrt{4\pi}$. For notations see the text.

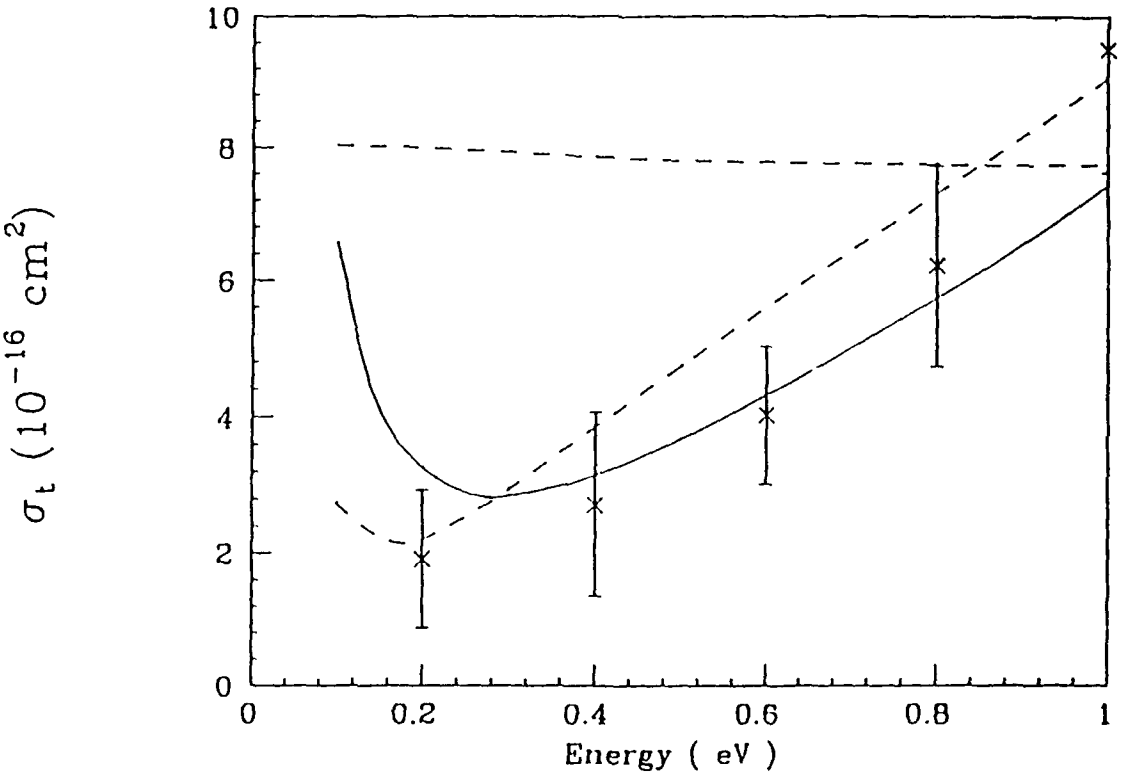

Fig. 6.2.18. Total cross sections for the e–SiH_4 elastic collisions below 1 eV. Theory: solid line, present SEP(JT) model; dashed line, present SEP(CP) model. The upper dash curve represents the static-exact-exchange (SEE) (without polarization). Experiment: crosses, Wan *et al.* [23].

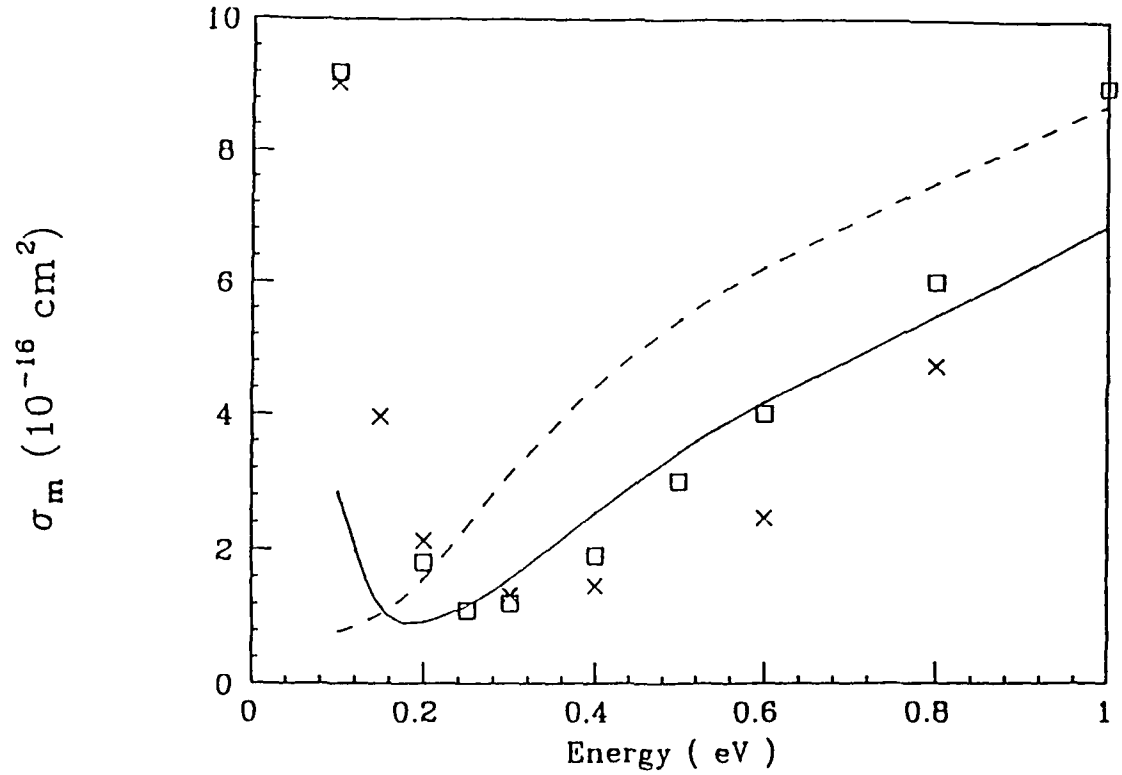

Fig. 6.2.19. Momentum transfer cross sections for the e–SiH_4 system in the present SEP(JT) (solid curve) and SEP(CP) (dashed curve) models. The swarm data are taken from Ref. 29 (crosses) and Ref. 30 (squares).

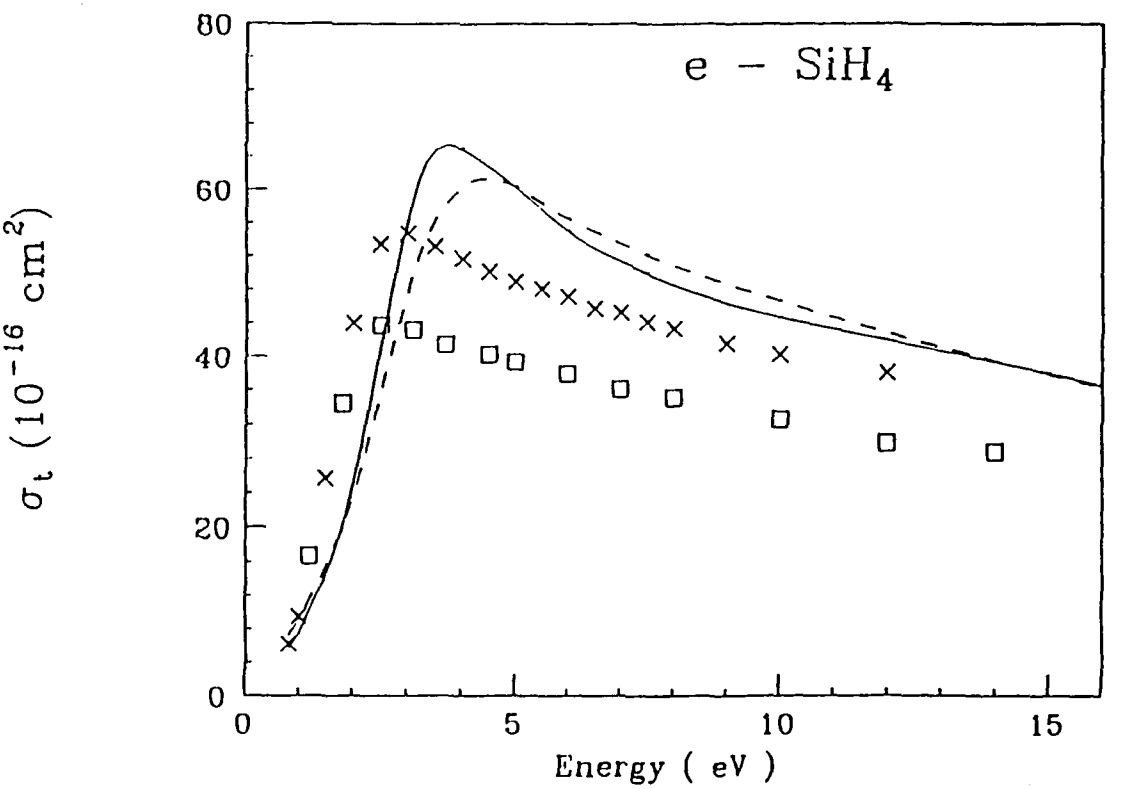

Fig. 6.2.20. Total cross sections for the e–SiH_4 elastic collisions at 1–15 eV. Theory: solid line, present SEP(JT) model; dashed line, present SEP(CP) model. The experimental points are from Ref. 23 (crosses) and Ref. 27 (squares).

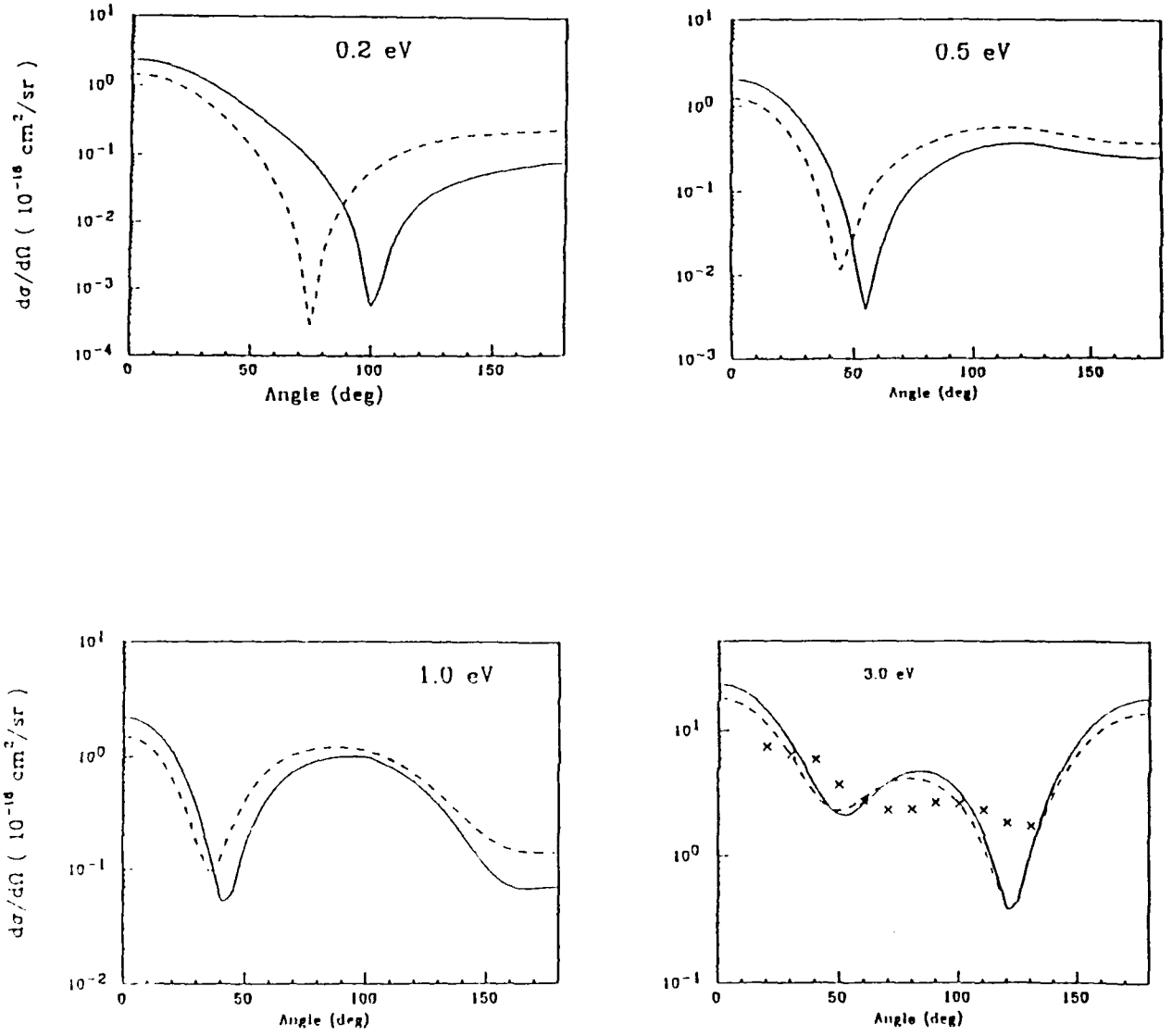

Fig. 6.2.21. Elastic differential cross sections for the e-SiH_4 scattering at 0.2, 0.5, 1 and 3 eV. Theory: solid curve, present SEP(JT) model; dashed line, present SEP(CP) model. At 3 eV, the measured values of Tanaka *et al.*[45] are shown by crosses.

6.3 Electron–GeH_4 Cross Sections

This is a rather too heavy spherical top molecule for which very recently DCS have been measured in the range of 2–100 eV [53]. No previous calculation exists for this collision system. Molecular wave functions and consequently the density and various interaction potentials were determined using the HONDO and INTERFACE programs (see Section 4.3). This part of the calculation was done at a simpler level than the one described above for other gases. A spherical approximation [54] was employed under the model exchange and polarization terms. A more rigorous treatment of this system is under progress; here our goal is to demonstrate that from the present techniques, it is possible to yield reliable cross sections even for such a heavy system. Strictly speaking, the following results correspond to the rotationally elastic channel.

First, in Figs. 6.3.1 (a) we show the electronic charge density for the GeH_4 molecule while in Fig. 6.3.1(b) the spherical part of static, exchange and polarization interactions are diplayed. The electronic charge density shown in Fig. 6.3.1(a) compares very well with previous calculations in the spherical description of GeH_4 molecule.

Figs. 6.3.2(a)–6.3.2(e) show our low energy (at 2, 3, 5, 7.5, and 10 eV) DCS together with the experimental data [53]. The validity of the spherical model depends on the fact that the rotational excitation channel is very weak compared to the elastic process. This is not true below 10 eV, where rotationally inelastic DCS are significant. The importance of rotationally inelastic channel is increased when strong interference effects make the elastic DCS become either smaller or bigger at a specific angle for each energy. Hence the ensuing DCS are characterized by a dip in the angular distribution. We, therefore, expect some significant discrepancy to appear between our theoretical DCS and the measured ones below 10 eV whenever the above feature may be present. Another source of approximations below 10 eV DCS is the treatment of exchange and polarization effects within the present model. Nevertheless, we see from Figs. 6.3.2(a)–(e) that there is a satisfactory agreement between theory and observation. However, the spherical model provides at times only a qualitative picture of the observed data since we see, for example, a very pronounced dip around 120^0 at 2 eV which is instead very shallow in the experimental data.

In Figs. 6.3.2(a)–(e), we have shown all results both on a linear as well as on a lograthmic scales. The higher angle dip in the DCS is more pronounced on the log scale; consequently we observe large discrepancy between theory and experiment at such angles.

This is probably due to the neglect of anisotropic terms in the SCE of the effective potential. Further, we see that at lower angles, the experimental DCS are very small as compared to computed values. As discussed by Boesten and Tanaka [53], the lowest angle DCS are rather too small in their measurements. It is also interesting to note that the background scattering is quite strong at 2 eV.

We now display our results at intermediate and high energies where our present model is likely to work markedly better [49]. In Figs. 6.3.2(f)-(i), we show our present DCS at 15, 20, 60 and 100 eV alongwith the measured points of Ref. 53 . We can see from these figures that there is indeed very good agreement between theory and experiment and that, in particular, the structure observed in the experimental DCS is clearly reproduced in our calculations at all energies above 10 eV.

Finally, we have displayed in Fig. 6.3.3 the computed integral and momentum transfer cross sections. We can see a shape-resonance feature around 5 eV which is caused by the d-wave component of our potential scattering mechanism. Note that in CH_4 and SiH_4 molecules this enhancement in the total cross section occurs around 7–8 eV and 2-3 eV respectively. Thus the 5 eV structure seen here in the e-GeH_4 case becomes quite interesting in comparison with other T_d-symmetry targets. Below 1 eV, we have also evidence of a minimum around 0.2 eV, but such a structure is very sensitive to the approximations involved in including exchange and polarization effects and therefore we expect that it will need possible confirmation from more extensive calculations that are presently planned in our laboratory.

In order to further confirm the 5 eV feature in the e-GeH_4 elastic scattering, we have plotted DCS as a function of energy in Fig. 6.3.4. The experimental DCS of Boesten and Tanaka [53] clearly exihibit this enhancement around 5 eV; this shape resonance phenomena is also present in our calculations (Fig. 6.3.4). It is still to be seen if measured total cross sections and more accurate calculations reveal this structure.

It is still interesting to note, however, that the present calculations, which effectively decouple each contributing partial wave in the spatial region where the potential exists, are indeed presenting a fairly good description of the scattering process. Since the coherent sum of angular momenta carried out to yield the DCS is a result of dynamical interference between trajectories, we are able to say that the present *spherical* potential is realistically treating such interference effects. The lack of angular anisotropy in the chosen interac-

tion prevents us from correctly including, however, the potential coupling which causes additional interference in the multichannel S–matrix of the full problem [1]. However, it appears from the present results that, at least above 10 eV, such further effects are rather negligible and that the heavy GeH_4 target can be considered as being essentially still during the interaction ($\tau_{\rm coll} << \tau_{\rm rot}$) and is approximately spherical when probed by the impinging electron. Thus, the possible adiabatic convolution of the scattering amplitude over rotational eigenstates can be approximately treated via its spherical component only: i.e., we can write,

$$\begin{aligned} f_{\rm tot} &= \sum_{i,f} f(\Omega) \\ &\simeq \sum_{i,f} \langle \psi_i | f(\Omega; \hat{\mathbf{r}}_{N+1}) | \psi_f \rangle \\ &\simeq \sum_{i,f} \langle \psi_i \sum_{\lambda,m} f_{\lambda m}(\Omega) X_{\lambda m}(\hat{\mathbf{r}}_{N+1}) | \psi_f \rangle \\ &\simeq \sum_{i,f} \langle \psi_i | f_{00}^{i \rightarrow f}(\Omega) | \psi_f \rangle \\ &\simeq \sum_{i,f} f_{00}(\Omega) \delta_{if} \end{aligned} \tag{6.3.1}$$

where Ω is the space–fixed orientation, $\hat{\mathbf{r}}_{N+1}$ is the body–fixed electron–molecule orientation vector and the $|\psi_i\rangle$ is rotational eigenfunction of the molecule. Because of time scale considerations, vibrational excitations are even less likely to occur.

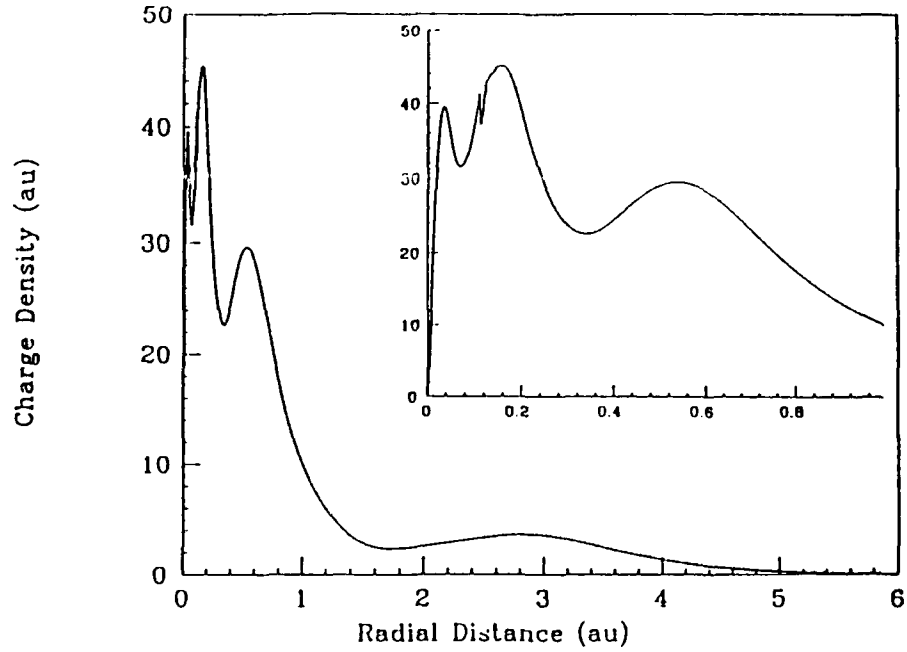

Fig. 6.3.1(a). Electronic Charge density of the GeH_4 molecule.

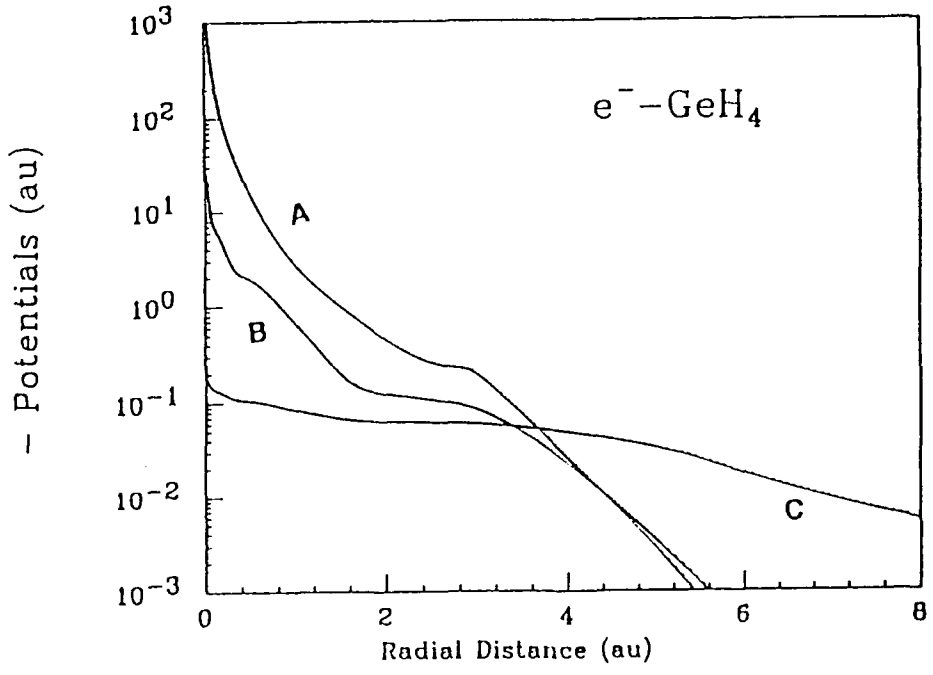

Fig. 6.3.1(b). Various potential terms (in atomic units) for the e–GeH_4 system. A, V_{st}; B, V_{ex}; C, V_{pol}.

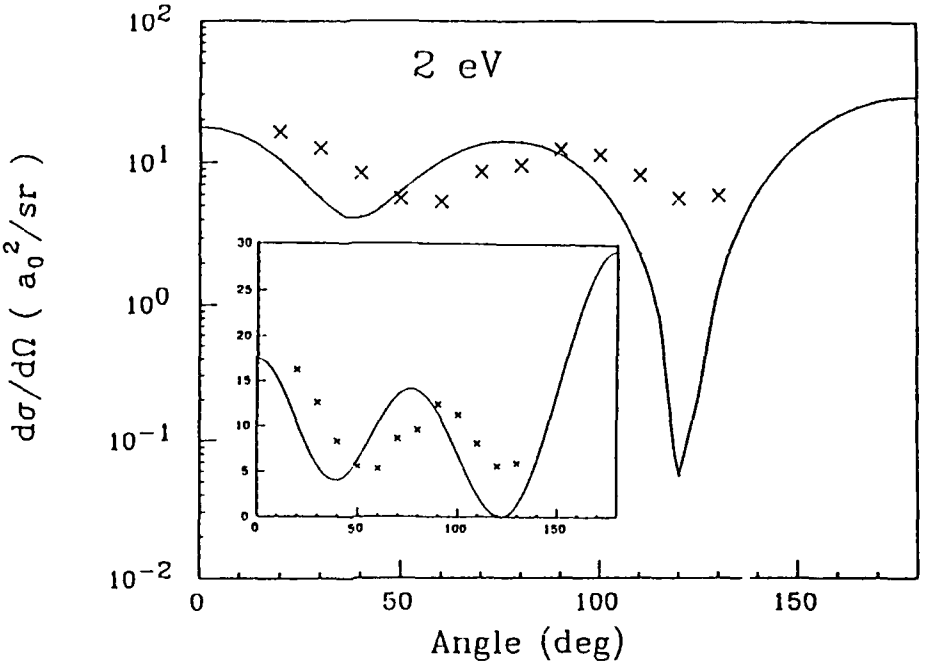

Fig. 6.3.2 (a). Differential cross sections for the e-GeH_4 system at 2 eV in the present SEP model (solid line). The crosses are the experimental points from Ref. 1. Note that we have shown both the linear and log scales.

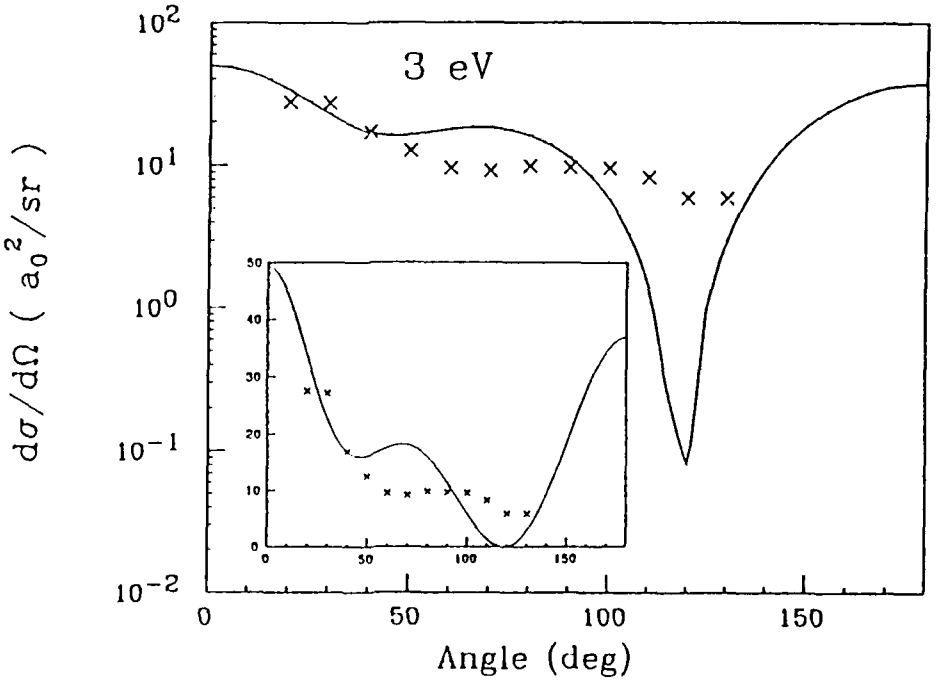

Fig. 6.3.2 (b). Differential cross sections for the e-GeH_4 system at 3 eV in the present SEP model (solid line). The crosses are the experimental points from Ref. 1. Note that we have shown both the linear and log scales.

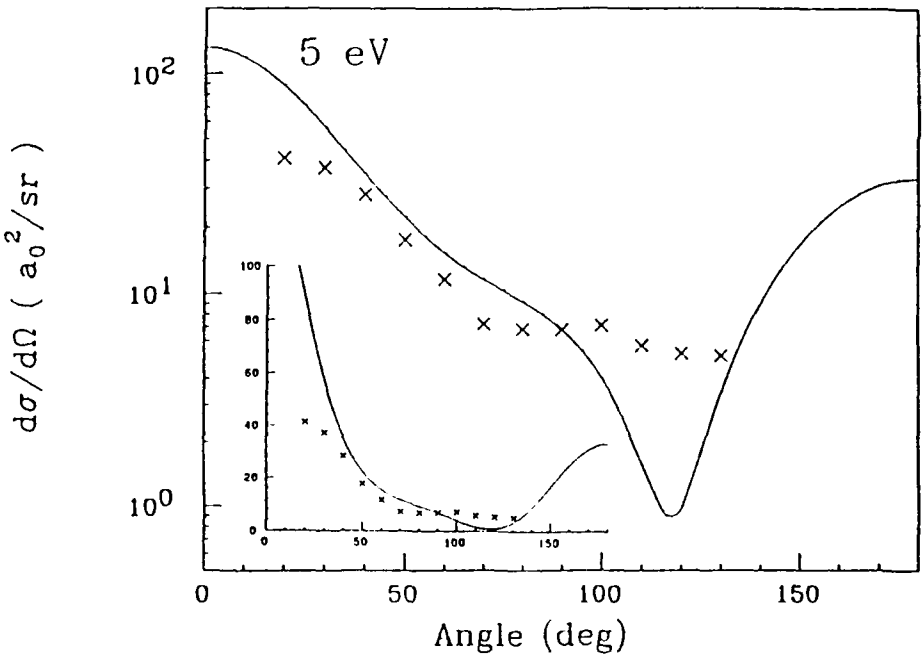

Fig. 6.3.2 (c). Differential cross sections for the e-GeH_4 system at 5 eV in the present SEP model (solid line). The crosses are the experimental points from Ref. 1. Note that we have shown both the linear and log scales.

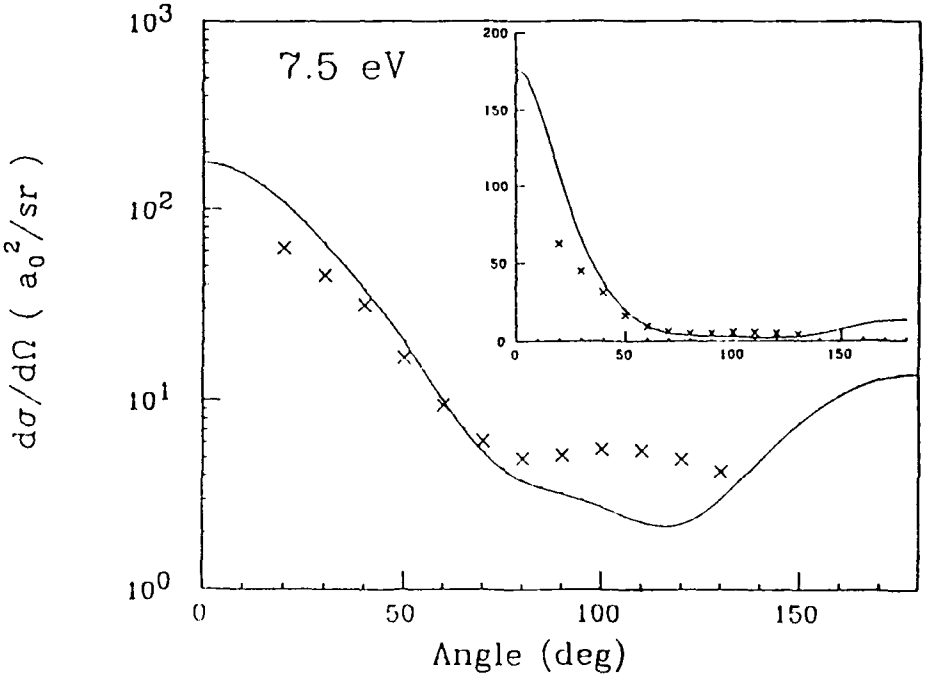

Fig. 6.3.2 (d). Differential cross sections for the e-GeH_4 system at 7.5 eV in the present SEP model (solid line). The crosses are the experimental points from Ref. 1. Note that we have shown both the linear and log scales.

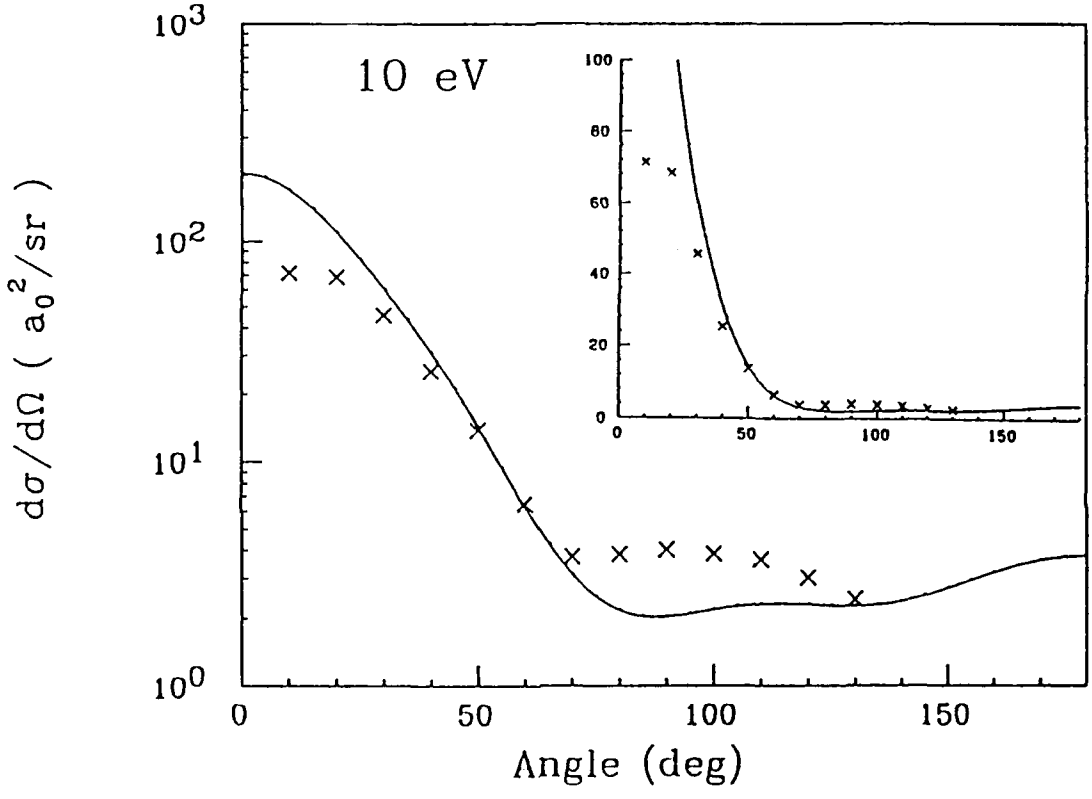

Fig. 6.3.2 (e). Differential cross sections for the e-GeH_4 system at 10 eV in the present SEP model (solid line). The crosses are the experimental points from Ref. 1. Note that we have shown both the linear and log scales.

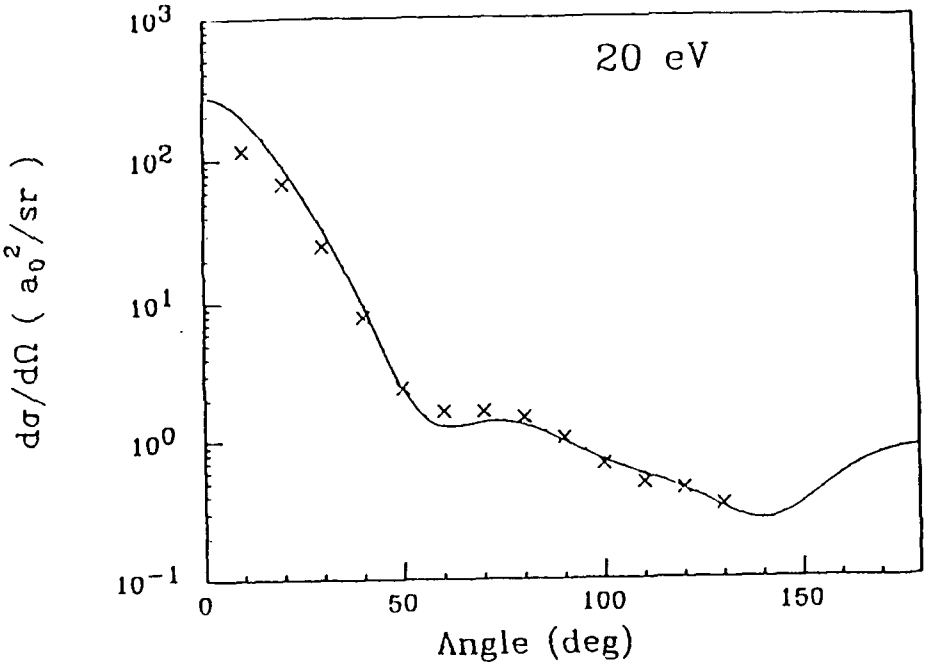

Fig. 6.3.2 (g). Differential cross sections for the e-GeH_4 system at 20 eV in the present SEP model (solid line). The crosses are the experimental points from Ref. 1. Note that we have shown both the linear and log scales.

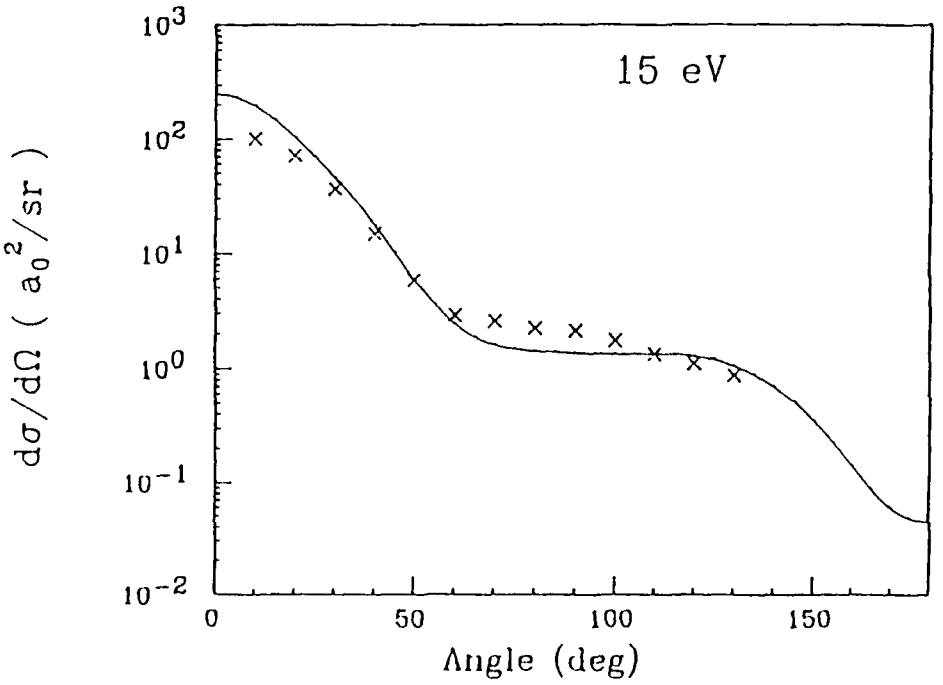

Fig. 6.3.2 (f). Differential cross sections for the e-GeH_4 system at 15 eV in the present SEP model (solid line). The crosses are the experimental points from Ref. 1. Note that we have shown both the linear and log scales.

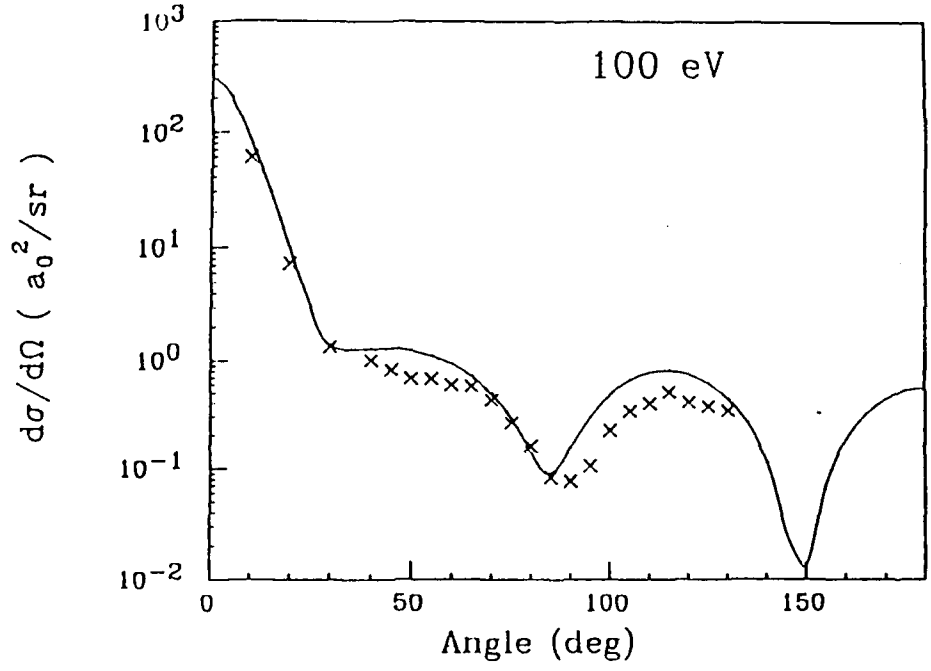

Fig. 6.3.2 (i). Differential cross sections for the e-GeH_4 system at 100 eV in the present SEP model (solid line). The crosses are the experimental points from Ref. 1. Note that we have shown both the linear and log scales.

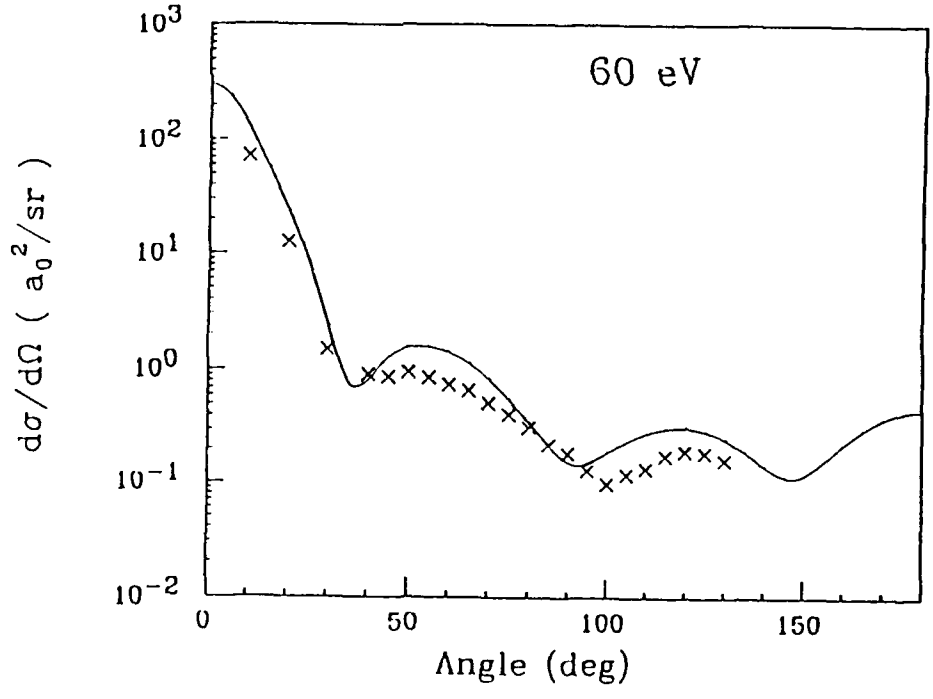

Fig. 6.3.2 (h). Differential cross sections for the e- GeH_4 system at 60 eV in the present SEP model (solid line). The crosses are the experimental points from Ref. 1. Note that we have shown both the linear and log scales.

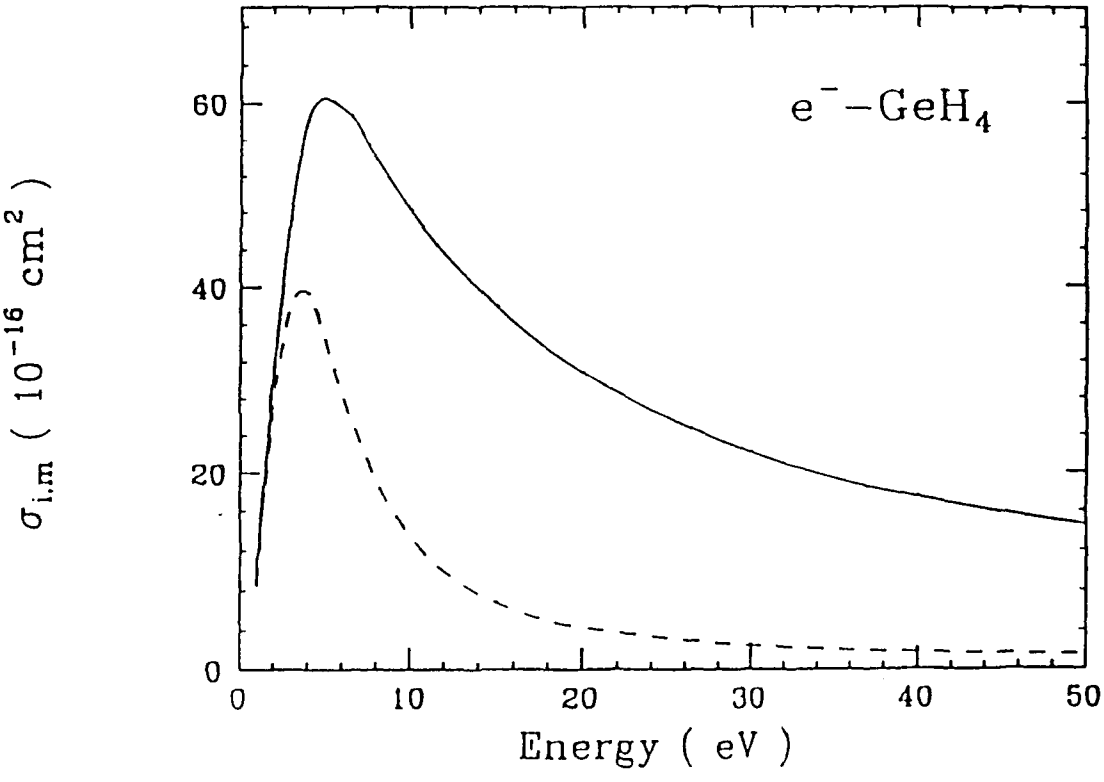

Fig. 6.3.3. Integral (solid line) and momentum transfer (dashed line) computed cross sections for e-GeH_4 for collision energies from 1 to 100 eV.

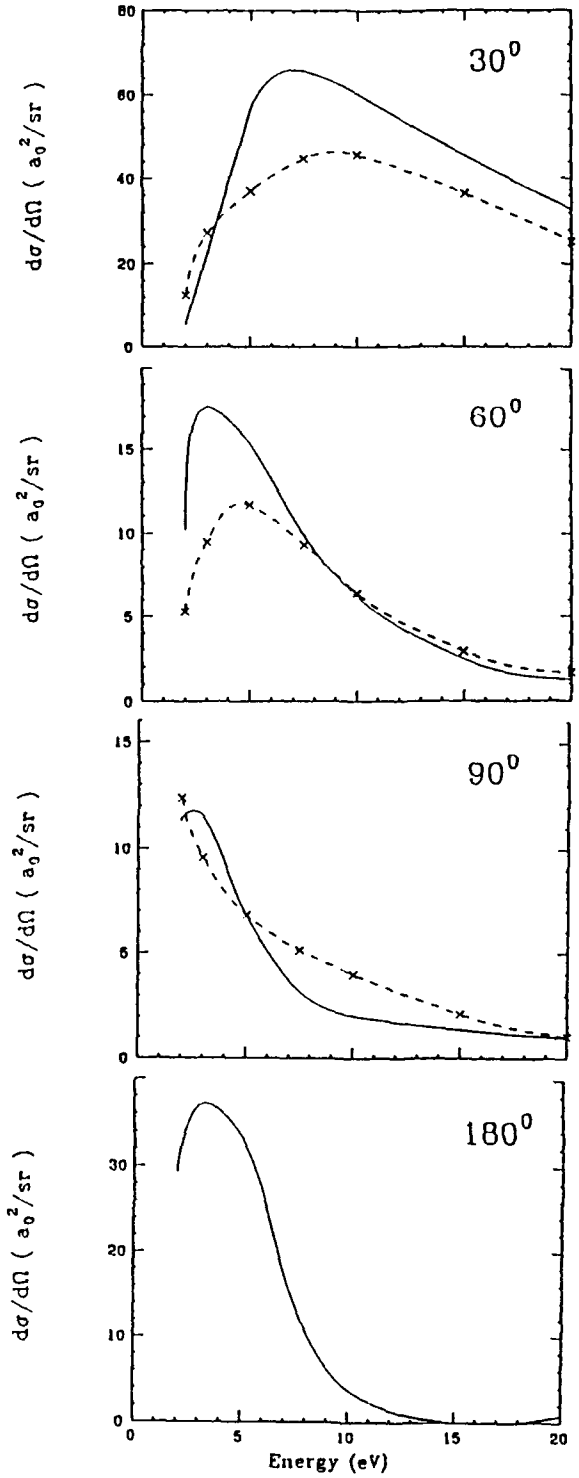

Fig. 6.3.4 Experimental (crosses) and theoratical(solid line) DCS as a function of energy at few selected angles.

6.4 Electron–NH_3 Cross Sections

There are recent measurements on the e–NH_3 total [54-55] and differential [56] cross sections in the present energy region; however, no *ab initio* calculation (with exact exchange plus polarization effects) exists in order to make a proper comparison with the experiment. The Schwinger multichannel variational (SMV) calculations of Pritchard *et al.* [57] are carried out only at the fixed-nuclei static–exchange level; consequently, in the absence of polarization effects, it may not be proper to compare these SMV results with experimental cross sections. More recently, Parker *et al.* [58] have employed complex Kohn variational principle to study e–NH_3 problem at the *ab initio* level. The only other fixed–nuclei close–coupling calculations employing model exchange and polarizations potentials are due to Jain and Thompson [59] and Gianturco [60].

Encouraged by the success of our present calculations on the CH_4, SiH_4, and GeH_4 molecules, we have extended our ESEP theory (Section 4) for the e–NH_3 case where recent measured data are available. We are in the process of completing these results by carrying out a careful checking on the convergence of the final DCS and integral quantities. As is well known, for a polar molecule, the ANA theory predicts infinite cross section in the forward direction. Here we restrict ourselves only to the eigenphase sum, partial cross sections, and momentum transfer cross sections. We also present DCS and integral parameters, but these numbers can be considered only prelimenary at this time. In Tables 6.4.1, 6.4.2, and 6.4.3, we have provided our results on the eigenphase sums, partial cross section and momentum transfer parameters in the ESE (without polarization) and ESEP (with polarization) models. These tables show that the polarization effects introduce significant changes in the collisional quantities.

First in Fig. 6.4.1, we compare the ESE (dashed curve) and ESEP (solid lines) eigenphase sums for all the three symmetries (A_1, A_2, and E). In the next figure 6.4.2, we have displayed similar data on the partial cross sections. As mentioned above, the effects of polarization force is significant at all energies shown in these figures. Next in Fig. 6.4.3, we illustrated our $\sigma_t$and $\sigma_m$cross sections along with experimental data. We see a qualitative agreement between our theory and measurements. The enhancement in both the integral and momentum transfer cross section around 10 eV is faithfully reproduced by our calculations.

Finally, we show our preliminary angular functions in Fig. 6.4.4 at 8.5 and 15 eV

along with measured points. We have shown our theoretical results at all angles. Also shown in this figure are the static-exchange (without polarization) SMV calculations of McKoy and coworkers [57]. It is clear that theoretical curves are very close with relative measurements of Ref. 56. We have used the same normalization criterion as in Ref. 57. A more careful analysis of our DCS in terms of convergence and aslo the normalization of experimental data with respect to our results will make this comparison (Fig. 6.4.4) even better. Also our calculated values in Fig. 6.4.4 are taken at 8.0 eV rather than at 8.5 eV as is the case with measured [56] and calulated [57] values. Unfortunately, the experimental DCS on the low energy e–NH_3 scattering are not available properly. The measured values of Shyn [56] are only preliminary and definitive conclusion about the agreement between theory and experiment is very hard to draw at this moment.

We are considering another possiblity of testing convergence of our DCS with respect to the use of Born theory in closure formulae. Recently, Parker *et al.* [58] have suggested the use of closure formula at the level of scattering amplitude rather than at the cross section level.

Table 6.4.1

Eigenphase sums (in radians) for the e–NH_3 elastic collisions in the ESE and ESEP models.

Energy (eV)	ESE A_1	ESEP A_1	ESE A_2	ESEP A_2	ESE E_x	ESEP E_x
0.01	0.1791	0.4367	0.0049	0.005	0.0461	0.0495
0.025	0.0832	0.3964	0.0061	0.0065	0.0484	0.0569
0.05	−0.00857	0.3535	0.00745	0.0084	0.0495	0.0663
0.075	−0.0718	0.3245	0.0085	0.0099	0.0491	0.0739
0.10	−0.0671	0.302	0.0094	0.0113	0.0477	0.0803
0.25	--0.2407	0.2164	0.0132	0.0181	0.0297	0.1054
0.50	−0.4105	0.1293	0.017	0.0271	−0.0143	0.1247
0.75	−0.5299	0.0611	0.019	0.0343	−0.0619	0.1347
1.0	−0.6274	−0.00047	0.0194	0.0399	−0.108	0.1427
2.0	−0.9284	−0.2081	0.0089	0.0509	−0.2521	0.1942
3.0	−1.1656	−0.3666	−0.0088	0.0547	−0.3352	0.2930
4.0	−1.3569	−0.484	−0.0228	0.0627	−0.376	0.4335
5.0	−1.511	−0.569	−0.0309	0.0762	−0.3829	0.6071
6.0	−1.6359	−0.629	−0.0349	0.0933	−0.3543	0.8079
8.0	−1.819	−0.6929	−0.035	0.134	−0.2024	1.228
10.0	−1.932	−0.705	−0.023	0.185	0.001	1.578
15.0	−2.0545	−0.6535	0.0367	0.329	0.4134	2.1325
20.0	−2.0938	−0.606	0.0999	0.462	0.6568	2.441

Table 6.4.2

Partial cross sections (in units of 10^{-16} cm^2) for the e–NH_3 elastic collisions in the ESE and ESEP models.

Energy (eV)	ESE A_1	ESEP A_1	ESE A_2	ESEP A_2	ESE E_x	ESEP E_x
0.01	2043.3	2792.0	83.33	83.32	709.323	710.6
0.025	737.01	1028.4	33.34	33.35	283.59	284.58
0.05	342.89	483.02	16.68	16.69	141.62	142.93
0.075	220.61	308.14	11.12	11.13	94.25	95.56
0.10	167.28	223.1	8.35	8.36	70.55	71.84
0.25	65.38	78.0	3.35	3.36	27.867	28.968
0.50	36.67	34.42	1.68	1.70	13.81	14.52
0.75	24.70	21.05	1.12	1.14	9.29	9.71
1.00	19.79	14.83	0.841	0.865	7.13	7.32
2.00	12.525	6.71	0.42	0.44	4.087	3.932
3.00	10.288	5.02	0.28	0.30	3.262	3.273
4.00	9.186	4.63	0.218	0.240	3.082	3.605
5.00	8.46	4.589	0.181	0.212	3.167	4.366
6.00	7.90	4.657	0.157	0.20	3.375	5.235
8.00	7.056	4.874	0.125	0.193	3.978	6.463
10.00	6.42	5.05	0.107	0.198	4.505	6.723
15.00	5.276	5.07	0.095	0.242	4.700	5.982
20.0	4.473	4.717	0.102	0.289	4.210	5.106

Table 6.4.3.

Total and momentum transfer cross sections (10^{-16} cm^2) for electron scattering with NH_3 molecules.

Energy (eV)	Theory (σ_t)	Expt.[1] (σ_t)	Expt.[2] (σ_t)	Theory (σ_m)	Expt.[3] (σ_m)
0.01					
0.025	1566.3	–	–	791.42	–
0.050	768.54	–	–	371.91	–
0.075	503.25	–	–	233.67	–
0.10	371.15	–	–	167.70	–
0.25	138.68	–	–	56.71	–
0.50	65.24	–	–	24.67	–
0.75	41.57	–	–	14.88	–
1.00	30.29	14.7±1.3		10.4	10.0
2.00	14.98	10.9±0.9	11.0	4.93	5.1
3.00	11.84	11.2±0.9*	11.0	4.94	5.1
4.00	12.04	12.0±1.0	12.5	6.70	6.25
5.00	13.48	14.5±1.2	15.75	8.96	8.2
6.00	15.24	15.5±1.3	18.0	11.11	9.1
8.00	17.85	17.1±1.4	22.0	13.78	9.8
10.0	18.52	17.5±1.5	23.5	14.06	10.2
15.0	17.93	16.0±1.5	20.0	12.12	–
20.0	15.09	14.2±1.2	17.25	9.08	

[1]Ref. 54

[2]Ref. 55

[3]Ref. 57

* at 3.1 eV

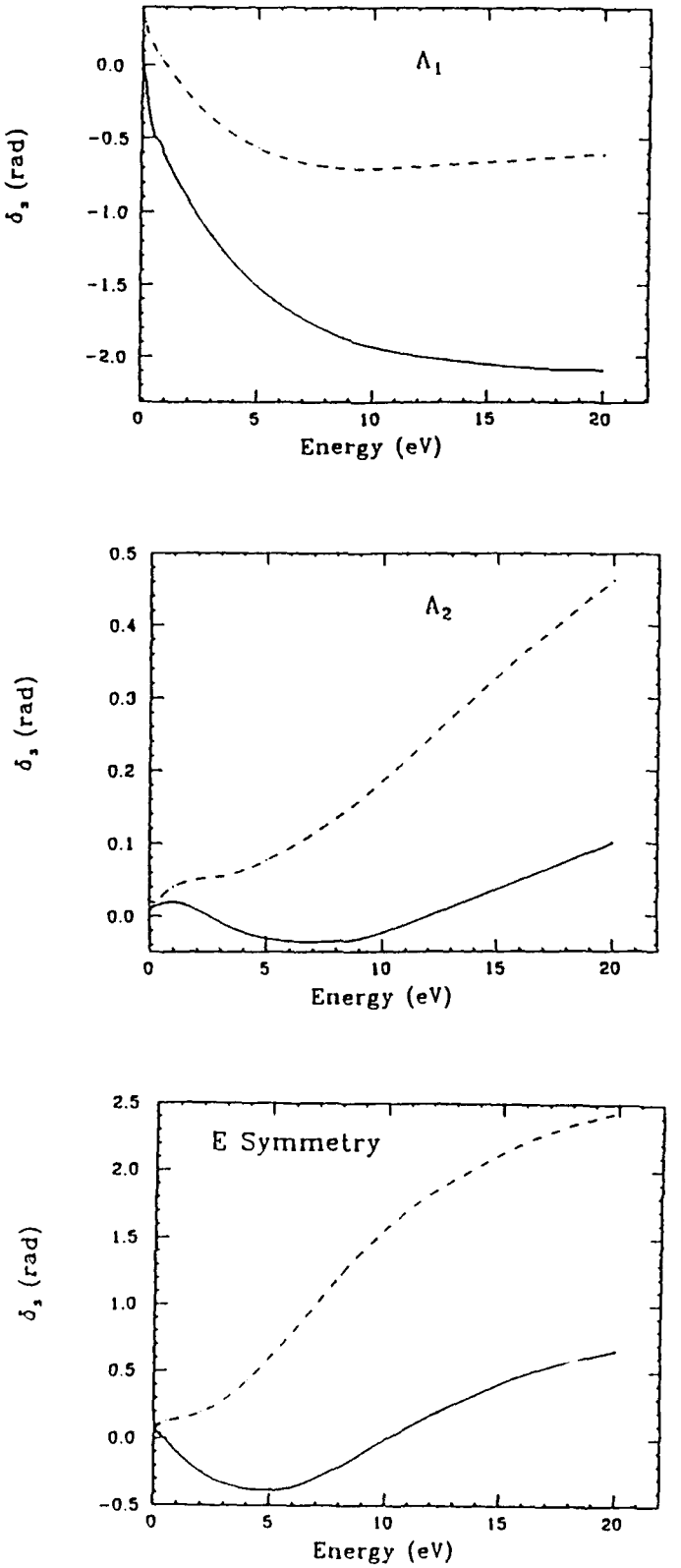

FIG. 6.4.1 e–NH_3 eigenphase sums in the ESE (solid) and ESEP (dashed) models.

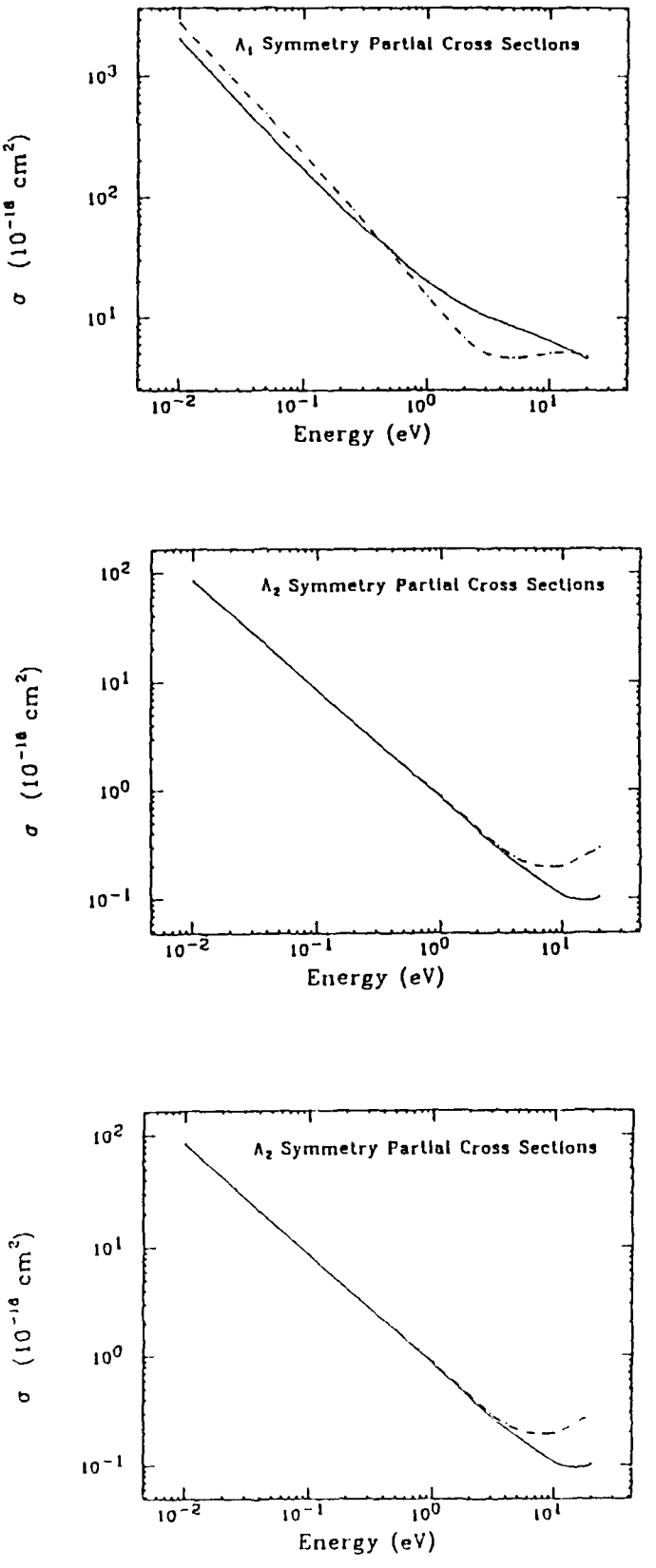

FIG. 6.4.2 e NH_3 partial cross sections in the ESE (solid) and ESEP (dashed) models.

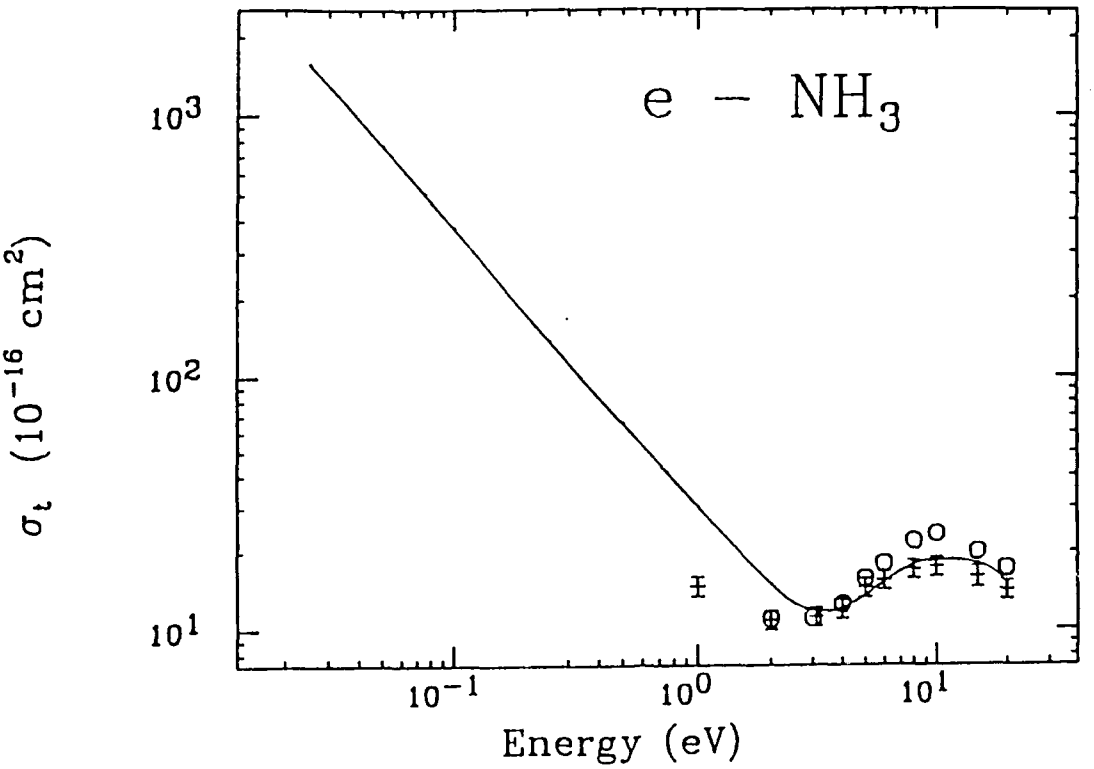

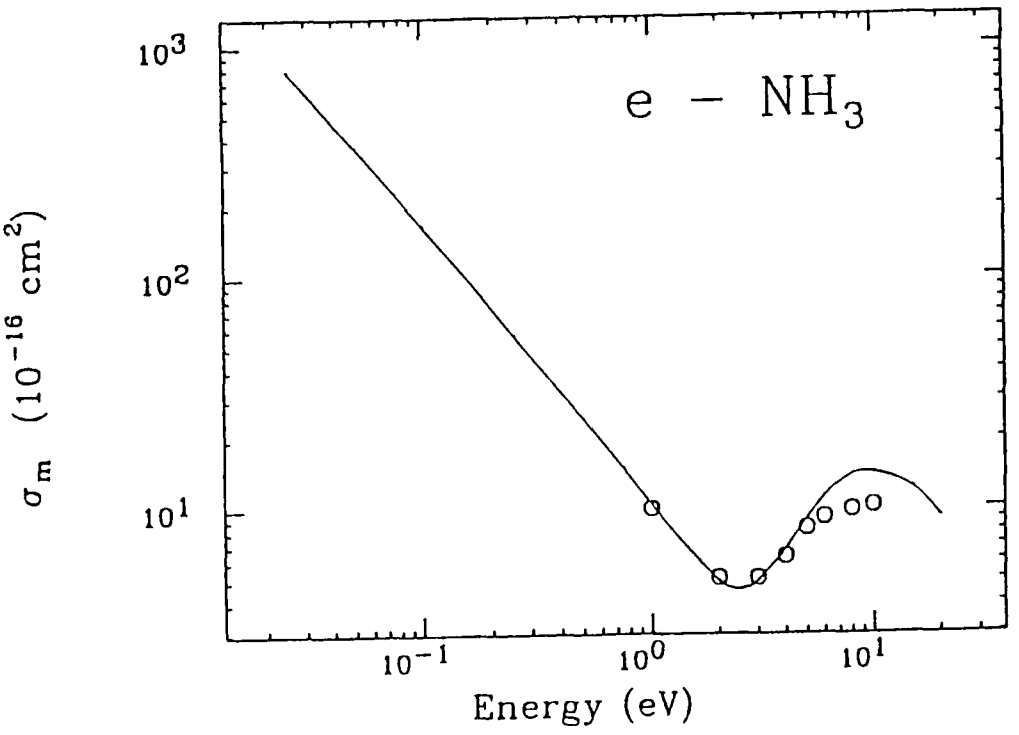

FIG. 6.4.3 Total (σ_t) and momentum transfer (σ_m) cross section in the present ESEP model (solid line). Expt. : +, Ref. 54; open circles, Ref. 55 ; for σ_m, the open circles are the recommended values of Itikawa as given in Ref. 57.

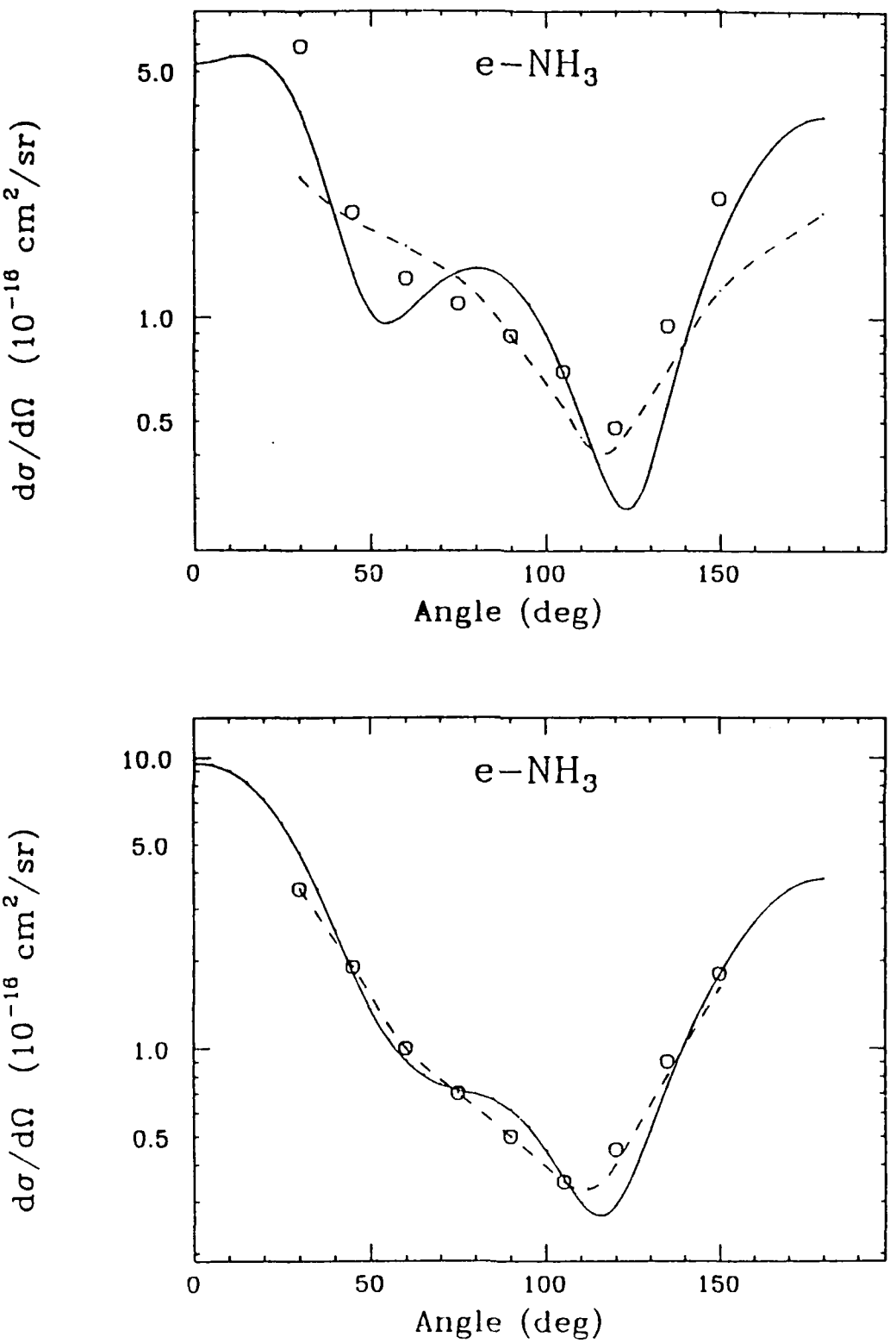

FIG. 6.4.4 e NH_3 DCS at 8 and 15 eV in the present ESEP model (solid line). The dashed curves are the SMC calculations from Ref. 57. The expt. points (relative data) are from Ref. 56.

6.5 Electron–H_2O Cross Sections

We are in the process of determining final converged cross sections (DCS, σ_t, σ_m) for elastic and rotationally inelastic processes. The H_2O molecule is polar molecule with above critical value of the dipole moment. Thus the dipole moment of water molecule is capable of supporting infinite number of bound states of the incoming electron. We are modifying our existing codes in order to include full contribution of the higher partial waves which is important in the forward angle scattering. There are several recent measurements on the σ_t[61-64], σ_m[65] and the DCS [66–68] parameters for the e–H_2O system. We will make a comparison between our theory and these measured data. In addition, SMV results [69] and other calculations [70] will also be included in the comparison.

Here, we show the values of eigenphase sums (Table 6.5.1) and partial cross sections (Table 6.5.2) for all the four symmetries A_1, A_2, B_1, and B_2. In these tables, we have included our calculations with and without polarization effects. Again we see considerable effect of polarization force in the e–H_2O scattering. In this case, there is no resonance or RT effects. This is mainly due to the dominance of dipole scattering.

Table 6.5.1:

Eigenphase sums for e–H_2O scattering in the ESE and ESEP models

E	A_1		A_2		B_1		B_2	
(eV)	ESE	ESEP	ESE	ESEP	ESE	ESEP	ESE	ESEP
0.5	−0.463	−0.332	−0.0024	0.0129	−0.167	−0.1296	−0.023	0.066
1.0	−0.713	−0.544	−0.0362	−0.0114	−0.326	−0.272	−0.070	−0.0091
2.0	−1.051	−0.853	−0.125	−0.090	−0.563	−0.488	−0.209	−0.127
3.0	−1.306	−1.088	−0.196	−0.155	−0.725	−0.636	−0.299	−0.210
4.0	−1.483	−1.248	−0.236	−0.190	−0.845	−0.743	−0.358	−0.270
5.0	−1.600	−1.350	−0.254	−0.202	−0.931	−0.818	−0.383	−0.303
6.0	−1.676	−1.409	−0.258	−0.199	−0.986	−0.863	−0.375	−0.306
7.5	−1.732	−1.441	−0.244	−0.177	−1.03	−0.889	−0.318	−0.273
10.0	−1.752	−1.426	−0.205	−0.121	−1.06	−0.897	−0.179	−0.1869
15.0	−1.747	−1.383	−0.139	−0.033	−1.09	−0.893	0.072	−0.0179

Table 6.5.2:

Partial Cross Sections for e–H_2O scattering in the ESE and ESEP models

E	A_1		A_2		B_1		B_2	
(eV)	ESE	ESEP	ESE	ESEP	ESE	ESEP	ESE	ESEP
0.5	48.40	45.30	3.26	3.28	16.14	15.74	15.03	15.2
1.0	27.28	24.51	1.66	1.64	9.79	9.25	7.74	7.62
2.0	16.62	13.94	1.05	0.938	6.61	6.02	4.33	4.10
3.0	12.38	10.72	0.787	0.709	5.32	4.72	3.29	3.03
4.0	10.68	9.31	0.636	0.564	4.67	4.10	2.91	2.61
5.0	9.66	7.50	0.531	0.471	4.28	3.74	2.78	2.43
6.0	8.93	7.998	0.453	0.402	3.97	3.47	2.74	2.33
7.5	7.63	6.550	0.362	0.322	3.56	3.11	2.78	2.27
10.0	7.31	6.107	0.270	0.248	3.08	2.72	3.08	2.37
15.0	6.28	5.485	0.208	0.215	2.55	2.33	3.46	2.66

7. EFFECT OF GAS TEMPERATURE ON THE CROSS SECTION

At a given temperature T, a typical polyatomic molecule has many rotational states populated. From theoretical point of view, it is easier to calculate rotational excitation cross sections from the ground state ($J = 0$) to any final J value of a given molecular system. In many practical cases, the transfer of rotational angular momentum J_t ($|J'-J| \leq J_t \leq J+J'$) in any scattering event involves very high values of J and J'. For spherical top molecules, the differential cross sections (DCS) for rotational excitation from any initial state J to a final state J' can be evaluated as follows [9-15],

$$\frac{d\sigma}{d\Omega}(J \rightarrow J'; k^2, \theta) = \sum_{J_t=|\Delta J|}^{2J+\Delta J} \frac{(2J+1+2\Delta J)}{(2J+1)(2J_t+1)} \frac{k'}{k_t} \frac{d\sigma}{d\Omega}(0 \rightarrow J_t; k^2, \theta), \qquad (7.1)$$

where k' and k_t are kinematic factors of the wavevector of projectile in the $J \rightarrow J'$ and $0 \rightarrow J_t$ cases respectively and $J' = J + \Delta J$. In the summation over J_t in Eq. (7.1), usually only a few terms are needed with small J_t values. For example, in the present case of CH_4 and SiH_4 molecules, the $J_t = 0, 3, 4$, and 6 values are sufficient (note that the $J_t = 1, 2$ and 5 values are not allowed for molecules having T_d point symmetry group). Thus, given a set of cross sections for a few $0 \rightarrow J_t$ transitions only, Eq. (7.1) can easily be used to determine rotational excitation quantities from any initial J value including very high ones. This is essential when one needs to average the cross section over the distribution of rotational states at a given temperature. Eq. (7.1) is valid under the adiabatic-nuclear-rotation (ANR) approximation, i.e., the incident and scattered electron is moving much faster than the rotational motion of the molecule. In circumstances where the ANR approximation fails (for example, near the threshold energy or a sharp shape resonance, or for a polar molecule), Eq. (7.1) may not be valid. In the present case of spherical top molecules and the energy range of 0.5-20 eV, the ANR approximation is valid and we use Eq. (7.1) to generate various cross sections with different initial J values for all possible final J' values allowed by the J_t selection rule.

If one neglects the kinematic factors (k' and k_t) from Eq. (7.1), the cross sections between the rotational states J and $J' = J \pm \Delta J$ can further be written as [12-13],

$$\frac{d\sigma}{d\Omega}(J \rightarrow J \pm \Delta J) = (1 \pm \frac{2\Delta J}{2J+1}) A(|\Delta J|), \qquad (7.2)$$

with

$$A(|\Delta J|) = \sum_{J_t=|\Delta J|}^{2J \pm \Delta J} \frac{d\sigma}{d\Omega}(0 \rightarrow J_t)/(2J_t+1). \qquad (7.3)$$

where we assume that $2J - |\Delta J|$ is larger than any J_t that contributes appreciably to the sum in Eq. (7.3). In other words, we assume that $d\sigma/d\Omega(0 \rightarrow J_t)$ is almost zero for $J_t \geq 2J - |\Delta J|$, so that the upper limit of the summation in Eq. (7.3) is equivalent to infinity. Thus, we can easily write $|\Delta J|$ in the argument of A and not J or ΔJ. The Eqs. (7.2)-(7.3) above are exact under the adiabatic-rotation approximation. The values of $d\sigma/d\Omega$ for various $|\Delta J|$ will be given and discussed later for both the molecules.

The $d\sigma/d\Omega\,(0 \rightarrow J_t)$ can be expanded as,

$$\frac{d\sigma}{d\Omega}(0 \rightarrow J_t) = \frac{k_t}{k} \sum_L A_L(0 \rightarrow J_t) P_L(\cos\theta), \tag{7.4}$$

where $P_L(\cos\theta)$ are Legendre polynomials and the expansion A_L coefficients are given by [27, see Section 4.4],

$$A_L(0 \rightarrow J_t) = \frac{(-1)^L}{4k^2} \sum_{\ell\ell'\bar{\ell}\bar{\ell}'} BC(\ell L\bar{\ell};000)C(\ell' L\bar{\ell}';000)(-1)^{J_t} W(\ell\ell'\bar{\ell}\bar{\ell}';J_t L) M^{J_t m}_{\ell\bar{\ell}} M^{J_t m^*}_{\ell'\bar{\ell}'}. \tag{7.5}$$

The **M** matrix is defined as,

$$M^{JM}_{\ell\ell'} = \sum_{mm'hh'p\mu} (-1)^m \bar{b}^{p\mu}_{\ell hm} C(\ell J\ell';mm'M) b^{p\mu}_{\ell' h'm'} \mathbf{T}^{p\mu}_{\ell h,\ell' h'}, \tag{7.6}$$

and $B = [(2\ell+1)(2\ell'+1)(2\bar{\ell}+1)(2\bar{\ell}'+1)]^{\frac{1}{2}} i^{\ell-\ell'}(-i)^{\bar{\ell}-\bar{\ell}'}$. The C-coefficients are the usual Clebsch-Gordan coefiecients and the **T**-matrix is defined in terms of scattering **S** matrix as $\mathbf{T} = (\mathbf{S}-\mathbf{1})$ where $\mathbf{S} = (\mathbf{1}+i\mathbf{K})/(\mathbf{1}-i\mathbf{K})^{-1}$ is written in terms of reaction **K** matrix for each symmetry $(p\mu)$. In Eqs. (7.5)-(7.6), W(abcd;ef) is the well known Racah coefficient and the $b^{p\mu}_{lhm}$ coefficients are expansion terms in the definition of symmetry adapted basis functions in terms of real spherical harmonics [1]. For the case of total and momentum transfer cross sections, Eq. (7.5) can be greatly simplified to give simple expressions [see Eqs. 4.4.9-4.4.10].

Here we have investigated the behaviour of various scattering parameters on the initial rotational state J and temperature of the gas. This is important because in rotational equilibrium at room temperature or higher, the gas molecules occupy many different rotational states. A typical Maxwellian rotational state distribution for the CH_4 and SiH_4 gases is shown in Fig. 7.1 at 300 and 500 K. We see from Fig. 7.1 that for CH_4 the most probable initial states at 300 K are distributed around $J = 6$ (and $J = 8$ at 500 K),

while for the heavier SiH_4 case, the initial state has an even higher value of $J = 8$ (and $J = 11$ at 500 K). In addition, we also study the dependence of the rotationally elastic and inelastic processes on the initial state J. Very recently, Müller *et al.* [52] have measured state–to–state rotational excitation cross sections from the broadened (because of rotational process) energy–loss peaks by using an analysis of Shimamura [14]. Shimamura [9–15] has described in a series of papers the various aspects of rotational transitions in molecules and established several important theorems (see later) regarding the dependence of collisional parameters on the initial rotational state and the gas temperature T.

The basic scattering parameter is the differential cross section as a function of scattering angle (θ) and energy (k^2) for any rotational transition $J \rightarrow J + \Delta J$. A large set of cross sections can be obtained for state–to–state rotational transitions and rotationally summed quantities; however, it would be meaningful to derive compact information from this huge amount of cross section data. For example, the differential moments (the dependence on θ and k^2 is suppressed),

$$\frac{dS}{d\Omega}(\mu; J) = \sum_{J'} (E_{J'} - E_J)^{\mu} \frac{d\sigma}{d\Omega}(J \rightarrow J'), \tag{7.7}$$

and the integral moments $S(\mu; J)$ characterize the behaviour of the electron–molecule system. The zeroth–order integral moment with $\mu = 0$, $S(0; J)$, is the usual integral (or total) cross section (summed $\sigma_t(J)$ or state–to–state $\sigma_t(J \rightarrow J')$), while first–order integral moment, $S(1; J)$, is the energy–loss or stopping cross section. Another useful parameter is the momentum transfer cross section (summed $\sigma_m(J)$ or state–to–state $\sigma_m(J \rightarrow J')$) which is obtained by integrating the differential cross section (Eq. 7.1) with the weighted factor of $(1 - \cos\theta)$. In Eq. (7.7), $E_J = BJ(J + 1)$ is rotational energy of the molecule in Jth level and B is the molecular rotational constant. For CH_4 and SiH_4 molecules the values of B are taken to be 65.11 meV and 35 .5 meV respectively. Higher order moments ($\mu \geq 2$) in Eq. 7.7 provide information on statistical fluctuations of the energy–loss spectrum from its mean value.

In practice, all observable physical quantities are connected with these moments averaged over the rotational distribution function $N(J; T)$, namely

$$< S(\mu) > = \sum_J N(J; T) S(\mu; J) \Big/ \sum_J N(J; T), \tag{7.8}$$

where $N(J;T) = g(J)e^{-E_J/\kappa T}$ is the Maxwellian distribution function, κ is the Boltzmann constant and $g(J) = (2J+1)^2$ is the statistical weight of the Jth state of a spherical top. In the definition of $N(J;T)$, we have neglected the effect of nuclear spins.

Another interesting aspect is the relationship between rotational excitation and deexcitation processes. Shimamura [12-13] has derived partial sum rules for the $J \rightarrow J \pm \Delta J$ rotational transitions. From Eqs. (7.2)-(7.3), we see that (denoting the cross section quantity in general by a)

$$\frac{a(J \rightarrow J + \Delta J)}{a(J \rightarrow J - \Delta J)} = \frac{2J + 1 + 2\Delta J}{2J + 1 - 2\Delta J}, \tag{7.9}$$

and the sum $a(J \rightarrow J + \Delta J) + a(J \rightarrow J - \Delta J)$ is a constant equal to $2A(|\Delta J|)$. However, if we include the effects of kinematic factors, particularly at the lower bound of the present energy region, Eq. (7.9) may be true only approximately. Shimamura [12–13] has also discussed the relationship between weighted rotational excitation and de-excitation quantities, i.e., $\Delta E^{+} a(J \rightarrow J + \Delta J)$ and $\Delta E^{-} a(J \rightarrow J - \Delta J)$. Here $\Delta E^{\pm}$ are transition energies given by $B\Delta J[\pm(2J+1) + \Delta J]$. We will also discuss these partial sum rules and ratios for the CH_4 and SiH_4 cross sections.

We have therefore carried out a systemetic study on the dependence of differential cross section (Eq. 7.1) and moments (Eq. 7.7) on the initial rotational state J and of the averaged quantities (using Eq. 7.8) on the gas temperature T. We will compare our predictions with the theorems as discussed by Shimamura [9–15] regarding the J or T dependence of various physical quantities. All our results are presented only for the spherical top molecules (CH_4 and SiH_4). The basic scattering quantity, i.e., $d\sigma/d\Omega(0 \rightarrow J_t; k^2, \theta)$, is taken from our recent *ab initio* calculations [see Sections 6.1 and 6.2] on the e–CH_4 and SiH_4 systems. These calculations treat electron–exchange interaction exactly via iterative procedure and the charge correlation and polarization effects are included approximately in a parameter–free perturbative approach (see Section 4.5). The final results on rotationally summed differential, integral, and momentum transfer cross sections (see Sections) compared very well with experimental data. In particular, at very low energies (below 1 eV), where various correlation terms (such as the polarization and exchange) play rather crucial role, our calculations [4–5] reproduced all salient features in the differential as well as integral cross sections (for example, the Ramsauer Townsend minimum in the total cross section) both in quality and quantity. Therefore, in the following analysis, we assume that the input data on the state–to–state differential cross sections are of reliable quality.

Our previous calculations [4] on the e–CH_4 state–to–state rotational transitions were in qualitative agreement with the experimentally extracted values of Müller *et al.* [52]. There were, however, some differences between theory and experiment for these rotationally inelastic channels where cross sections are very small compared to the pure elastic case. For example, for the $0 \rightarrow 3$ transition, calculated values show zero cross section in the forward direction, while experimental points exihibit no such behaviour. This is one of the purposes of this article, i.e., to resolve this discrepancy between theory and experiment.

7.1 Sum Rules for Rotationally Summed Parameters

It has been shown by several authors (see Ref. 15 for details) that the zeroth–order moments (Eq. 7.7), differential or integral, are independent of the initial rotational state J and hence on the gas temperature T. It is also shown for spherical top molecules [12–13] that the first–order moment is also independent on J and T, i.e., $S(0;J) = S(0;0); S(1;J) = S(1;0)$. In addition, the second and third order moments are shown to depend linearly on the energy E_J of the initial state [14]. In Table 7.1, we have given our actual calculations on the state–to–state rotational excitation cross sections for the e–CH_4 system at 5 eV for the DCS (at few angles only), $\sigma_t(J \rightarrow J')$ and $\sigma_m(J \rightarrow J')$. Only the $J = 0, 1, 2$ and 7 cases are shown in Table 7.1. In Table 7.2, the state–to–state moments $S(1;JJ'), S(2;JJ')$, and $S(3;JJ')$ are given at two energies of 0.2 and 5 eV. Here also we have shown only the $J = 0, 1, 2$, and 7 cases. In Table 7.2, we have also given the summed (over J') quantities (this sum includes $J_t = 6$ transition also) for all the moments up to $\mu = 3$. We can clearly see from these tables for CH_4 molecule that the differential, integral, and various moments are independent of J and hence on the gas temperature T. The higher order moments depend very weakly on the initial J value (see Table 7.2).

A similar situation exists for the case of SiH_4 molecule (not shown). In all these results (Tables 7.1 and 7.2) the initial and final wave vectors (k and k') are considered to be different. Although, in Tables 7.1 and 7.2 we have shown our results up to $J = 2$ and $J = 7$ only, the $J \geq 3$ results exihibit exactly the same J-independent behaviour for all the moments mentioned above; we cheked our data up to $J = 100$ value with maximum value of J_t to be 6. Thus, the moments $< S(\mu) >$ (Eq. 7.8) for μ up to 3 are nearly independent of rotational temperature. The higher order moments are very small; nevertheless, a weak dependence on J (as discussed by Shimamura [14]) is visible here in our calculations (Table 7.2). In addition, for both the targets, CH_4 and SiH_4, the values of moments with $\mu \geq 4$

in the present energy region are rather too small to be of any physical significance.

If the effects of kinematic factor are taken into account by assuming the expansion [12–14],

$$\frac{k'}{k} = 1 - \frac{1}{2}(\frac{\Delta E}{\epsilon} - \ldots). \tag{7.1.1}$$

and by neglecting higher order terms, then Shimamura [14] has shown that for $\mu = 1$ and 2,

$$S(\mu; J) = S(\mu, 0)(1 - \frac{2E_J}{3\epsilon}), \tag{7.1.2}$$

Tables 7.1 and 7.2 show that even when kinematic effcts are taken into account, all the moments up to $\mu = 3$ are very weakly dependent on the J value. The magnitude of these higher order moments is too small to show any appreciable dependence as defined in Eqs. (7.1.1)–(7.1.2). Finally, in Table 7.3, we have provided our averaged moments, $\langle S(\mu) \rangle$ as a function of electron energy for both the molecules. All these moments preserve the shape–resonance behaviour around 7.5–10 eV (for the CH_4 molecule) and 3–4 eV (for the SiH_4 molecule) energy region.

7.2 Partial Sum Rules

Our results on the *partial* sum rules and the asymmetry between the $J \rightarrow J \pm \Delta J$ rotational transitions are as follows. Shimamura [12–13] has discussed these rules for spherical tops in general. In Table 7.3 (for the CH_4 molecule) we find that the partial-sum rule [12–13] for any physical quantity, say a,

$$a(J \rightarrow J + \Delta J) + a(J \rightarrow J - \Delta J) = 2A(|\Delta J|), \tag{7.2.1}$$

is approximately true. Here $A(|\Delta J|)$ can be differential, integral, and momentum transfer cross sections or the moments (Eq. 7.2–7.3). The values of $A(|\Delta J|)$ for the case of e–CH_4 collisions at 0.5 and 5 eV are given in Table 7.4 for $|\Delta J| = 1, 2, 3$, and 4. As assumed in Eqs. (7.2)–(7.3), the $d\sigma/d\Omega(|\Delta J|)$ are almost a constant for any initial J value. The difference between $A(|\Delta J|)$ with different initial J values is always less than 5% (at both 0.5 and 5 eV energies). There are only few cases (see Table 7.4) when $A(|\Delta J|)$ depends strongly on the initial and final J values; for example, the $|\Delta J| = 3$ case when $J = 3$ for both the energies. In addition, the validity of Eqs. (7.2)–(7.3) is less clear for 0.5 eV. As mentioned earlier, Eqs. (7.2)–(7.3) are valid under the adiabatic-rotation approximation, which may may break down at very low energies below 1 eV energy. This will affect the

analysis of experimental data to extract state–to–state DCS from the observed broadened peaks [13] (see later). The $|\Delta J| = 4$ transition at 0.5 eV also depends significantly on the initial J value. This is not surprising since at this rather low energy the inclusion of rotational Hamiltonian in the scattering calculation is important.

The individual excitation and de-excitation DCS at 90^0 for the e–CH_4 are plotted in Fig. 7.2 for the $\Delta J = \pm 3$ case and in Fig. 7.3 for the $\Delta J = \pm 4$ case. From Fig. 7.2, we see that in the high–J region, the ratio is independent of initial J value, i.e., the excitation and de–excitation intensities are equal. The excitation and de–excitation cross sections approach each from upper and lower ends respectively; however, the two curves are not symmetrical with respect to the mean values. The DCS plotted in Fig. 7.2 are very close (within 5%) to the analytic formula given in Eq. (7.9) because Eqs. (7.2) and (7.3) are approximately true. A similar behaviour is noticed for the $\Delta J = \pm 4$ case in Fig. 7.3. Curves in Figs. 7.2 and 7.3 give us idea of the high–J limit of the rotational excitation process. A similar situation exists for the case of e–SiH_4 scattering (not shown).

7.3 Rotationally Elastic and Inelastic Cross Sections

It is remarkable that experimentalists have been successful in obtaining absolute state–to–state rotational cross sections for the e–CH_4 system [52] at low impact energies. In order to extract these cross sections from their broadened energy–loss peaks, Müller *et al.* [52] used a theoretical analysis given by Shimamura [9] (based on the Eqs. 7.2–7.3) for the rotational excitation of spherical top molecules, which couples the line strength intensities of transitions from different initial rotational level. Like our assumption (see the introduction section), Müller *et al.* [52] have also assumed that the transfer of larger angular momenta ($J_t \geq 6$) is highly unlikely. Our earlier calculations [4] on the rotational transitions in CH_4 molecule by electron impact compared satisfactorily with the experimental data of Müller *et al.*. However, there were some qualitative differences between theoretical and experimental DCS in the forward scattering particularly for the $0 \rightarrow 3$ transition; all theoretical calculations on the $0 \rightarrow 3$ transition predict a zero value of the DCS at 0^0 angle [see Ref. 4], while the general trend of experimental DCS does not agree with the theoretical shape in this small angle scattering region. Even at higher angles, there are significant discrepancy in shape and magnitude of the DCS between theory and the measurement. For example, almost all theoretical $0 \rightarrow 3$ DCS predict a dip around 120^0 angle, while experimental values are rather flat in this angular region. This is one of the purposes of

this section, i.e., to investigate these state–to–state differential and integral cross sections with respect to their direct comparison with experimental data and the effect of rotational averaging for a particular ΔJ transition.

Müller *et al.* [52] have presented their measurements at 0.5, 5, 7.5, and 10 eV energies for the case of $0 \rightarrow 0$, $0 \rightarrow 3$, and $0 \rightarrow 4$ state–to–state rotational transitions in CH_4 molecule by electron impact. They employed Eqs. (7.2)–(7.3) to extract the absolute DCS as mentioned above. We have seen in the previous section that the neglect of kinematic factors in Eqs. (7.2)–(7.3) leads to significant error in the validity of these equations particularly at 0.5 eV. It is not clear that how much difference it will make in the final values of experimental DCS. In the following, we will discuss our results only at 7.5 eV and the corresponding discussion on other energies is almost same.

First we show our e–CH_4 DCS for both the $0 \rightarrow 3$ (Fig. 7.4) and $0 \rightarrow 4$ (Fig. 7.5) transitions with (solid curve) and without (dash curve) rotational averaging. The rotationally averaged curves (solid curve in Figs. 7.4–7.5) depend simply on the ΔJ=3 or 4 value. The experimental points [52] are also depicted for comparison. We immediately notice from Fig. 7.4 that the averaged (at 300 K) DCS improve drastically in the small angular region where the unaveraged DCS vanish at the zero angle. The overall shape of the DCS changes significantly when rotational averaging is performed. The backward scattering region is also affected with rotational averaging (see Fig. 7.4). In general, the averaged DCS are smaller and exihibit less structure in the DCS as compared with the unaveraged DCS. The $0 \rightarrow 4$ transition is also reduced significantly when rotational averaging is performed (Fig. 7.5). The pure elastic ($0 \rightarrow 0$) DCS (not shown) do not show any visible effect with and without rotational averaging. It may be appropriate to call our averaged DCS as $d\sigma/d\Omega(|\Delta J|)$ rather than from $J = 0$ to $J' = 3$ or 4. It may be questionable whether one should compare these $|\Delta J| = 3$ or 4 DCS with the data of Müller *et al.* [52]. In addition, because of a very weak broadening appearing in the energy-loss spectrum, large systematic errors are possible at lower angles in the data of Müller *et al.* [52].

In Figs. 7.6 and .7, we have displayed similar DCS for the two transitions ($0 \rightarrow 3$ and $0 \rightarrow 4$) with and without rotational averaging for the e–SiH_4 case. Here also the qualitative picture is same as discussed above for the CH_4 molecule. The averaged DCS depict less variation in the cross section as function of scattering angle (see Fig. 7.6). The $0 \rightarrow 4$ cross sections are reduced by almost a factor of four when averaging is taken into

account. No experimental data are available to compare our calculations shown in Figs. 7.6 and 7.7.

In Fig. 7.8, we have shown state–to–state DCS for the $\Delta J = +3$ transition at several initial J values. It is clear that only the $J = 0$ curve vanishes in the zero degree limit. The next $1 \rightarrow 4$ transition has a finite value at zero degree and is almost flat up to about 120^0. As the value of initial J is increased further, the DCS become independent of J. For example, $8 \rightarrow 11$ and $10 \rightarrow 13$ cross sections are almost identical. This situation exists for other energies also (not shown).

Finally in Figs. 7.9–7.12 we have shown the averaged integral ($\langle\sigma_t^{JJ'}\rangle$ and $\langle\sigma_m^{JJ'}\rangle$) cross sections for CH_4 and SiH_4 molecules respectively. These Figs. (7.9–.12) show that the averaged integral cross sections are reduced significantly; although the general shape does not change appreciably. In Table 7.3 we have given $\langle\sigma_t^{JJ'}\rangle$ at various gas temperatures of the CH_4. There is very little change in these cross sections going from 100 K to 500 K. Table 7.4 provides similar data for the case of SiH_4 molecule.

Müller *et al.* [52] have given the branch structure (see their Fig. 2(b)) after summing up all transitions with the same ΔJ. Earlier Read [69] has discussed the classification of rotational transition into branches. In this structure we can clearly see that the area of the plus branch (i.e., $\Delta J = +1, +2, +3$, and $+4$) is always larger than the corresponding area of the negative branch (i.e., $\Delta J = -1, -2, -3$, and -4). This is true in our calculations also (see Table 7.3) where DCS for the $+\Delta J$ are always higher than the $-\Delta J$ values. This is a consequence of the principle of detailed balance.

In Tables 7.5 and 7.6 we have provided state–to–state rotational excitation cross sections with and without rotational averaging for the CH_4 and SiH_4 cases respectively. We see a significant change in the cross sections at all energies shown in these tables. In general, the averaged quantities are reduced. At various gas temperatures (see Tables 7.5 and 7.6), the averaged cross sections differ from each other.

Finally, we can provide a large set of cross section data for both the targets on state–to–state rotational processes in the 0.1–20 eV energy range. The tabulated values of $d\sigma/d\Omega(|\Delta J| = 0, 1, 2, 3, 4, 5, 6)$ at 0.1–20 eV are also available from the PI at request.

Table 7.1.

State–to–State rotational excitation differential cross sections at 5 eV for e–CH_4 case. A number like 7.7355-02 means 7.736 $\times 10^{-2}$

$J \rightarrow J'$	DCS (15^0)	DCS (45^0)	DCS (90^0)	DCS (120^0)	$\sigma_t(JJ')$	$\sigma_m(JJ')$
$0 \rightarrow 0$	4.0032	1.1786	1.5889	7.736-02	18.292	16.338
$0 \rightarrow 3$	1.604-03	1.390-02	3.343-02	3.064-02	0.420	0.548
$0 \rightarrow 4$	8.519-02	7.385-02	5.439-02	5.866-02	0.799	0.772
$1 \rightarrow 1$	4.0032	1.1786	1.5889	7.736-02	18.292	16.338
$1 \rightarrow 2$	3.820-04	3.311-03	7.964-03	7.299-03	0.100	0.1306
$1 \rightarrow 3$	2.263-02	2.379-02	2.526-02	2.543-02	0.3474	0.3829
$1 \rightarrow 4$	2.909-02	3.057-02	3.245-02	3.268-02	0.4464	0.4920
$1 \rightarrow 5$	3.470-02	3.009-02	2.219-02	2.395-02	0.3261	0.3149
$2 \rightarrow 1$	1.376-04	1.193-03	2.869-03	2.629-03	3.603-02	4.703-02
$2 \rightarrow 2$	4.0129	1.1888	1.5997	8.826-02	18.441	16.502
$2 \rightarrow 3$	1.358-02	1.428-02	1.516-02	1.526-02	0.2085	0.2298
$2 \rightarrow 4$	1.746-02	1.836-02	1.950-02	1.965-02	0.2682	0.2957
$2 \rightarrow 5$	2.133-02	2.242-02	2.381-02	2.400-02	0.3276	0.3611
$2 \rightarrow 6$	2.459-02	2.133-02	1.572-02	1.697-02	0.2311	0.2232
$2 \rightarrow 7$	1.253-05	1.705-05	3.234-05	5.148-05	4.683-04	6.101-04
$7 \rightarrow 2$	1.401-06	1.907-06	3.617-06	5.757-06	5.237-05	6.823-05
$7 \rightarrow 3$	4.437-03	3.848-03	2.837-03	3.062-03	4.169-02	4.027-02
$7 \rightarrow 4$	5.840-03	6.140-03	6.520-03	6.570-03	8.968-02	9.887-02
$7 \rightarrow 5$	7.133-03	7.500-03	7.964-03	8.025-03	0.1095	0.1208
$7 \rightarrow 6$	8.424-03	8.856-03	9.404-03	9.476-03	0.1294	0.1426
$7 \rightarrow 7$	4.0129	1.1889	1.5997	8.828-02	18.441	16.502
$7 \rightarrow 8$	1.099-02	1.156-02	1.227-02	1.237-02	0.1688	0.1861
$7 \rightarrow 9$	1.227-02	1.290-02	1.370-02	1.381-02	0.1885	0.2078
$7 \rightarrow 10$	1.355-02	1.424-02	1.512-02	1.524-02	0.2080	0.2294
$7 \rightarrow 11$	1.447-02	1.254-02	9.249-03	9.984-03	0.1359	0.1313
$7 \rightarrow 12$	6.938-06	9.440-06	1.791-05	2.850-05	2.593-04	3.378-04

Table 7.2. Partial ($S(\mu; JJ')$) and total ($S(\mu; J)$), at 5 eV for the e-CH_4 collisions.

	E=0.2 eV			E=5eV		
$J \rightarrow J'$	$S(1; JJ')$	$S(2; JJ')$	$S(3; JJ')$	$S(1; JJ')$	$S(2; JJ')$	$S(3; JJ')$
$0 \rightarrow 3$	1.1239-03	6.4573-07	3.7099-10	1.2063	6.9304-04	3.9817-07
$0 \rightarrow 4$	3.4565-04	3.3098-07	3.1692-10	3.8270	3.6645-03	3.5084-06
$0 \rightarrow 6$	2.6083-04	5.2448-07	1.0547-09	2.0413-02	4.1046-05	8.2537-08
$1 \rightarrow 2$	2.712-04	1.558-07	8.952-11	2.874-01	1.651-04	9.485-08
$1 \rightarrow 3$	4.671-04	3.033-07	2.077-11	1.395	1.182-03	1.043-06
$1 \rightarrow 4$	5.924-04	3.846-07	2.634-10	1.793	1.519-03	1.340-06
$1 \rightarrow 5$	2.143-04	2.847-07	4.325-10	1.564	1.504-03	1.452-06
$1 \rightarrow 6$	8.727-05	1.755-07	3.529-10	6.805-03	1.368-05	2.752-08
$1 \rightarrow 7$	9.802-05	1.971-07	3.964-10	7.845-03	1.578-05	3.172-08
$2 \rightarrow 1$	9.891-05	5.683-08	3.265-11	1.035-01	5.947-05	3.416-08
$2 \rightarrow 2$	2.035-04	1.321-07	9.048-11	5.982-01	5.068-04	4.473-07
$2 \rightarrow 3$	2.821-04	1.832-07	1.254-10	8.372-01	7.092-04	6.260-07
$2 \rightarrow 4$	3.959-04	3.087-07	3.127-10	1.0787	9.171-04	8.159-07
$2 \rightarrow 5$	4.755-04	3.708-07	3.756-10	1.3175	1.120-03	9.965-07
$2 \rightarrow 6$	1.498-04	1.990-07	3.023-10	1.1085	1.066-03	1.029-06
$2 \rightarrow 7$	5.928-05	1.192-07	2.397-10	4.708-03	9.467-06	1.904-08
$2 \rightarrow 8$	6.506-05	1.308-07	2.631-10	5.330-03	1.072-05	2.155-08
$7 \rightarrow 1$	4.683-06	9.417-09	1.894-11	3.160-04	6.354-07	1.278-09
$7 \rightarrow 2$	7.762-06	1.561-08	3.139-11	5.265-04	1.059-06	2.129-09
$7 \rightarrow 3$	3.060-05	4.065-08	6.174-11	2.000-01	1.923-04	1.857-07
$7 \rightarrow 4$	1.428-04	1.113-07	1.128-10	3.607-01	3.067-04	2.728-07
$7 \rightarrow 5$	1.719-04	1.341-07	1.358-10	4.406-01	3.746-04	3.333-07
$7 \rightarrow 6$	1.995-04	1.556-07	1.576-10	5.203-01	4.424-04	3.935-07
$7 \rightarrow 7$	2.251-04	1.756-07	1.778-10	5.998-01	5.099-04	2.728-07
$7 \rightarrow 8$	2.484-04	1.937-07	1.962-10	6.791-01	5.773-04	5.136-07
$7 \rightarrow 9$	2.689-04	2.097-07	2.124-10	7.581-01	6.445-04	5.734-07
$7 \rightarrow 10$	2.861-04	2.231-07	2.260-10	8.368-01	7.114-04	6.329-07
$7 \rightarrow 11$	8.156-05	1.084-07	1.646-10	6.520-01	6.269-04	6.053-07
$7 \rightarrow 12$	2.956-05	5.943-08	1.195-10	2.607-03	5.242-06	1.054-08
$7 \rightarrow 13$	2.985-05	6.003-08	1.207-10	2.811-03	5.652-06	1.137-08
$S(\mu; 0)$	1.7304-03	1.5012-06	1.7426-09	5.0536	4.3986-03	3.9896-06
$S(\mu; 1)$	1.7303-03	1.5010-06	1.7423-09	5.0536	4.3986-03	3.9896-06
$S(\mu; 2)$	1.7300-03	1.5007-06	1.7418-09	5.0536	4.3985-03	3.9896-06
$S(\mu; 3)$	1.7296-03	1.5002-06	1.7410-09	5.0536	4.3985-03	3.9896-06
$S(\mu; 7)$	1.7267-03	1.4966-06	1.7353-09	5.0536	4.3985-03	3.9896-06

Table 7.3

Averaged moments, $\langle S(\mu) \rangle$, at 300 K for both the CH_4 and SiH_4 molecules as a function of impact energy. All quantities are in units of 10^{-20} cm^2. A number like 9.4689-03 means 9.4689×10^{-3}.

	CH_4			SiH_4		
E (eV)	$\langle S(1) \rangle$	$\langle S(2) \rangle$	$\langle S(3) \rangle$	$\langle S(1) \rangle$	$\langle S(2) \rangle$	$\langle S(3) \rangle$
0.5	9.4689-03	7.0219-06	6.5976-09	5.7035-02	1.9118-05	7.0480-09
0.8	1.9726-02	1.4905-05	1.3686-08	1.3850-01	4.7202-05	1.7437-08
1.0	2.9072-02	2.2578-05	2.0747-08	2.2140-01	8.5138-05	4.0045-08
2.0	2.0601-01	1.6459-04	1.4344-07	1.5960-01	7.1955-04	3.4236-07
3.0	8.7060-01	7.1289-04	6.2159-07	6.8700	4.2248-03	2.1843-06
4.0	2.4317	2.0627-03	1.8381-06	8.4114	4.2248-03	2.1843-06
5.0	5.0536	4.3985-03	3.9896-06	6.7770	3.4008-03	1.8326-06
7.5	11.083	9.8819-03	9.16-5-06	7.7804	4.4423-03	3.1630-06
10.0	11.586	1.0296-02	9.6791-06	9.1768	5.9293-03	4.7698-06
15.0	9.7749	8.6949-03	8.8677-06	7.1206	4.8130-03	4.0314-06

Table 7.4.

The state–to–state differential cross sections at 90^0 for e–CH_4 scattering at 0.5 and 5 eV. The 0.5 eV numbers are in units of 10^{-20} cm^2, while the 5 eV results are in units of 10^{-18} cm^2 .

J	$\Delta J = +1$	$\Delta J = -1$	$\Delta J = +2$	$\Delta J = -2$	$\Delta J = +3$	$\Delta J = -3$	$\Delta J = +4$	$\Delta J = -4$
	0.5 eV							
0	-	-	-	-	1.4404	-	0.1272	-
1	0.2068	-	0.2202	-	0.2191	-	0.0197	-
2	0.2208	0.2079	0.2254	-	0.2239	-	0.0196	-
3	0.2263	0.2226	0.2248	0.2232	0.2230	0.2090	0.0195	-
4	0.2260	0.2286	0.2242	0.2295	0.2221	0.2243	0.0194	0.0145
5	0.2257	0.2289	0.2236	0.2300	0.2211	0.2310	0.0193	0.0204
6	0.2254	0.2292	0.2230	0.2307	0.2202	0.2318	0.0191	0.0251
8	0.2247	0.2298	0.2217	0.2318	0.2184	0.2336	0.0189	0.0207
10	0.2242	0.2304	0.2205	0.2330	0.2165	0.2353	0.0187	0.0209
12	0.2236	0.2310	0.2193	0.2342	0.2146	0.2370	0.0185	0.0211
14	0.2230	0.2316	0.2181	0.2353	0.2128	0.2387	0.0182	0.0213
	5.0 eV							
0	-	-	-	-	3.3400	-	5.4400	-
1	0.4778	-	1.0823	-	1.0818	-	0.6051	-
2	1.0826	0.4781	1.0831		1.0824	-	0.6048	-
3	1.0836	1.0835	1.0829	1.0838	1.0820	0.4783	0.6044	-
4	1.0834	1.0847	1.0826	1.0851	1.0816	1.0843	0.6041	0.6059
5	1.0833	1.0848	1.0823	1.0854	1.0812	1.0858	0.6038	0.6073
6	1.0831	1.0850	1.0820	1.0857	1.0807	1.0862	0.6035	0.6076
8	1.0829	1.0853	1.0814	1.0862	1.0800	1.0871	0.6028	0.6082
10	1.0826	1.0855	1.0809	1.0868	1.0790	1.0879	0.6022	0.6089
12	1.0823	1.0858	1.0803	1.0874	1.0782	1.0888	0.6016	0.6095
14	1.0820	1.0861	1.0800	1.0879	1.0773	1.0896	0.6009	0.6101

Table 7.5

State–to–state rotational excitation cross sections with ($\langle\sigma_t^{JJ'}\rangle$) and without ($\sigma_t^{JJ'}$) rotational averaging for the case of e–CH_4 collisions. All numbers are in unit of 10^{-16} cm^2.

Energy (eV)	σ_t^{03}	$\langle\sigma_t^{03}\rangle^{100K}$	$\langle\sigma_t^{03}\rangle^{300K}$	$\langle\sigma_t^{03}\rangle^{500K}$
0.5	0.0025	0.0009	0.00081	0.00080
0.8	0.0047	0.00187	0.00162	0.00160
1.0	0.00614	0.00258	0.00227	0.00225
2.0	0.0326	0.0157	0.0146	0.0145
3.0	0.1151	0.0632	0.0585	0.0581
5.0	0.4200	0.3313	0.3012	0.2994
7.5	0.7381	0.7078	0.6310	0.6274
10.0	0.9028	0.7746	0.6771	0.6730
15.0	1.1891	0.7241	0.6239	0.6196
	σ_t^{04}	$\langle\sigma_t^{04}\rangle^{100K}$	$\langle\sigma_t^{04}\rangle^{300K}$	$\langle\sigma_t^{04}\rangle^{500K}$
0.5	0.00032	0.00011	0.000084	0.000082
0.8	0.0011	0.00033	0.000262	0.000257
1.0	0.0021	0.00062	0.00050	0.00049
2.0	0.0228	0.0061	0.00532	0.00521
3.0	0.1117	0.0304	0.00259	0.02536
5.0	0.7993	0.2251	0.1855	0.1814
7.5	1.8556	0.5437	0.4313	0.4220
10.0	1.8398	0.5627	0.4294	0.4201
15.0	1.2006	0.3879	0.2880	0.2819

Table 7.6

State–to–state rotational excitation cross sections with ($\langle\sigma_t^{JJ'}\rangle$) and without ($\sigma_t^{JJ'}$) rotational averaging for the case of e–SiH_4 collisions. All numbers are in units of 10^{-16} cm^2.

Energy (eV)	σ_t^{03}	$\langle\sigma_t^{03}\rangle^{100K}$	$\langle\sigma_t^{03}\rangle^{300K}$	$\langle\sigma_t^{03}\rangle^{500K}$
0.5	0.0342	0.0104	0.0104	0.0099
0.8	0.0793	0.0246	0.0239	0.0238
1 0	0.1132	0.0367	0.0356	0.0355
2.0	0.3571	0.1951	0.1908	0.1903
3.0	0.6039	0.6892	0.6780	0.6765
5.0	0.8118	0.7027	0.6905	0.6890
7.5	1.6663	0.8441	0.8279	0.8258
10.0	1.6637	0.8849	0.8706	0.8688
15.0	1.2393	0.6578	0.6479	0.6468
	σ_t^{04}	$\langle\sigma_t^{04}\rangle^{100K}$	$\langle\sigma_t^{04}\rangle^{300K}$	$\langle\sigma_t^{04}\rangle^{500K}$
0.8	0.0049	0.0012	0.0011	0.0011
1.0	0.0125	0.0033	0.0031	0.0031
2.0	0.3951	0.0953	0.0894	0.0885
3.0	2.2616	0.5456	0.5117	0.5068
5.0	2.0235	0.4945	0.4639	0.4595
7.5	1.3635	0.3766	0.3542	0.3509
10.0	1.3952	0.4233	0.3988	0.3952
15.0	0.9833	0.3146	0.2967	0.2941

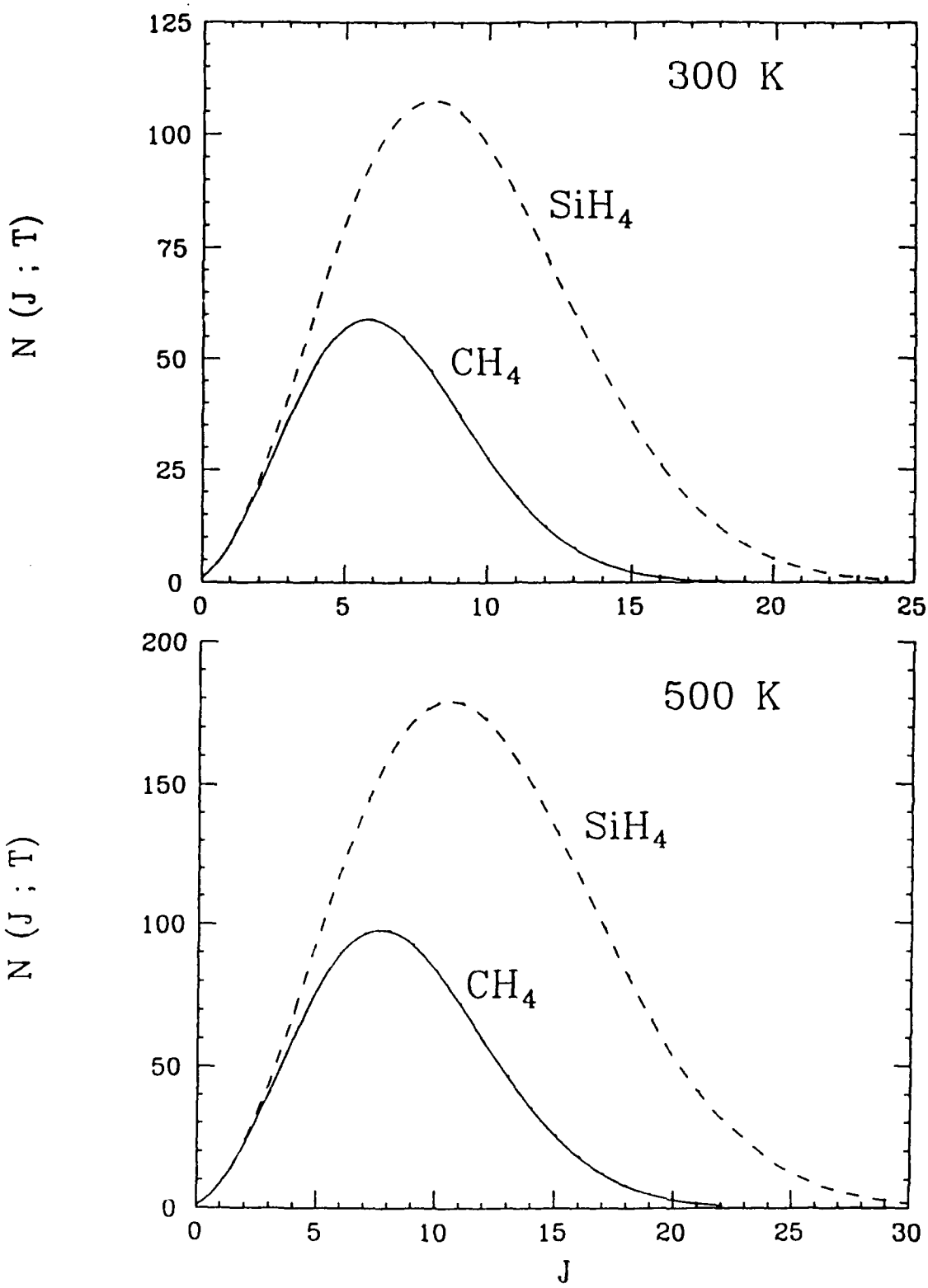

Fig. 7.1. Maxwellian distribution of the rotational states of CH_4 and SiH_4 molecules at 300 K and 500 K

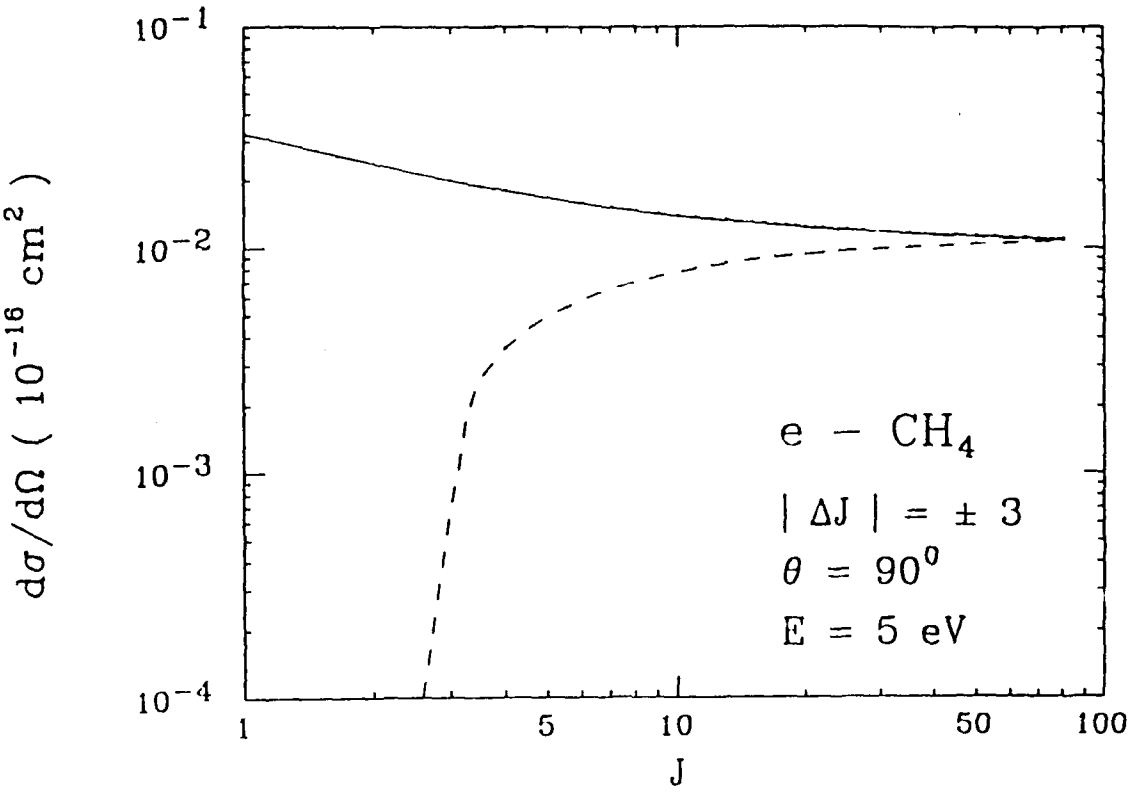

Fig. 7.2. Ratio of the excitation and de-excitation (for $\Delta J = \pm 3$) differential cross sections at 90^0 angle for e-CH_4 collisions at 5 eV. The solid curve represents the excitation, while dashed curve represents the de-excitation process.

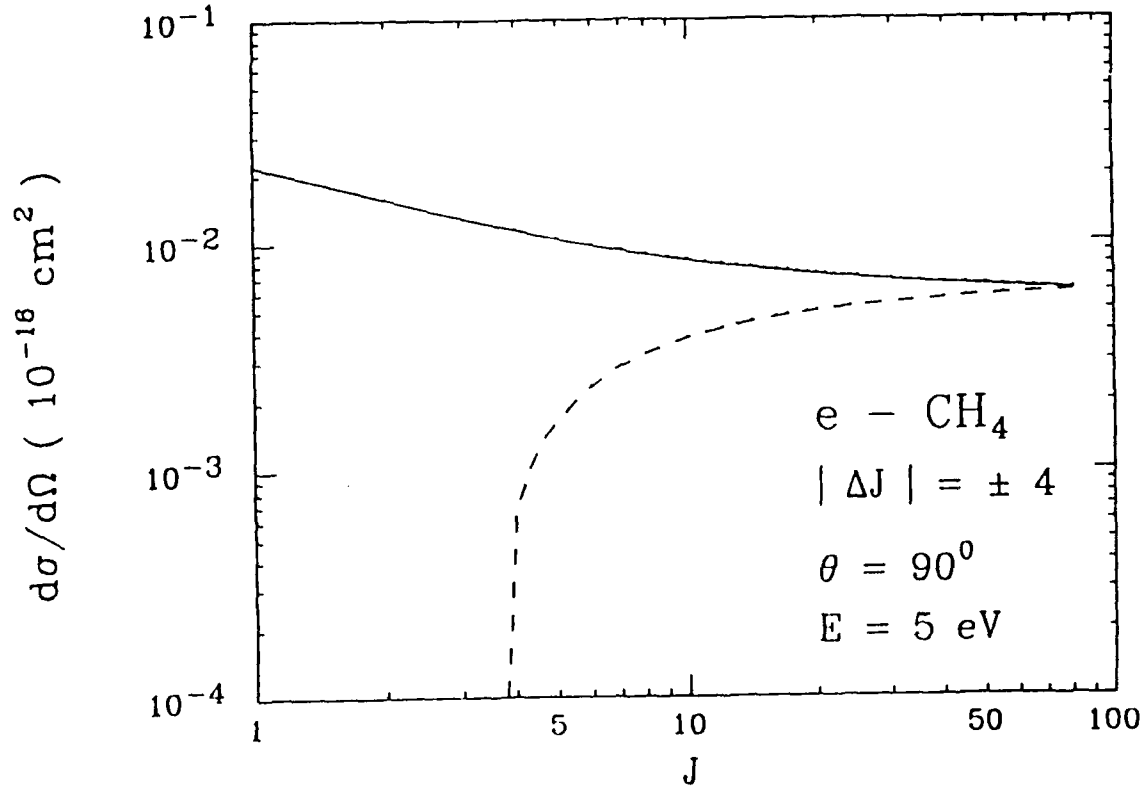

Fig. 7.3. Ratio of the excitation and de-excitation (for $\Delta J = \pm 4$) differential cross sections at 90^0 angle for e-CH_4 collisions at 5 eV. The solid curve represents the excitation, while dashed curve represents the de-excitation process.

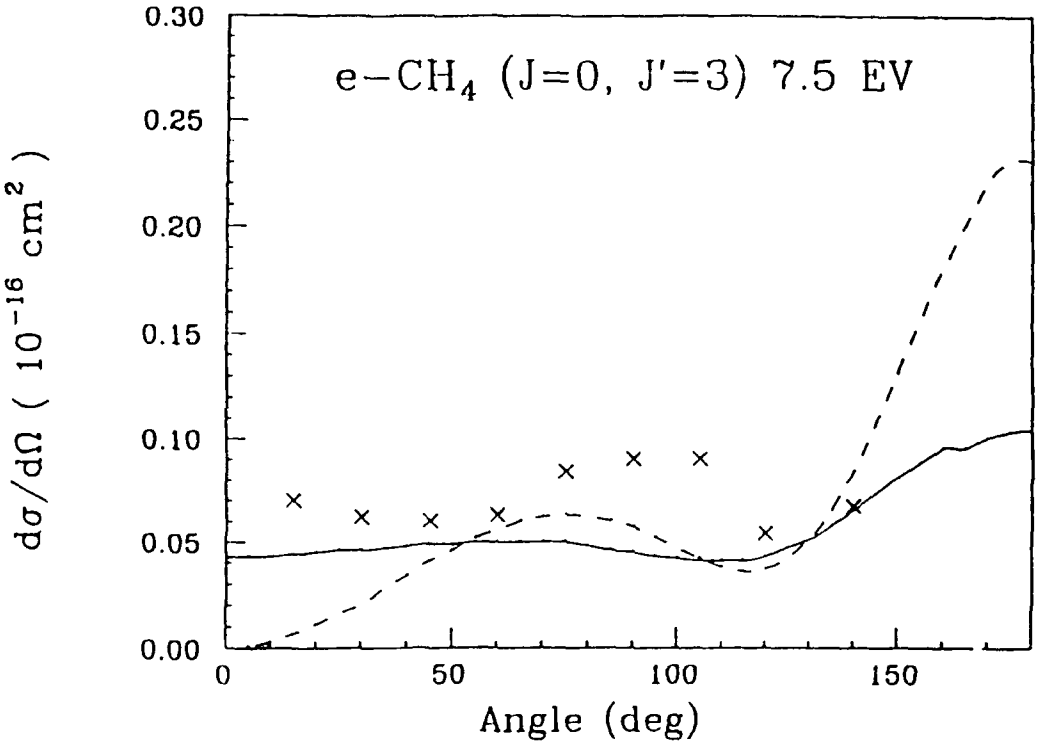

Fig. 7.4. $0 \rightarrow 3$ differential cross sections at 7.5 eV for the case of e-CH_4 collisions. Theoretical curves are the $0 \rightarrow 3$ (dashed line) and averaged $|\Delta J| = 3$ (solid line) values. The experimental data are from Ref. 4.

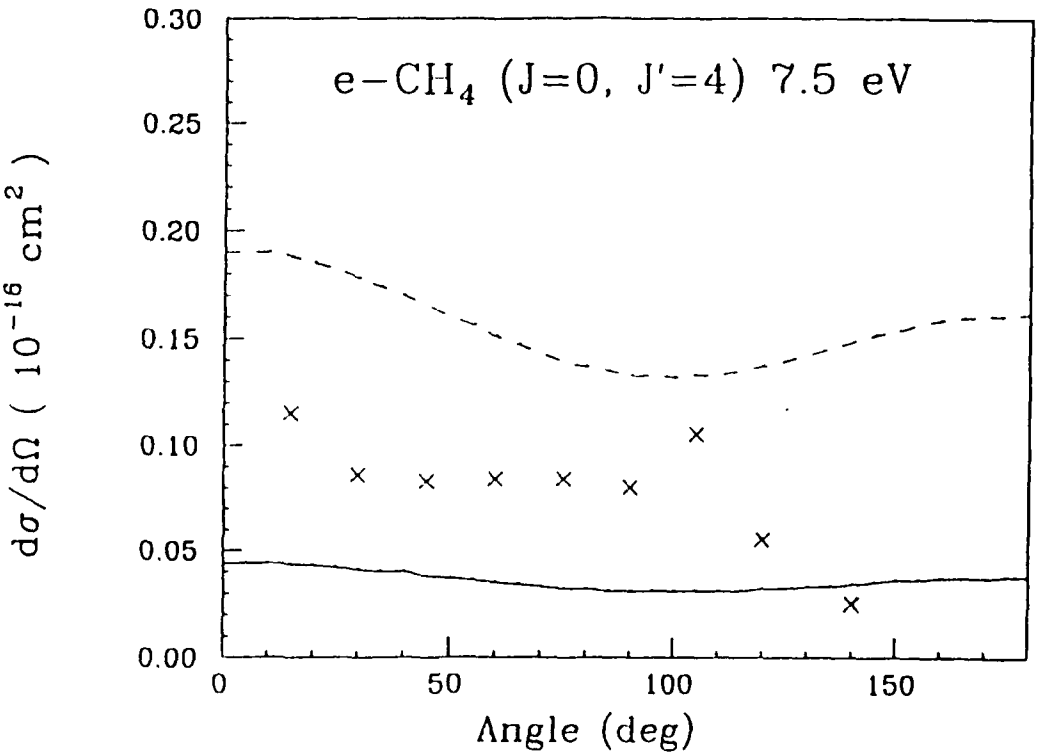

Fig. 7.5. $0 \rightarrow 4$ differential cross sections at 7.5 eV for the case of e CH_4 collisions. Theoretical curves are the $0 \rightarrow 3$ (dashed line) and averaged $|\Delta J| = 3$ (solid line) values. The experimental data are from Ref. 4.

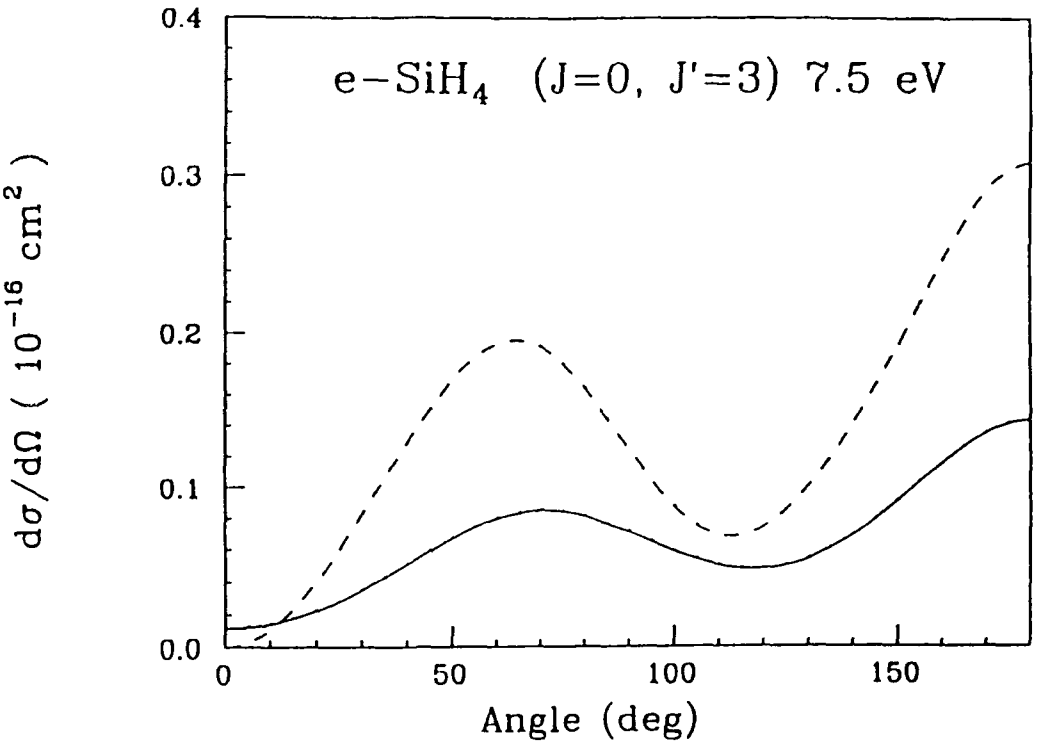

Fig. 7.6. $0 \rightarrow 3$ differential cross sections at 7.5 eV for the case of e–SiH_4 collisions. Theoretical curves are the $0 \rightarrow 3$ (dashed line) and averaged $|\Delta J| = 3$ (solid line) values. The experimental data are from Ref. 4.

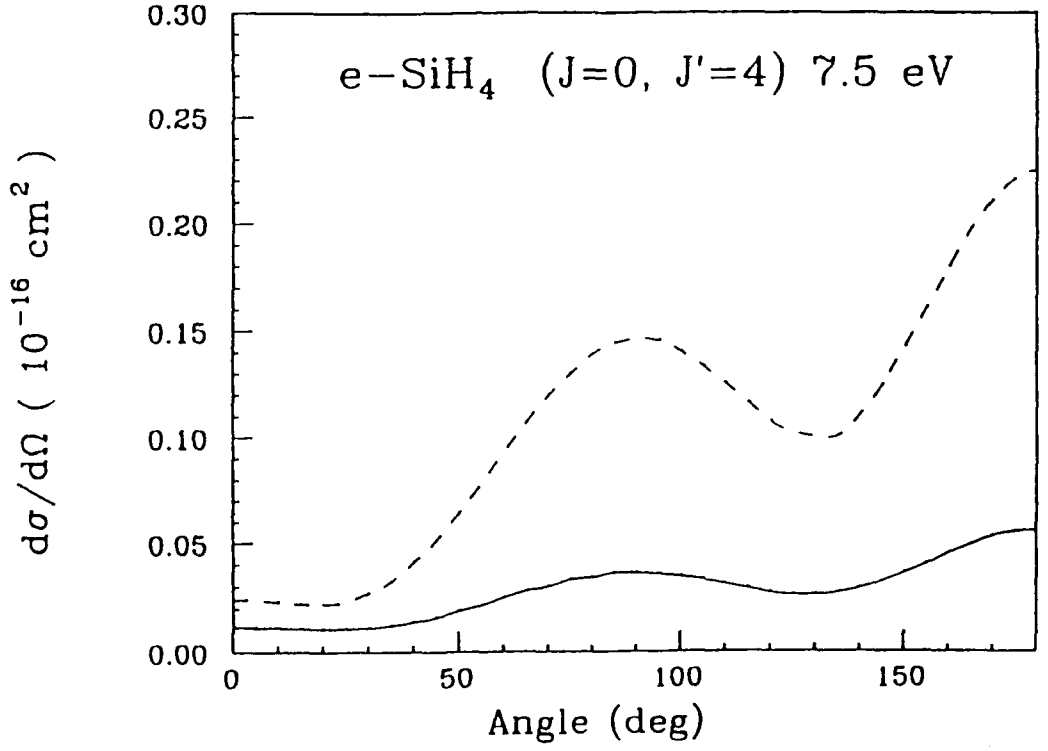

Fig. 7.7. $0 \rightarrow 4$ differential cross sections at 7.5 eV for the case of e–SiH_4 collisions. Theoretical curves are the $0 \rightarrow 3$ (dashed line) and averaged $|\Delta J| = 3$ (solid line) values. The experimental data are from Ref. 4.

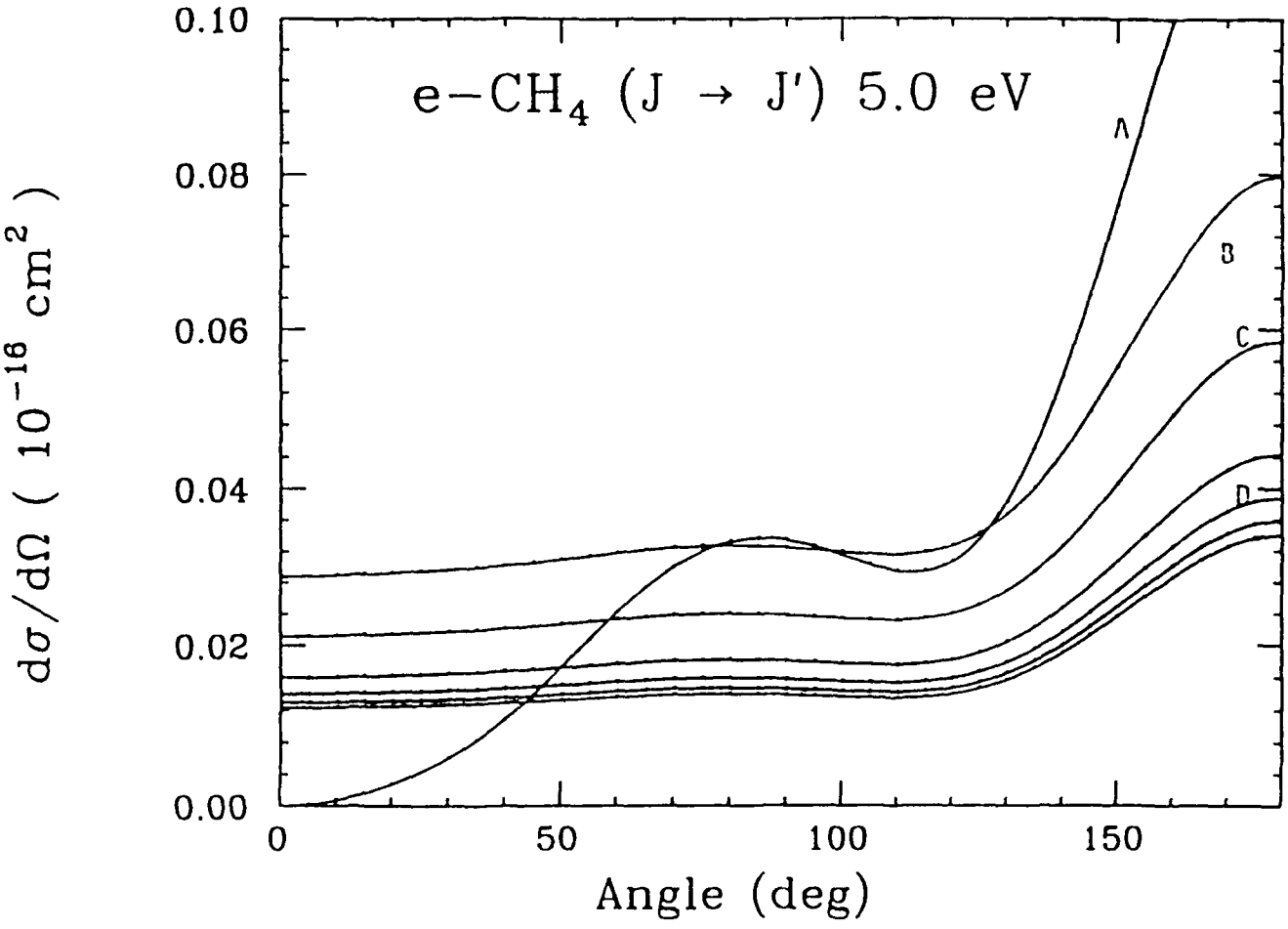

Fig. 7.8. State-to state differenntial cross section for the e-CH_4 collisions at 5 eV. A, $0 \rightarrow 3$; B, $1 \rightarrow 4$; C, $2 \rightarrow 5$; D, $4 \rightarrow 7$; E, $6 \rightarrow 9$; F, $8 \rightarrow 11$; G, $10 \rightarrow 13$.

FIG. 7.9

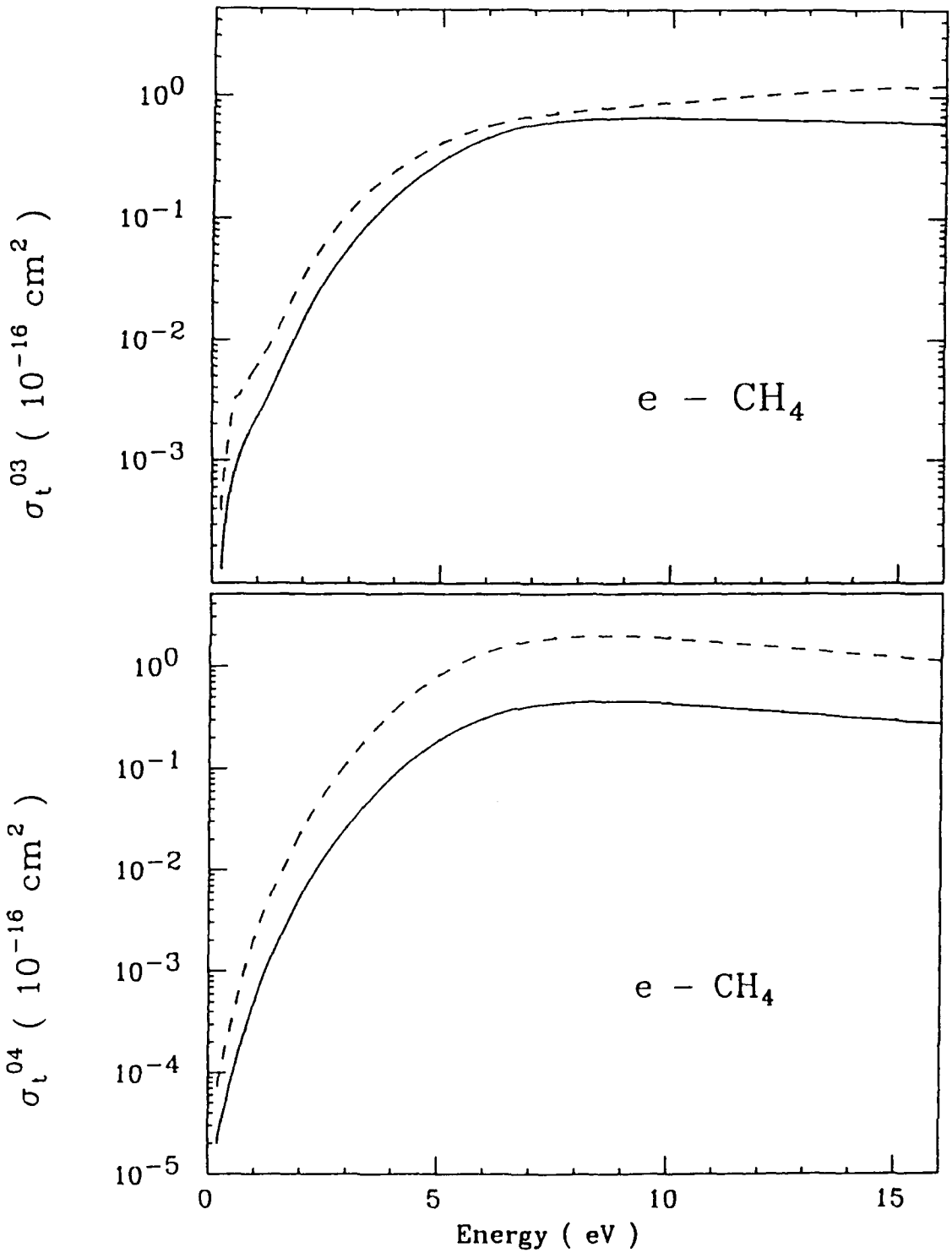

Fig. 7.9. State-to-state integral σ_t^{03} (upper set of curves) and σ_t^{04} (lower set of curves) cross sections for e CH_4 collisions with (solid line) and without (dash lines) rotational averaging.

FIG. 7.10

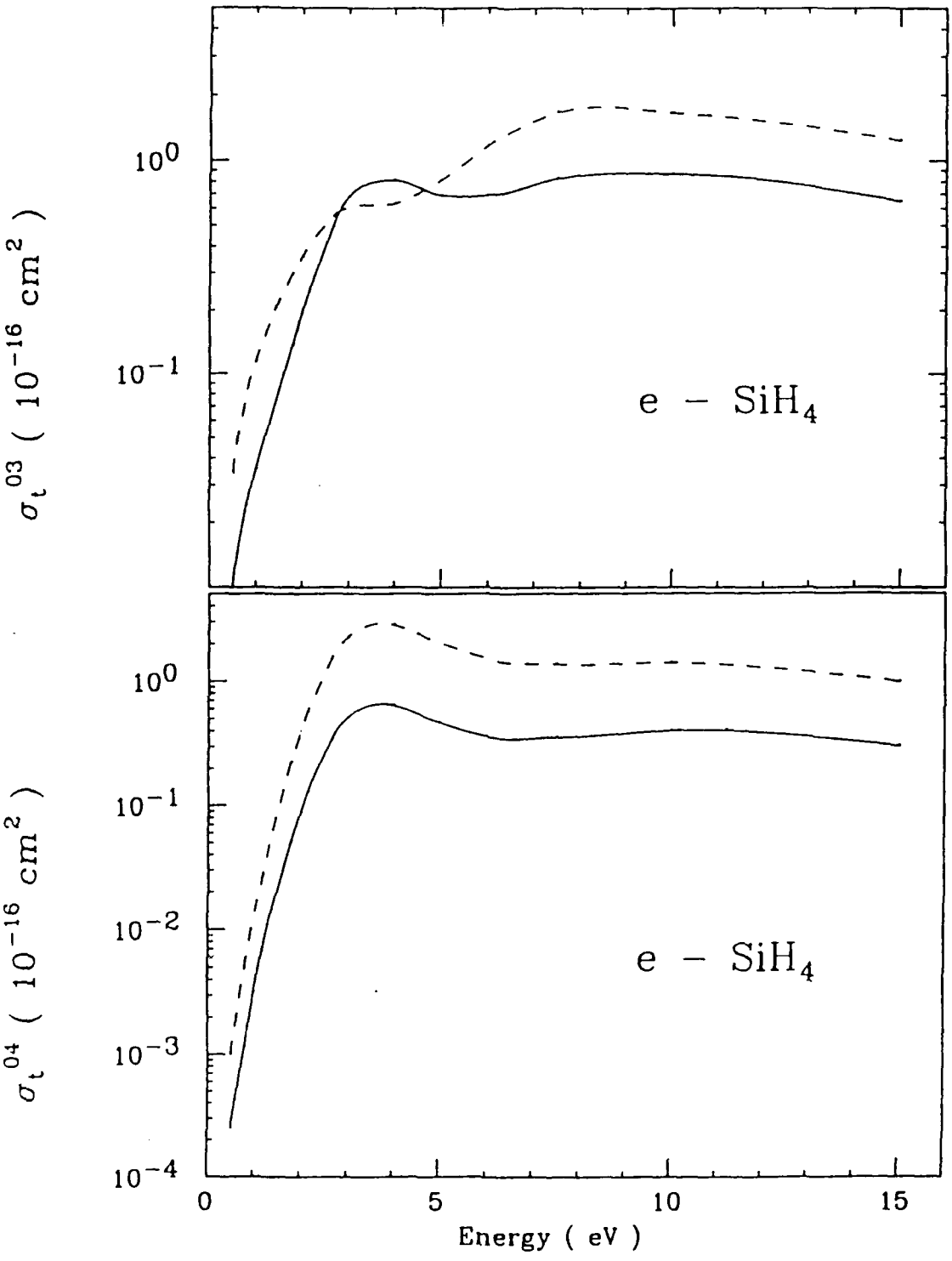

Fig. 7.10. State-to-state integral σ_t^{03} (upper set of curves) and σ_t^{04} (lower set of curves) cross sections for e-SiH_4 collisions with (solid line) and without (dash lines) rotational averaging.

FIG. 7.11

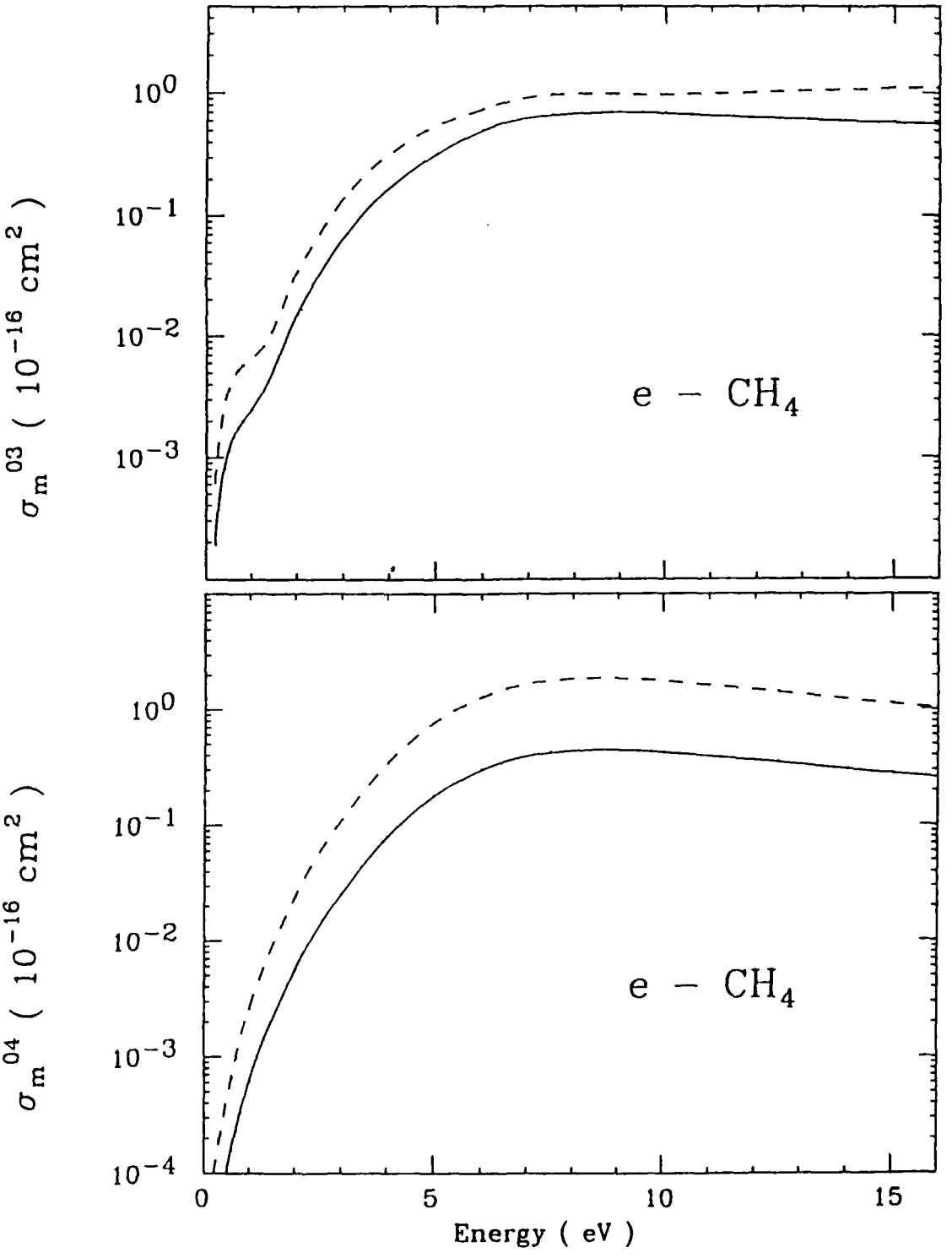

Fig. 7.11. State to-state integral σ_m^{03} (upper set of curves) and σ_m^{04} (lower set of curves) cross sections for e CH_4 collisions with (solid line) and without (dash lines) rotational averaging.

FIG. 7.12

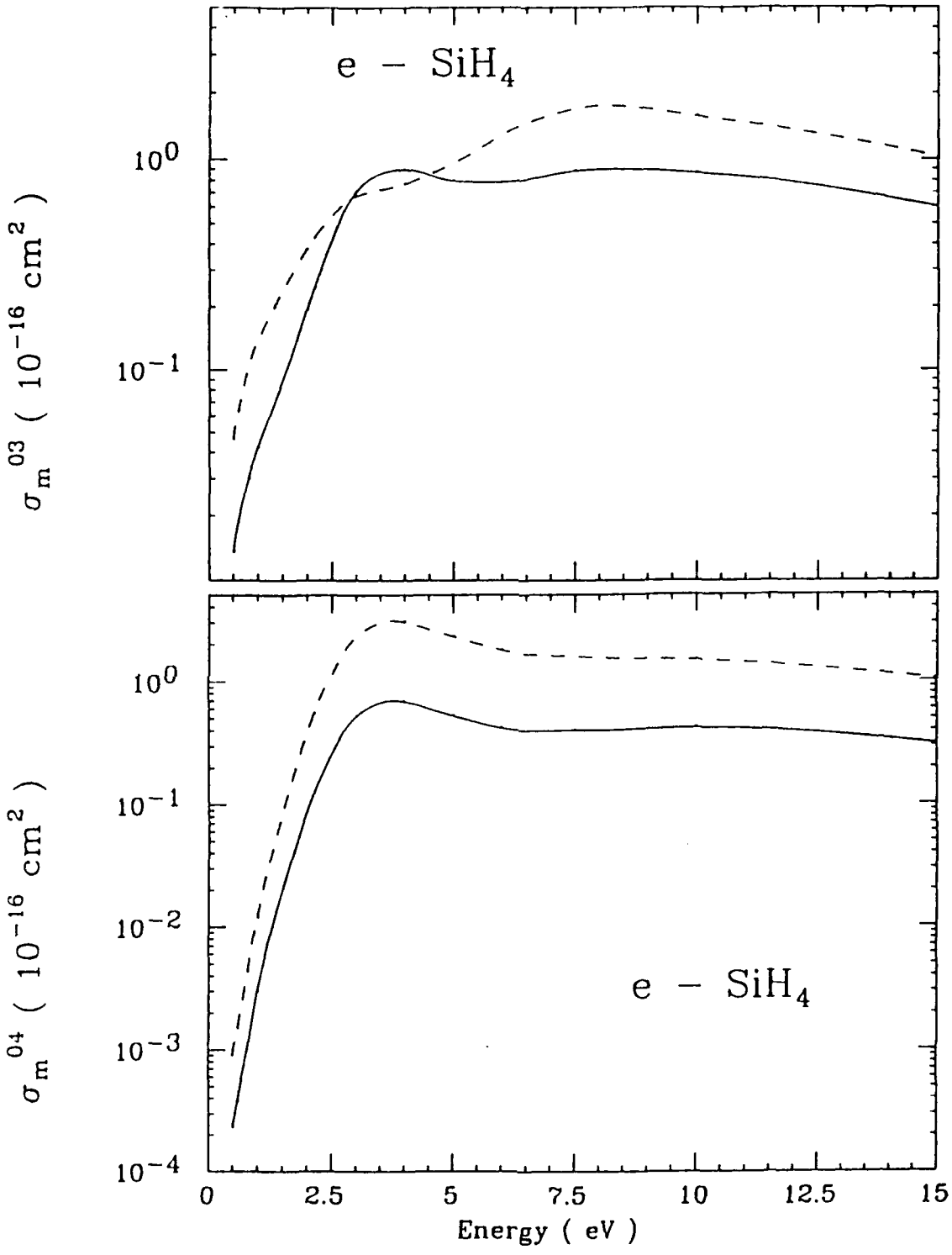

Fig. 7.12. State-to-state integral σ_m^{03} (upper set of curves) and σ_m^{04} (lower set of curves) cross sections for e-SiH_4 collisions with (solid line) and without (dash lines) rotational averaging.

8. CONCLUSIONS AND FUTURE PROGRAM

During the period of **June 1990 – June 1991**, the following research was completed and has been presented in this report:

We have presented rotationally elastic, inelastic and summed cross sections for electron scattering with several polyatomic molecules (CH_4, SiH_4, GeH_4, H_2O, and NH_3) in a highly sophisticated close–coupling non–empirical theory. Exchange effects are included exactly, while polarization corrections are considered approximately but without involving any fitting parameter. Results are compared with measurements where such data are available. No previous theoretical investigation is available on these molecules in such detail and energy range. This study has drawn several important conclusions: (1) exchange effects at the exact level and model polarization potentials can describe low energy e–molecule scattering quite accurately, (2) polarization effects should be included in a theory where target orbitals are relaxed in the presence of incoming particle, (3) the effect of gas temperature on the cross sections is crucial for rotationally inelastic channels, (4) a single–center approach can be useful for many polyatomics without any convergence problem, (5) the iterative scheme is quite promising tool in future if employed in an optimized way as suggested in this study.

During the **June 1991 – May 1992** *period, we plan to do the following:*

Our e–NH_3 and H_2O results presented here are not complete yet. We hope to get these data ready very soon. In addition, the calculations on the GeH_4 molecule are being repeated in full close–coupling approach rather than the spherical model. We are in the process of undertaking some big molecules such as the CF_4, SF_6, CCl_4, etc., to investigate low energy electron behaviour. These targets have been studied in the laboratory quite recently. Our present investigation will be extended to study vibrational excitation process in the present energy regime. In addition, molecular wave functions for open shell targets and radicals and ions of polyatomic molecules will be calculated from existing molecular structure codes.

During the **June 1992 – May 1993** period, we plan to do the following:

Our present computer codes are fully capable of carrying out accurate calculations for closed–shell molecules. We plan to modify them in order to study open–shell (such as the radicals of polyatomic molecules) and ionic molecules. For such targets, the theoretical work is almost non-existential. We hope to finish during the next few years the detailed results on several big molecules such as SF_6, CF_4, CCl_4, PbH_4 for elastic, rotational and vibrational channels.

9. REFERENCES

[1]. F A Gianturco and A Jain, Phys. Rep., **143**, 348 (1986).

[2]. P McNaughten and D G Thompson, J. Phys. **B21**, L703 (1988).

[3]. A. Jain, C A Weatherford, P McNaughten and D G Thompson, Phys. Rev. **A40**, 6730 (1989).

[4]. P McNaughten, D G Thompson and A Jain, J. Phys. **B23**, 2405S (1990).

[5]. A Jain and D G Thompson, J. Phys. **B24**, 1087 (1991).

[6]. A Jain, F A Gianturco and D G Thompson, J. Phys. **B24**, L255 (1991).

[7]. A Jain, Phys. Rev. **A44**, 772 (1991).

[8]. B I Schneider *et al*, article in " Aspects of Electron–Molecule Scattering and Photoionization ", ed. by A Herzenberg (AIP, 1990). pp. 83.

[9]. I Shimamura, Chem. Phys. Lett., **73**, 328 (1980).

[10]. I. Shimamura, Prog. of Theo. Phys., **68**, 178 (1982).

[11]. I. Shimamura, J. Phys. **B15**, 93 (1982).

[12]. I Shimamura, Phys. Rev. **A28**, 1357 (1983).

[13]. I Shimamura, Phys. Rev. **A23**, 3350 (1981).

[14]. I Shimamura, Z. Phys. **A309**, 107 (1982).

[15]. I Shimamura, Phys. Rev. **A42**, 1318 (1990).

[16]. A Jain, Z Phys. D: Atoms, Molecules and Clusters, **21**, 153 (1991).

[17]. F A Gianturco, Vi D Martino and A Jain (submitted in Nuovo di Cimento, 1991).

[18.] A Jain, K L Baluja, Vi D martino and F A Gianturco, Chem. Phys. Lett. (accepted for publication).

[19]. see for example a review by N F Lane, Rev. Mod. Phys. **52**, 29 (1980) for the subject of ANA. see also M A Morrison, Aus. J. Phys. **36**, 239 (1983).

[20]. S Hara, J. Phys. Soc. Japan, **22**, 710 (1967).

[21]. S S Salvini and D G Thompson, J. Phys. **B14**, 3797 (1981).

[22]. A Jain and D G Thompson, J. Phys. **B15**, L631 (1982).

[23]. J A Pople and P Schofield, Phil. Mag. **2**, 591 (1957).

[24]. A Temkin, Phys. Rev. **107**, 1004 (1957).

[25]. J K O'Connel and N F Lane, Phys. Rev. **A27**, 1893 (1983); F A Gianturco, A Jain and L C Pantano, J. Phys. **B20**, 571 (1987).

[26]. W Sohn, K H Kochem, K M Scheuerlein, K Jung and H Ehrhardt, J. Phys. **B19**, 3625 (1986).

[27]. A Jain, Ph.D. thesis (Queen's University, Belfast) 1983.

[28]. D M Chase, Phys. Rev. **104**, 838 (1956).

[29]. D W Norcross and L A Collins, Adv. At. Mol. Phys. **18**, 341 (1982).

[30]. D W Norcross and N T Padial, Phys. Rev. **A25**, 226 (1982).

[31]. G Herzberg, in " Molecular Spectra and Molecular Structure", Vol. III. (Krieger, 1990)

[32]. P G Burke and M J Seaton, Methods in Comp. Phys. **10**, 1-80 (1971).

[33]. L A Collins and D W Norcross, Phys. Rev. **A18**, 478 (1978).

[34]. A Jain (to be submitted for publication).

[35]. J Ferch, B Granitz and W raith, J. Phys. **B18**, L445 (1985).

[36]. A. Garscadden, G L Duke and W F Bailey, Appl. Phys. Lett. **43**, 1012 (1983).

[37]. H -X Wan, J H Moore and J A Tossell, J. Chem. Phys. **91**, 7340 (1989).

[38]. W J Pollock, Trans. Faraday Soc. **64**, 2919 (1968).

[39]. J C Giordan, J. Am. Chem. Soc. **105**, 6544 (1983).

[40]. S Mori, Y Katayama and O Sueoka, At. Coll. Res. Jpn. **11**, 19 (1985).

[41]. M Tronc, A Hitchcock and F Edard, J. Phys. **B22**, L207 (1989).

[42]. Y Ohmori, M Shimozuma and H Tagashira, J. Phys. **D19**, 1029 (1986).

[43]. M Kurachi and Y Nakamura, J. Phys. D, Appl. Phys. **22**, 107 (1989).

[44]. M Hayashi (private communication).

[45]. H Tanaka, L Boesten, H Sato, M Kimura, M A Dillon and D Spence, J. Phys. **B23**, 577 (1990).

[46]. A Jain and D G Thompson, J. Phys. **B20**, 2861 (1987).

[47]. A K Jain, A N Tripathi and A Jain, J. Phys. **B20**, L389 (1987).

[48]. F A Gianturco, L C Pantano and S Scialla, Phys. Rev. **A36**, 557 (1987).

[49]. A Jain, J. Chem. Phys. **78**, 1289 (1987).

[50]. J Yuan, J. Phys. **B22**, 2589 (1989).

[51]. C Winstead and V McLoy, Phys. Rev. **A42**, 5357 (1990).

[52]. R Müller, K Jung, K H Kochem, W Sohn and H Ehrhardt, J. Phys. **B 18**, 3971 (1985).

[53]. L Boesten and L Tanaka (private communication).

[54]. O Sueoka, S Mori and Y Katayama, J. Phys. **B20**, 3237 (1987).

[55]. C Szmytkowski, K Maciag, G Karwasz and D Filipovic (private communication).

[56]. T W Shyn (private communication).

[57]. H P Pritchard, M A P Lima and V McKoy, Phys. Rev. **A39**, 2392 (1989).

[58]. S D Parker, C W McCurdy and T N Rescigno, Bull. Am. Phys. Soc. **36**, 1266 (1991).

[59]. A Jain and D G Thompson, J. Phys. **B16**, 2593 (1983).

[60]. F A Gianturco (to be published).

[61]. V F Sokolov and Yu A Sokolova, Sov. Tech. Phys. Lett. **7**, 268 (1981).

[62]. O Sueoka, S Mori and Y Katayama, J. Phys. **B19**, L373 (1986).

[63]. A Zecca, G Karwasz, S Oss, R Grisenti and R S Brusa (private communication).

[64]. C Szmytkowski, Chem. Phys. Lett. **136**, 363 (1987).

[65]. J L Pack, R E Voshall and L Rosenberg, Phys. Rev., **125**, 1300 (1962).

[66]. K Jung, Th Antoni, R Müller, K H Kochem and H Ehrhardt, J. Phys. **B15**, 3535 (1982).

[67]. A Danjo and H Nishimura, J. Phys. Soc. Japan, **54**, 1224 (1985).

[68]. T W Shyn and S Y Cho, Phys. Rev. **A36**, 5138 (1987).

[69]. L M Brescansin, M A P Lima, T L Gibson and V McKoy, J. Chem. Phys. **85**, 1854 (1986).

[70]. H Sato, M Kimura and K Fujima, Chem. Phys. Lett. **145**, 21 (1988).

☆U.S. Government Printing Office:1992—648-127/62118